© 2012 Young Joo Lee

FINITE-ELEMENT-BASED SYSTEM RELIABILITY ANALYSIS AND UPDATING OF FATIGUE-INDUCED SEQUENTIAL FAILURES

BY

YOUNG JOO LEE

DISSERTATION

Submitted in partial fulfillment of the requirements
for the degree of Doctor of Philosophy in Civil Engineering
in the Graduate College of the
University of Illinois at Urbana-Champaign, 2012

Urbana, Illinois

Doctoral Committee:

Associate Professor Junho Song, Chair and Director of Research
Professor Billie F. Spencer, Jr.
Professor Arif Masud
Professor Harry R. Millwater, Jr., University of Texas at San Antonio

ABSTRACT

Fatigue is one of the main causes of structural failure. In fact, many structural systems such as bridges, offshore platforms, and aircraft are subjected to the risk of fatigue-induced failure caused by repeated loading over their life cycle. Therefore, structural systems should be designed and maintained such that they have an adequate level of structural redundancy to prevent local fatigue-induced failures from progressing toward system-level failure such as collapse, which may result in complete loss of the structural system and catastrophic consequences. For decision-making with respect to the design, maintenance and retrofit of robust structural systems, it is thus essential to estimate their reliability and identify critical sequences of local failures leading to system failures. In addition, it is desirable to update the original reliability based on inspection results, which will facilitate reliability-based structural maintenance based on the actual conditions of structures.

Performing reliability analysis and updating of fatigue-induced sequential failure of a structural system is a challenging task. First, the reliability analysis should be performed at the system level in conjunction with sophisticated finite element analysis to account for the complex behavior of the structure during fatigue-induced sequential failures including the impact of load re-distribution caused by failures at other locations. Second, one might need to explore a huge number of failure sequences to estimate the failure risk accurately, especially for complex structural systems with high level of redundancy. Third, for accurate system reliability updating, precise system reliability estimation should be performed first and then the results should be incorporated into a method that can update the original reliability based on inspection results.

This thesis proposes novel finite-element-based methods for system reliability analysis and updating for structures that are subject to the risk of fatigue-induced sequential failures. First

of all, a new computational framework is developed which performs finite element reliability analysis (FE-RA) at the system level. While many of the existing FE-RA software packages aim at reliability analysis at the *component* level or have the limited capability of their FE modules, the new framework enables us to perform *system* reliability analysis in conjunction with sophisticated finite element analysis. Secondly, a new Branch-and Bound method employing system reliability Bounds (termed the B^3 method) is developed to perform system reliability analysis for the fatigue-induced sequential failures of structures. Describing sequential failures as disjoint events, the B^3 method enables us to estimate the system-level failure probability and identify critical failure sequences, more accurately and efficiently than other existing methods. The B^3 method was originally developed for reliability analysis of discrete structures such as a truss, but the method is further developed for its applications to continuum structures. Lastly, a new reliability updating method employing the B^3 method is proposed to update the system reliability analysis results based on structural inspections. The approach can update the original failure probability of structures based on various conditions observed during inspections for both truss and continuum structures. All of the proposed methods are applied to numerical examples of structural systems, and the results are compared with those by Monte Carlo simulations, which show that the proposed methods can perform system reliability analysis and updating in conjunction with finite element analysis, accurately and efficiently.

Dedicated to my family

ACKNOWLEDGEMENTS

First of all, I wish to express my deep appreciation to my advisor, Professor Junho Song. Since I started my Ph.D. study, he has given me passionate advice, constant support, and continuous encouragement. I have learned so many things from him, and his insightful guidance has been the key to my research accomplishments and academic growth. He has been the perfect role model as a researcher, teacher, advisor, mentor, and person, and I believe that it was one of the best decisions of my life to join his research group as a doctoral student.

I was greatly honored to have Professor Billie F. Spencer, Jr., Professor Arif Masud, and Professor Harry R. Millwater, Jr., on my dissertation committee. It was also my great honor to have Doctor Eric J. Tuegel on my preliminary exam committee. All of them kindly served on my committee and provided insightful suggestions and feedback, which were crucial elements in improving my Ph.D. research.

I would like to thank all of the former and current members of Professor Song's Structural System Reliability Group: Dr. Seung-Yong Ok, Dr. Won Hee Kang, Dr. Tam Hong Nguyen, Hyun-woo Lim, Derya Deniz, Nolan Kurtz, Junho Chun, Paul Lee, and Roselyn Kim. It was my great pleasure to share this time and have research discussions with them. Furthermore, I am grateful to my friends at the University of Illinois at Urbana-Champaign, especially to Do Soo Moon, Jae Hyuk Kwack, Ki Won Park, Yong Won Seo, Young Suk Kim, Dae-Jin Kim, Kyoung Soo Park, Sung-Han Sim, Heui Hwang Lee, Moo Chul Shin, Seung Jae Lee, Liang Chang, Hong Ki Jo, Nam Jeong Choi, Su Yun Ham, and Tae Sung Hwang. I also owe my thanks to my English tutor, Mr. Bruce Norris, for his great and passionate teaching for more than two years.

This work was mainly supported by the Midwest Structural Science Center (MSSC) under a cooperative agreement from the U.S. Air Force Research Laboratory Air Vehicles Directorate (contract number FA8650-06-2-3620). Additional support was provided by the National Science Foundation (NSF) and the University of Illinois at Urbana-Champaign, and I gratefully acknowledge their financial support.

Lastly, I would like to show my deepest gratefulness to my parents, Tae Ho Lee and Cha Sook Park, and my brother, Young Jae Lee, for their love and support throughout my life. I also would like to thank my lovely wife, Min Kyoung Lee, to whom I owe the most for her endless love, understanding, support, and encouragement. I hope this experience during my Ph.D. years will help build a beautiful life with our lovely daughter, Yuna.

Table of Contents

List of Figures

List of Tables

1. INTRODUCTION

In recent decades, structural reliability theory has flourished to help engineers across various disciplines model uncertainties and quantify their impacts on analysis, design, and maintenance. Many methods and tools have been developed and applied to structural systems in civil, mechanical, nuclear, marine, and aerospace engineering (Thoft-Christensen 1998, Haldar 2006, Frangopol and Maute 2003, Moan 2005). A structural system often requires sophisticated methods of structural reliability analysis due to its complex failure mechanism. One of the examples showing such a challenge is the reliability analysis of structural systems subjected to sequential failures induced by fatigue.

Fatigue is one of the main causes of the failure of structures. Many structural systems such as bridges, offshore platforms, and aircraft are subjected to the risk of failures caused by repeated loading over their life cycle (Byers *et al*. 1997, Karamchandani *et al*. 1992). However, it is difficult to predict fatigue-induced failures because fatigue is a complex process including various uncertainties, as proved by many laboratory experiment data (Haldar 2006). For this reason, many structural reliability methods were developed to analyze the uncertainties in terms of failure probability.

Most of the existing studies about fatigue reliability focus on predicting the fatigue life of individual structural members. However, it is noted that a structure should be designed and maintained in terms of the system-level performance to achieve an adequate level of structural redundancy that would prevent local fatigue-induced failures from progressing toward exceedingly large damage such as structural system collapse. Although the system-level redundancy plays such an important role in preventing the failure of local members from

initiating the collapse of the structural system, there have been few research efforts for fatigue life prediction considering the system-level redundancy.

For risk-informed structural design against fatigue-induced sequential failures, it is essential to estimate the reliability of a structural system and to identify critical sequences of local failures leading to a system failure. In addition, an adequate level of structural reliability needs to be guaranteed through structural maintenance such as inspection, as well as proper structural design, and it is thus required to update the original reliability based on inspection results.

For accurate reliability analysis and updating of fatigue-induced sequential failures, it is necessary to develop an integrated reliability analysis framework that can address the followings: First, structural reliability analysis should be performed in conjunction with finite element (FE) analysis, so that structural responses which appear in the limit-state function describing the structural failure mode of interest can be evaluated accurately during reliability analysis. Even though there are a few computational platforms that link structural reliability analysis with FE analysis, most of them still have some limitations in that they perform reliability analysis at the component level without considering system-level failures or have FE modules with limited capabilities in their applications.

Second, the sequential failure of a structure needs to be described as a complex "system" event which is a logical function consisting of multiple "component" events representing the failures of physical structural members or the occurrence of various failure modes. There have been many research efforts to develop an accurate and efficient method for the risk analysis of the many failure modes. In most cases, however, the existing methods aim to quantify the risks of individual local failures only. Such component reliability analysis may cause errors in

estimating the actual risk, and system reliability should be introduced to calculate the risk of sequential failure of structures accurately.

Third, for a complex structural system, there exist a huge number of failure sequences to explore, which may require overwhelming computational and time costs. Thus, for an efficient risk analysis of sequential failure, it is indispensable to have a smart algorithm that minimizes the number of failure sequences to explore. Although many research efforts have been made to develop efficient searching schemes, these methods are still either time-consuming or prone to miss critical failure sequences. In addition, the methods may underestimate the risk due to heuristic rules or assumptions that are often introduced to enhance the efficiency of the search.

Fourth, while fatigue-induced sequential failure is a critical failure mode of various structures, most of the existing studies of the system-level reliability analysis of fatigue-induced sequential failure have been undertaken for offshore structures, which are often modeled as discrete structures (e.g., truss). However, it is noted that reliability analysis for fatigue-induced sequential failure is important not only for discrete structures, but also for continuum structures such as subsystems in aircraft structures. Therefore, it is required to develop a novel method to perform system reliability analysis of fatigue-induced sequential failures for continuum structures.

Lastly, it is beneficial to develop a new method to update the original reliability, which was calculated during structural design, based on the observations from structural inspections. Practically, the safety of a structural system can be guaranteed through not only proper structural design, but also structural maintenance such as inspection. However, many of the existing methods developed for reliability updating focus on structural components, and there are few studies about reliability updating for sequential failure of a structural system. For an effective

inspection planning, it is thus essential to develop a new method for estimating the reliability of structures against fatigue-induced sequential failures and updating the original reliability based on inspections accurately.

These challenges motivated the research reported in this thesis, which focuses on developing novel frameworks and methods for system reliability analysis and reliability updating of fatigue-induced sequential failures based on finite element simulations. In order to overcome the aforementioned challenges, an FE-SRA (finite element system reliability analysis), an efficient path-searching algorithm, and a reliability updating technique are developed. First, an FE-SRA framework was developed by use of a newly-developed interface code that integrates a reliability analysis package and FE analysis software. This has been demonstrated through examples of structural systems. Second, a new branch-and-bound method that employs system reliability bounds (termed the B^3 method) has been developed. The B^3 method was first developed for system reliability analysis for discrete structures, and then further developed for continuum structures. The method enables us to estimate system-level failure probability and to identify critical fatigue-induced failure sequences accurately and efficiently, and is applicable to many types of structures from truss to continuum. Lastly, a reliability updating method employing the B^3 method was developed to update the original reliability information of a structure based on inspection results.

This Ph.D. thesis summarizes these developments and discusses the future research plan. Chapter 2 describes the newly-developed FE-SRA framework and the interface code named as FERUM-ABAQUS. Chapter 3 presents the B^3 method which is developed for the system reliability analysis of fatigue-induced sequential failures in discrete structures. Chapter 4 discusses the further development of the B^3 method for its applications to continuum structures.

Chapter 5 introduces the new reliability updating method employing the B^3 method. Lastly, Chapter 6 summarizes the major finding of this study and provides future research topics.

2. FINITE ELEMENT SYSTEM RELIABILITY ANALYSIS (FE-SRA)

For accurate reliability analysis of fatigue-induced sequential failures, it is necessary to perform the reliability analysis at the system level in conjunction with sophisticated finite element (FE) analysis. This chapter introduces a new FE-SRA (finite element system reliability analysis) framework, which will be introduced in the next chapters as a crucial element of system reliability analysis and updating for fatigue-induced sequential failures.

2.1. Literature Review

In recent years, many research efforts have been made to perform structural reliability analyses with more realistic and complex structural models. The examples include suspension bridge (Imai and Frangopol 2002), wing torque box of aircraft (Lee *et al*. 2008), pylon of cable-stayed bridge (Song *et al*. 2008, Kang *et al*. 2012), and bridge structure system (Song and Kang 2009). In addition, sophisticated reliability methods have been developed to deal with complex failure mechanisms such as failure of rigid-plastic structure (Song and Der Kiureghian 2003), progressive yielding failure of indeterminate truss structure (Song and Kang 2009), and fatigue-induced sequential failures of truss structure (Karsan and Kumar 1988, Karamchandani *et al*. 1992, Wang *et al*. 2006).

In such reliability analyses, it is essential to account for the uncertainties in loading, material properties, geometry, etc. Structural reliability analysis requires describing the limit-state of interests mathematically, in terms of structural response quantities such as strain, displacement, stress, force, and energy (Sudret and Der Kiureghian 2000). If the limit-state can be represented by a simple algebraic function of random variables representing the

aforementioned uncertainties, one can easily perform reliability analysis. In dealing with many complex structural systems or failure mechanisms, however, sophisticated structural analyses employing a finite element model are needed to evaluate the structural response that appears in the limit-state function during the reliability analysis. Therefore, it is necessary to perform structural reliability analysis (RA) in conjunction with finite element (FE) analysis, which is often termed as finite element reliability analysis (FE-RA) in the literature (Sudret and Der Kiureghian 2000, Haukaas 2003, Lee *et al*. 2008).

There have been active research efforts to connect the computational modules of FE analysis with those for reliability analysis, which resulted in computer software packages such as reliability package in OpenSees (Haukaas 2003), FERUM (Haukaas *et al*. 2003), and RELSYS (Estes and Frangopol 1998). Despite these recent advances, there are still two research needs in FE-RA.

First, many of the existing FE-RA software packages mainly perform "component" reliability analysis. In other words, the FE reliability analysis is performed for individual failure modes of a structural member or location that are represented by single limit-state functions. This may lead to an inaccurate estimate on the failure probability of a structural system because the overall system-level risk of a structure often needs to be described by means of a "system" event, i.e. a logical function of "component" events representing physical components or various failure modes (Song and Der Kiureghian 2003, Song and Kang 2009, Lee *et al*. 2008). The failure of a structure may be described as a series, parallel, or general system event (Song and Der Kiureghian 2003, Song and Kang 2009, Lee *et al*. 2008), and this type of reliability analysis is often termed as system reliability analysis (SRA).

Another limitation of the existing FE-RA software packages is the limited capability of their FE modules. For accurate risk estimation, it is desirable that reliability software employs a finite element model that can represent the structural behavior most accurately. However, most of the existing FE-RA packages contain an FE analysis program whose capability and applicability are somewhat limited. In order to have more versatile FE-RA computing platform, therefore, it is desirable to develop an interface code between a reliability analysis code and general-purpose FE software such as ABAQUS® rather than employing an FE code included in the reliability software package.

To overcome these challenges, advanced FE-RA software packages have been developed in recent years, such as NESSUS (SwRI 2009) and STRUREL (Gollwitzer *et al*. 2006) by combining a module of system reliability analysis with FE analysis software. In this Ph.D. research, an FE-SRA (FE system reliability analysis) framework that employs a new system reliability analysis method is developed (Lee *et al.* 2008), and an interface code between FERUM and ABAQUS® (termed the FERUM-ABAQUS) is developed as a computational platform of the research. FERUM (Finite Element Reliability Using Matlab) is a reliability analysis package developed by researchers at the UC Berkeley, which allows us to perform various reliability analyses (Haukaas *et al*. 2003). ABAQUS is widely used commercial software for FE analysis. By using these two software packages specialized in their own areas, it becomes possible to take full advantages of them and solve challenging problems. This chapter describes the proposed FE-SRA framework and demonstrates the interface code, FERUM-ABAQUS, with numerical examples of an aircraft wing torque box and a bridge pylon.

2.2. FE-SRA Using FERUM-ABAQUS

2.2.1. FE component reliability analysis

The first step of FE-SRA is to perform FE reliability analyses to compute the probabilities of all component failure events that are considered significant. Such an FE component reliability analysis is described as

$$P_i = P\left[g_i(\mathbf{X}) \le 0\right] = \int_{g_i(\mathbf{x})\le 0} f_{\mathbf{X}}(\mathbf{x})d\mathbf{x}\ ,\quad i = 1,...,n \tag{2.1}$$

in which P_i and $g_i(\mathbf{X})$ respectively denote the probability and the limit-state function of the i-th component event, $\mathbf{X}$ is the vector of the random variables representing the uncertainties in the given problem, $f_{\mathbf{X}}(\mathbf{x})$ is the joint probability density function (PDF) of $\mathbf{X}$, and n is the total number of component events in the given system event. As previously stated, one approach to compute this probability by FE reliability analysis is to link a reliability analysis algorithm with an FE code so that the algorithm can import the values and/or sensitivities of $g_i(\mathbf{X})$ with respect to $\mathbf{X}$, from the computational simulation. Figure 2.1 illustrates this approach and the data flows.

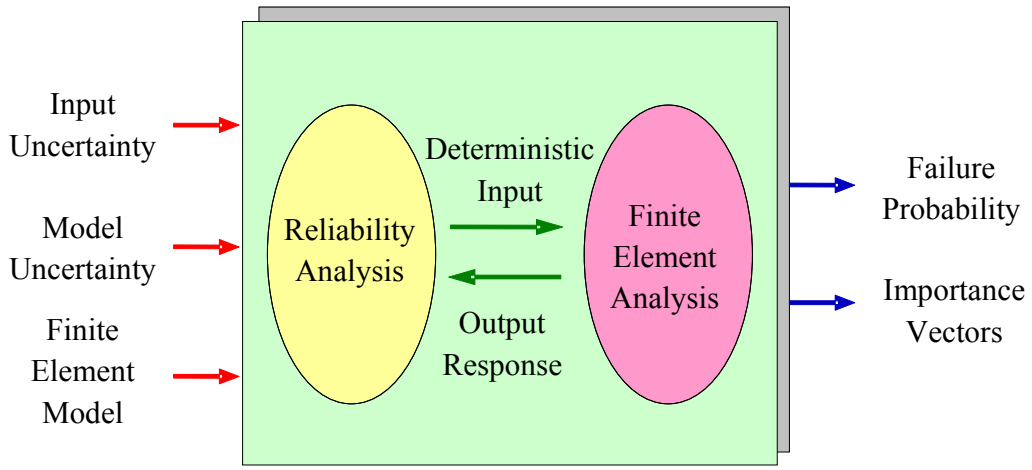

Figure 2.1 Data flows during FE reliability analysis

For the numerical examples in this chapter, the first order reliability method (FORM) (see Der Kiureghian 2005 for a review) in an open-source reliability code FERUM is used to calculate the probability of "component" event in Eq. (2.1). The nonlinear constrained optimization problem during FORM analysis needs the values and gradients of the limit-state function at each step of the iteration. FERUM-ABAQUS is employed so that FERUM can obtain the output responses that appear in the limit-state functions (e.g., strain, displacement, stress, force, and energy results) and their gradients from an FE-based computational simulation.

The component FE reliability analyses provide the probabilities of all the component failure events considered. For an accurate SRA, we also need to quantify the statistical dependence between the component failure events. For example, if component reliability analysis is performed by FORM, it is required for SRA to obtain the normalized negative gradient vectors (Der Kiureghian 2005) of the limit-state function, that is

$$\boldsymbol{\alpha}_i = -\nabla G_i(\mathbf{u}_i^*) / \left\| \nabla G_i(\mathbf{u}_i^*) \right\| \tag{2.2}$$

where $\nabla G_i(\cdot)$ and $\mathbf{u}_i^*$ respectively denote the gradient vector of the i-th limit-state function $G_i(\mathbf{u})$ and the most probable point (or "design point") in the space of uncorrelated standard normal random variables $\mathbf{u}$. In this thesis, the gradient vectors and the normalized gradient vectors are given as row vectors. In system reliability analysis, these normalized gradient vectors are used to quantify the statistical dependence between the component events, and the procedure will be explained in the following section.

An important by-product of FORM analysis is a set of importance measures that provide information as to the order of importance of the random variables. First, when the random variables $\mathbf{X}$ of a reliability problem are statistically independent, the order of importance of random variables can be determined in terms of the normalized negative gradient vectors in Eq. (2.2). However, when the random variables are statistically dependent, the following importance measure (Der Kiureghian 2005) should be introduced to define the relative importance of the random variables $\mathbf{X}$:

$$\boldsymbol{\gamma}_i = \frac{\boldsymbol{\alpha}_i \mathbf{J}_{\mathbf{u},\mathbf{x}} \mathbf{D}}{\left\| \boldsymbol{\alpha}_i \mathbf{J}_{\mathbf{u},\mathbf{x}} \mathbf{D} \right\|} \tag{2.3}$$

where $\mathbf{J}_{\mathbf{u},\mathbf{x}}$ denotes the Jacobian matrix of the transformation from $\mathbf{X}$ to $\mathbf{u}$, and $\mathbf{D}$ denotes the diagonal matrix of standard deviations of $\mathbf{X}$. The importance measure in Eq. (2.3) is a unit row vector defining the relative importance of the original random variables, and a positive (or negative) value of this vector indicates that the relevant random variable is of load (or capacity)

type. The element-squares of γ_i are widely used to quantify the relative contributions of the random variables to the variance of the limit-state function.

Lastly, FORM analysis provides us with the sensitivities of the failure probability P_i with respect to statistical parameters (e.g., mean and standard deviation) of random variables (Bjerager and Krenk 1989). However, these sensitivities may have a scaling problem as sensitivity measures. For this reason, they are generally normalized by multiplying standard deviation of random variables to these sensitivities. For example, for the *j*-th random variable (i.e. X_j, j=1,…,N_{rv}) where N_{rv} is the total number of random variables,

$$\delta_{i,j} = \frac{\partial P_i}{\partial \mu_j}\sigma_j \tag{2.4a}$$

$$\eta_{i,j} = \frac{\partial P_i}{\partial \sigma_j}\sigma_j \tag{2.4b}$$

in which μ_j and σ_j respectively denote the mean and standard deviation of the *j*-th random variable. The details of the importance measures and sensitivities from FORM can be found in Der Kiureghian (2005).

2.2.2. FE system reliability analysis

The main goal of SRA is to evaluate the probability of a system event that describes the failure of a structural system, that is

$$P_{sys} = P\left[\bigcup_k \bigcap_{i\in C_k} g_i(\mathbf{X}) \le 0\right] \tag{2.5}$$

where C_k denotes the index set of components in the *k*-th cut-set. This general "cut-set" formulation can also represent "series" systems (all the cut-sets have only one component) and

"parallel" systems (there is only one cut-set). In particular, when FORM is used for the component reliability analyses in Eq. (2.5), P_{sys} can be approximately computed as

$$P_{sys} \cong P(\mathbf{\Omega}) = P\left[\bigcup_{k}\bigcap_{i\in C_k}\left(\beta_i - Z_i \le 0\right)\right] = \int_{\mathbf{\Omega}} \varphi_N(\mathbf{z};\mathbf{R})\, d\mathbf{z} \tag{2.6}$$

where Ω denotes the failure domain approximated as a polyhedron determined by linear half spaces, $\beta_i = \boldsymbol{\alpha}_i \mathbf{u}_i^*$ is the reliability index of the *i*-th component event, $\mathbf{Z} = \{Z_i\}$, i = 1,…,*n* is the vector of standard normal random variables approximately describing the component events by $\beta_i - Z_i \le 0$, $\varphi_N(\mathbf{z};\mathbf{R})$ is the joint PDF of $\mathbf{Z}$, and $\mathbf{R}$ is the correlation coefficient matrix of $\mathbf{Z}$ in which the correlation coefficient between Z_i and Z_j is computed as $\rho_{ij} = \boldsymbol{\alpha}_i \boldsymbol{\alpha}_j^{\mathrm{T}}$ (Hohenbichler and Rackwitz 1983).

In order to compute the probability of this logical function of component events from the results of individual component reliability analyses, various SRA algorithms have been developed, such as theoretical bounding formulas (Ditlevsen 1979), sequentially conditioned importance sampling (SCIS) (Ambartzumian *et al*. 1998), the product of conditional marginals (PCM) method (Pandey 1998), the multivariate normal integral method by Genz (1992) (applicable to series and parallel systems), and the first-order system reliability methods (Hohenbichler and Rackwitz 1983) (applicable to series and parallel systems directly, and to cut-set and link-set systems indirectly in conjunction with bounding formulas). However, these existing methods for system reliability analysis are applicable to "series" and "parallel" systems, but not to "general" system events. In addition, they are not flexible in incorporating various types and amount of available information on components and their statistical dependence.

For these reasons, SRA methods such as the linear programming (LP) bounds method (Song and Der Kiureghian 2003, Der Kiureghian and Song 2008), the matrix-based system reliability (MSR) method (Kang *et al*. 2008, Song and Kang 2009, Nguyen *et al*. 2010b, 2011, Song and Ok 2010, Lee *et al*. 2011, Kang *et al*. 2012), and the sequential compounding method (SCM) (Kang and Song 2010) have been recently developed. These methods are capable of solving general system events with various merits. A more comprehensive review on SRA methods can be found in Kang (2011). In the examples of this chapter, FE-SRA employs the MSR method which is summarized as follows.

First, consider a system event whose i-th component, $i = 1,\ldots,n$ has two distinct states, e.g. the failure and survival. The sample space can be subdivided into m ($=2^n$) mutually exclusive and collectively exhaustive (MECE) events. These are named the "basic" MECE events and denoted by e_j, $j = 1,\ldots,m$. Then, any system event can be represented by an ''event" vector $\mathbf{c}$ whose j-th element is 1 if e_j belongs to the system event and 0 otherwise. Let $p_j = P(e_j)$, $j = 1,\ldots,m$, denote the probability of e_j. Due to the mutual exclusiveness of e_j's, the probability of the system event E_{sys}, i.e. $P(E_{sys})$ is the sum of the probabilities of e_j's that belong to the system event. Therefore, the system probability is computed by the inner product of the two vectors, that is,

$$P\left(E_{sys}\right) = P_{sys} = \sum_{j:e_j \subseteq E_{sys}} p_j = \mathbf{c}^{\mathrm{T}}\mathbf{p} \tag{2.7}$$

where $\mathbf{p}$ is the ''probability" vector that contains p_j's and $\mathbf{c}$ is the "event" vector each of whose elements has 1 or 0 depending on whether e_j belongs to E_{sys} or not. The formulation in Eq. (2.7) can be generalized to compute the probabilities of multiple system events under multiple conditions of component failures by a single matrix multiplication (Lee *et al*. 2011).

Furthermore, the MSR method provides us with the normalized parameter sensitivities of the system failure probability, i.e. the sensitivities of system failure probability with respect to one-standard-deviation-changes of statistical parameters of random variables, based on the component-level parameter sensitivities as shown in Eqs. (2.4a) and (2.4b).

$$\delta_{sys,j} = \frac{\partial P_{sys}}{\partial \mu_j} \sigma_j \tag{2.8a}$$

$$\eta_{sys,j} = \frac{\partial P_{sys}}{\partial \sigma_j} \sigma_j \tag{2.8b}$$

More details about the MSR method can be found in Song and Kang (2009), and the method is selected as an SRA method in this chapter because of the following merits over other existing methods: First, the probability of a system event is calculated by a simple matrix multiplication regardless of the complexity of the system definition. Second, the matrix-based formulation helps identify/handle the system events conveniently and compute the corresponding probabilities efficiently. Third, even when one has incomplete information on the component failure probabilities and/or their statistical dependence, the matrix-based framework still enables obtaining the narrowest possible bounds on any general system event using the LP bounds method. Fourth, once the probability of the system event is obtained, one can easily calculate the probabilities of other system events, conditional probabilities and component importance measures without additional probability calculations. Fifth, the recent developments of matrix-based computer languages and software have rendered matrix calculations more efficient and easier to implement. Finally, the MSR method can account for the statistical dependence between components and compute the sensitivity of the system reliability with respect to design parameters for general system events.

2.3. Numerical Example I: Wing Torque Box

2.3.1. Problem description

The proposed framework for FE-SRA and the interface code, FERUM-ABAQUS, are demonstrated by a numerical example of a 4-bay wing torque box (Lee *et al*. 2008) shown in Figure 2.2.

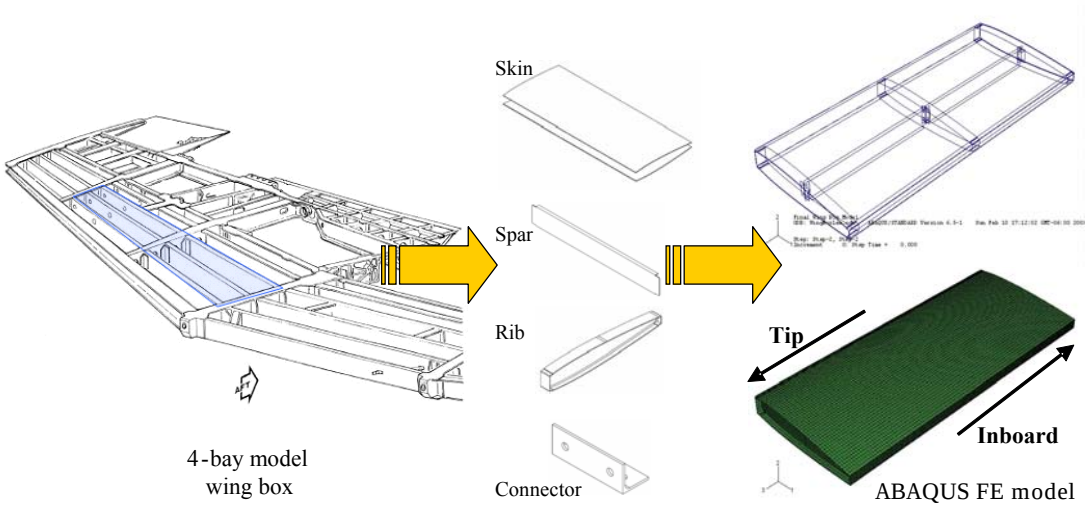

Figure 2.2 Wing torque box example

This is a hypothetical example created to test the existing and new methods for quantifying the risk and uncertainty in a sub-structure of generic aircraft structures. The initial drawing was created by Air Force Research Laboratory (AFRL) for the purpose of this research. Its dimensions are 1.52 meters (60 inches) length, 0.64 meters (25.2 inches) width, and 7.6 to 10.2 centimeters (3.0 to 4.0 inches) height. It is assumed that the main material of the wing box is Aluminum 7075-T6, which shows linear elasticity until it reaches yielding stress. The

structural system consists of numerous physical parts such as skins, spars, ribs, and connectors as shown in Figure 2.2. During FE reliability analyses, statistically independent random variables are assigned to describe the uncertainties in the material yield strengths and Young's modulus of all the parts individually.

In this example, three reference load combinations (A, B and C) are considered to represent random loading conditions. Each operational loading for the 4-bay wing box model is described by the combination of moments and torques applied to each end of the box, and a pressure distribution on the lower surface. These load combinations are results of the 4-bay model being a portion of a complete wing. One of the three load cases is shown in Figure 2.3 with the corresponding spatial distribution of Von-Mises stress computed by an FE analysis. It was noted that the maximum stress under the given load case "A" occurs at the front side of the inboard edge. The other two loading cases resulted in maximum stresses at similar locations. The actual loads can vary with the structural characteristics and flight patterns of aircraft, and environmental effects such as humidity and barometric pressure.

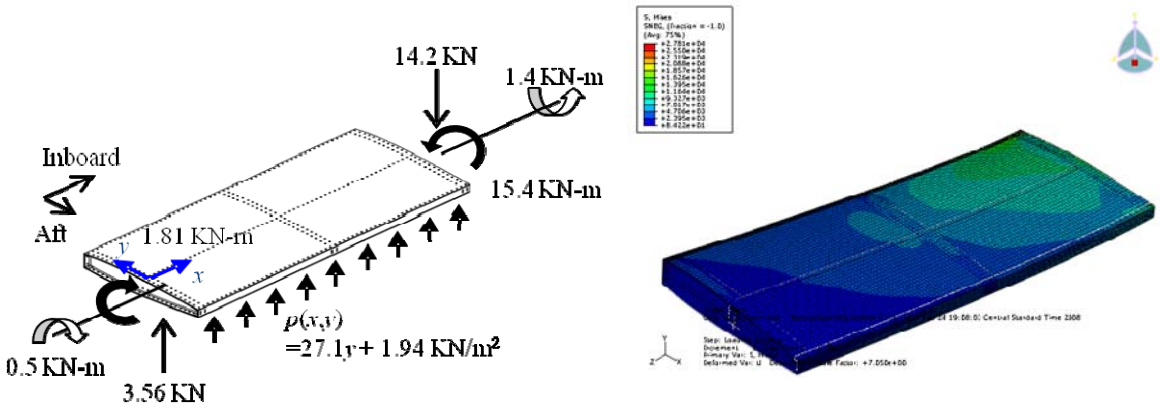

Figure 2.3 Reference load case "A" and corresponding stress distribution by FE analysis

This example accounts for three kinds of uncertainties by use of random variables: (1) Young's modulus; (2) yield strength; and (3) load scale factor in the load spectrum. The first two characterize the uncertainty in the material properties and capacities while the third represents the uncertainties in loads and demands. Table 2.1 summarizes the mean, coefficient of variation (c.o.v.) and the type of distribution used for each type of uncertainty in this example.

	Mean	c.o.v.	Distribution Type
Young's modulus	71,700 (MPa)	0.100	Normal
Yield strength	524 (MPa)	0.050	Lognormal
Load scale factor	0.300	0.400	Lognormal

Table 2.1 Statistical properties of random variables

The wing torque box is composed of two skins, three ribs, four spars (one front spar, one rear spar, and two middle spars), and many connectors. Since they are usually manufactured using separate raw materials, statistically independent random variables are assigned to Young's moduli of the nine parts. From preliminary FE reliability analyses, it was observed that the contribution of Young's moduli of the connectors to the variance of the limit-state function is insignificant. Therefore, a single random variable represents Young's moduli of all the connectors. This assumption helps reduce the number of random variables during FE reliability analyses. As a result, in this example ten random variables represent the uncertainty in Young's moduli (two for skins, three for ribs, four for spars, and one for connectors).

The statistical properties of the material yield strength were extracted from Military Handbook 5 (U.S. Department of Defense 2005), now known as Metallic Material Properties

Databook (MMPD), which provides two classes of guidelines on yield strength of the target material: A-basis and B-basis. These are nominal values of the strengths defined as of the thresholds of 99% and 90% exceedence probabilities, respectively. Assuming that the strengths follow a normal distribution, the mean and standard deviation of the experimental data of yield strength were back-calculated.

The uncertain time variation of the intensity of the loading during a flight is characterized by use of FALSTAFF spectrum (Van Dijk and De Jonge 1975). It is assumed that all the loads in each load case, e.g., bending moment, torsion and pressure are in-phase and thus uniformly scaled by the spectrum. The FALSTAFF spectrum is normalized to the considered load cases so that 1.0 in the spectrum corresponds to the magnitudes in the given load case. Figure 2.4 shows the exceedence plot of peak values in the FALSTAFF spectrum. Based on this plot, the distribution of load scale factor is fitted to a log-normal distribution whose mean and c.o.v. are 0.30 and 0.40, respectively (See Figure 2.5).

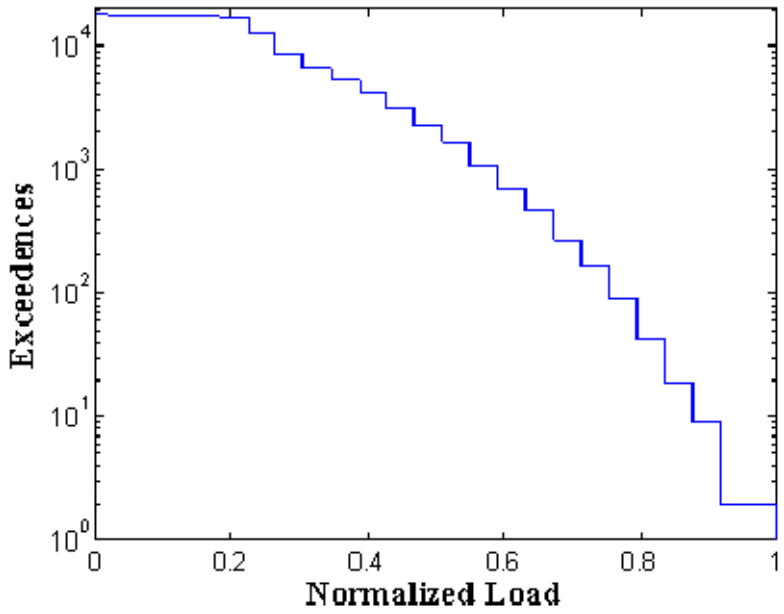

Figure 2.4 Exceedence Plot for FALSTAFF spectrum (Peak)

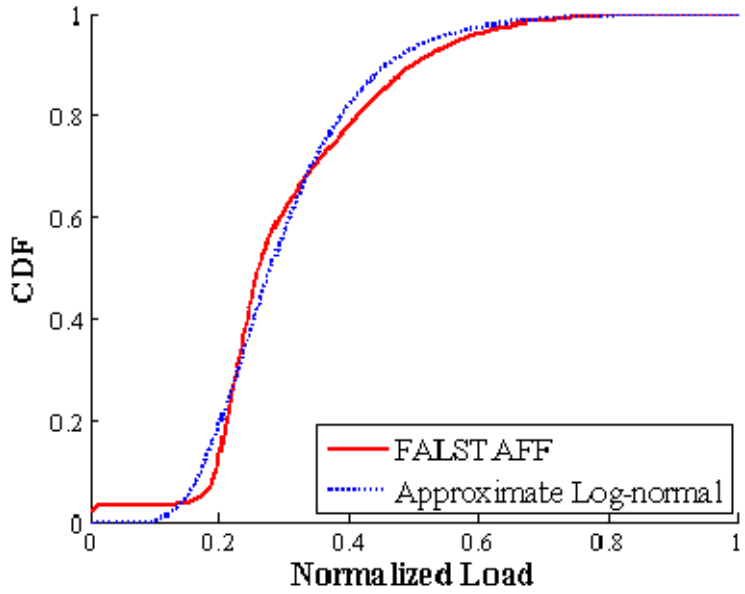

Figure 2.5 Fitting plot to FALSTAFF spectrum

All the random variables are assumed to be uncorrelated except the three random variables used for the load scale factors. The statistical dependence between three loading cases is not known, so a parametric study is performed by varying correlation coefficient between the load cases.

This example focuses on the failure due to yielding. Therefore, the failure of the *i*-th component is described by use of a limit-state function

$$g_i(\mathbf{X}) = \sigma_y^i(\mathbf{X}) - \sigma^i(\mathbf{X}) \le 0 \tag{2.9}$$

where $\sigma_y^i(\mathbf{X})$ is the yield strength of the physical part (e.g., spars, skins), and $\sigma^i(\mathbf{X})$ is the maximum Von-Mises stress estimated by FE analysis.

2.3.2. Analysis results

Before performing reliability analyses, the maximum Von-Mises stress response of each part is computed by deterministic FE analyses by use of the mean values of the random variables in Table 2.1. The results are shown in Table 2.2.

Maximum stress (MPa)	Load A	Load B	Load C
Upper skin	128.9	120.2	168
Lower skin	**132 (E_6)**	129.3	188.3
Front spar	**143.8 (E_4)**	**162.2 (E_3)**	**301.4 (E_1)**
Middle spar (Inboard)	71.6	73.2	151.3
Middle spar (Tip)	38.1	63.1	137.9
Rear spar	77.9	92	210.6
Rib (Inboard)	85.8	**132.2 (E_5)**	**269.8 (E_2)**
Rib (Middle)	21.7	35.6	72.6
Rib (Tip)	16.8	34.8	69.5

Table 2.2 Maximum stress response for each part under three loading cases

The results of this preliminary deterministic analysis help identify important component events to be considered during system reliability analysis. Two yielding failure events with top maximum stress results for each load cases are selected as shown in Table 2.2 (in bold). These component events are denoted by E_1 to E_6. FE reliability analyses of these component events are performed individually by FORM using FERUM-ABAQUS. Table 2.3 shows the component failure probabilities.

Component event	Failure probability ($\times 10^{-2}$)
E_1 (Load C; Front spar)	5.51989
E_2 (Load C; Rib inboard)	2.85896
E_3 (Load B; Front spar)	0.07515
E_4 (Load A; Front spar)	0.02923
E_5 (Load B; Rib inboard)	0.01010
E_6 (Load A; Lower skin)	0.01087

Table 2.3 Probabilities of component failure events by FORM analysis

The importance measure in Eq. (2.3) quantifies the relative contribution of the random variables to the total variance of the limit-state function. In this example, the load sale factors are identified as the most important ones with around 98% contribution for each component failure event. This relative importance may change if other failure modes such as fatigue are considered for reliability analyses.

FORM analysis provides the sensitivity of the failure probability with respect to the statistical parameters as well. Using these component-level sensitivities, it is possible to compute the sensitivity-based importance measures in Eqs. (2.4a) and (2.4b). For example, the results for

the component event E_1 are shown in Table 2.4, which confirms the dominance of the uncertainty in the loading to the component failure probability.

Random variables		$\delta_{1,j} = \frac{\partial P_1}{\partial \mu_j}\sigma_j$	$\eta_{1,j} = \frac{\partial P_1}{\partial \sigma_j}\sigma_j$
Young's modulus	Connector	−0.0011	0
	Rib (Inboard)	−0.0973	0.0014
	Rib (Middle)	−0.0019	0
	Rib (Tip)	0.001	0
	Lower skin	−1.203	0.2071
	Upper skin	0.0442	0.0003
	Front spar	1.3034	0.2431
	Middle spar (Inboard)	−0.0666	0.0006
	Middle spar (Tip)	−0.002	0
	Rear spar	−0.021	0.0001
Load scale factor	Combination A	0	0
	Combination B	0	0
	Combination C	3.402	5.317
Yield strength (Front spar)		−1.4354	0.3575

Table 2.4 Sensitivity-based importance measures for E_1 ($\times 10^{-2}$)

In order to compute the system probability in Eq. (2.4), the correlation coefficient matrix **R** is constructed by the inner product of the negative normalized gradient vectors, i.e. $\rho_{ij} = \boldsymbol{\alpha}_i \boldsymbol{\alpha}_j^{\mathrm{T}}$. Table 2.5 shows the correlation coefficient matrix when the correlation coefficient between the scale factors of different load cases is assumed to be 0.4.

Correlation	E_1	E_2	E_3	E_4	E_5	E_6
E_1	1	0.961	0.426	0.425	0.395	0.379
E_2		1	0.397	0.398	0.413	0.414
E_3			1	0.425	0.959	0.380
E_4				1	0.396	0.942
E_5		Symmetric			1	0.415
E_6						1

Table 2.5 Correlation matrix with six component failure events

One noticeable fact from this table is that there are strong correlations between the following event pairs: (E_1 and E_2), (E_3 and E_5), and (E_4 and E_6). These pairs respectively represent failure events under load cases A, B, and C, which also proves that loading scale factors are most contributory to the failure events.

These results of component reliability analysis are used for system reliability analysis. Let us first consider the series system event of the identified components:

$$E_{sys} = \bigcup_{i=1}^{6} E_i \tag{2.10}$$

This means that the structural system "fails" if any of these six component events occurs. For the component failure events whose probabilities and correlations are shown in Tables 2.3 and 2.5, the probability of the system event in Eq. (2.10) is computed by the MSR method. Table 2.6 compares the results by the MSR method with those by theoretical bounding formulas, i.e. Uni-component bounds (Boole 1854) and Bi-component bounds formulas (Ditlevesen 1979). The results by the MSR method are included in the relatively wider bounds by theoretical bounding formulas. It is also noteworthy that the system failure probability is higher than the probability of the most likely component failure event E_1. This means that component FE reliability analysis

may underestimate the risk of the overall system particularly when there is no dominant component event.

Method	System failure probability ($\times 10^{-2}$)
MSR	5.7431
Uni-component bounds	5.5199 ~ 8.5042
Bi-component bounds	5.7104 ~ 5.7451

Table 2.6 Failure probability of series system

In order to investigate the effect of statistical dependence between different load cases on the system failure probability, FE system reliability analyses are performed with varying correlation coefficients between the three load scale factors. As previously stated, the correlation matrix in Table 2.5 is calculated with the assumption that the correlation coefficient between the scale factors of different load cases is 0.4. However, the correlation between the component events is affected by the correlation coefficient between load scale factors, which therefore affects the system probability as well. For a series system event, for example, it is known that high correlation between component events reduces the failure probability. Figure 2.6 shows the effect of the statistical dependence between the load scale factors on the system reliability estimates. Figure 2.6a shows the probabilities from the MSR method, Uni-component bounds, and Bi-component bounds. Figure 2.6b compares the results from the MSR method and Bi-bounds only to show the effect of the statistical dependence more clearly.

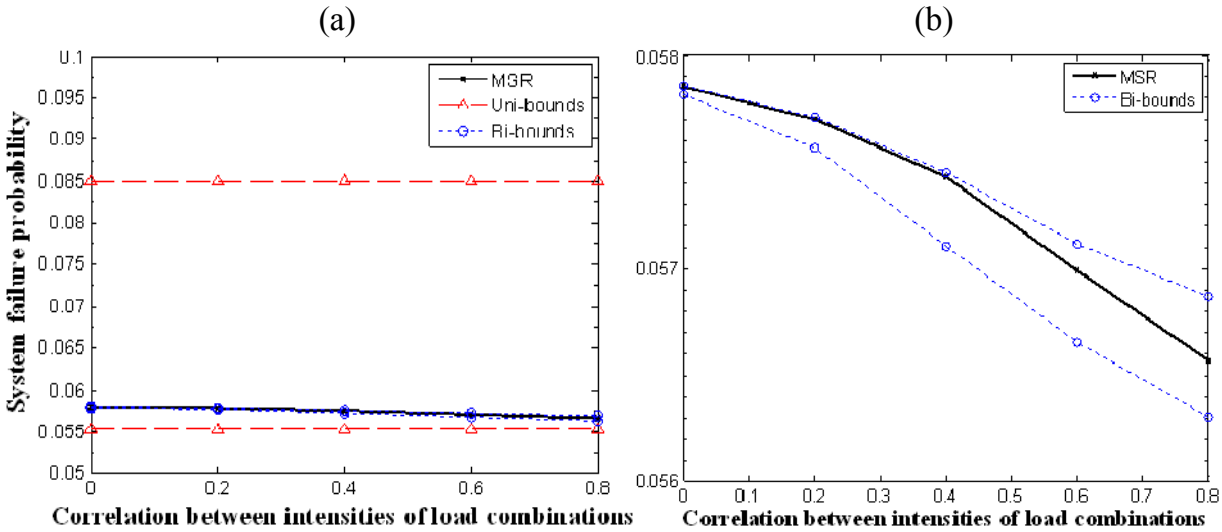

Figure 2.6 Parametric study on the effect of correlation between load scale factors

An important merit of the MSR method is that the method can estimate the probabilities of other system events of interest without significantly increasing computational cost. For example, suppose we are interested in the probability of a system event that the yielding failure occurs "only" by load case B, i.e.

$$E_{sys} = (E_3 \cup E_5) \cap \overline{E}_1 \overline{E}_2 \overline{E}_4 \overline{E}_6 \tag{2.11}$$

Using the matrix procedure of the MSR (Song and Kang 2009) described in Eq. (2.8), one can easily find the new system vector that corresponds to the event in Eq. (2.11). The probability of this system event is computed as 4.1407×10^{-4} by the MSR analysis.

In addition, the MSR method enables us to compute the sensitivities of the failure probability of the series system in Eq. (2.10) with respect to the means and standard deviations of

the random variables using the MSR method. Table 2.7 shows the sensitivity-based importance measures of the dominant random variables.

Random variables		$\delta_{sys,j} = \frac{\partial P_{sys}}{\partial \mu_j}\sigma_j$	$\eta_{sys,j} = \frac{\partial P_{sys}}{\partial \sigma_j}\sigma_j$
Young's Modulus	Rib (Inboard)	−0.0614	0.00249
	Lower skin	−1.0731	0.19713
	Front spar	1.1415	0.23371
	Middle spar (Inboard)	−0.0641	0.00056
Load scale factor	Combination A	0.02004	0.0685
	Combination B	0.04757	0.1483
	Combination C	3.4817	5.5713
Yield strength	Front Spar	−1.4894	0.38171
	Rib (Inboard)	−0.00729	0.00348
	Lower skin	−0.00155	0.00078

Table 2.7 Sensitivities of failure probability of series system ($\times 10^{-2}$)

2.4. Numerical Example II: Bridge Pylon

2.4.1. Problem description

This section provides another numerical example to demonstrate the proposed FE-SRA framework and FERUM-ABAQUS, a pylon structure of cable stayed bridge (Song *et al*. 2008, Kang *et al*. 2012), which is shown in Figure 2.7.

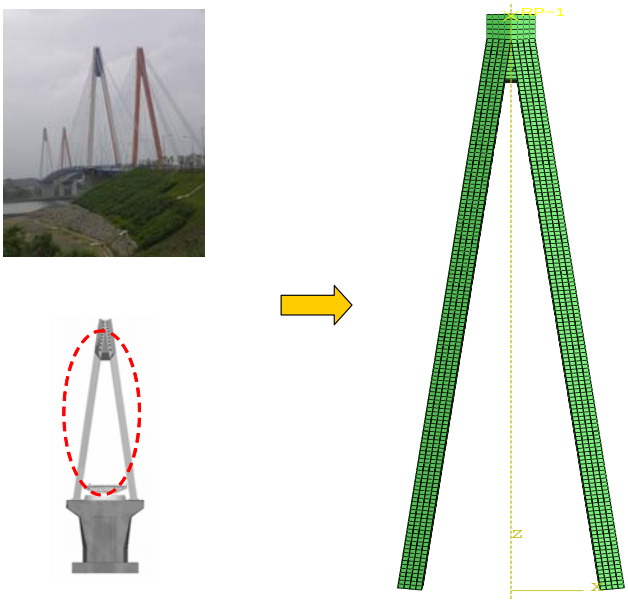

Figure 2.7 Pylon structure of cable stayed bridge

The dimensions of the pylon structure are chosen based on an actual bridge design. The 70-meter-long pylon has two symmetric arms, each of which consists of a main body with trapezoidal cross-section, 13 stiffeners, and 23 diaphragms. The dimensions of the left arm are shown in Figure 2.8.

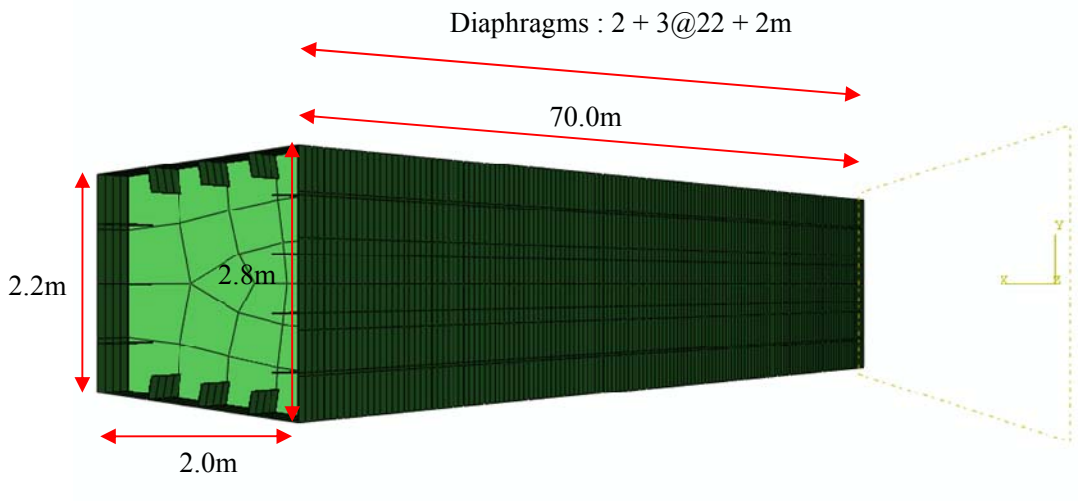

Figure 2.8 FE model of the left arm of the Pylon

Real bridge structures are usually exposed to various kinds of loads. These loads are often combined into load cases based on possible loading scenarios. This example considers the following load combinations consisting of four types of design loads, i.e. dead load (D), live load (L), wind load in service (WL) and wind load out of service (W), which are widely used in bridge design practice:

$$\begin{aligned} &\text{Load Combination 1 (LC1): } D + L + WL \\ &\text{Load Combination 2 (LC2): } D + W \end{aligned} \tag{2.12}$$

The dead load (D) includes the self-weight and the pre-stress force of the cables. The live load (L) includes the loads caused by the traffic and the pedestrians. The in-service wind load (WL) represents the wind loads when the bridge is in service. The out-of-service wind load (W) models the wind loads when vehicles are prohibited to pass over the bridge due to the strong winds. In this example, the pylon structure is modeled independently from the entire bridge system by

giving proper boundary conditions: the bottom end of the pylon is assumed to be fixed, and a reasonable axial force, shear force, and moment are specified at the top end to describe the reactions to cable anchors. Figure 2.9 shows the free body diagrams of the pylon structure and boundary conditions for the four types of loads that are considered.

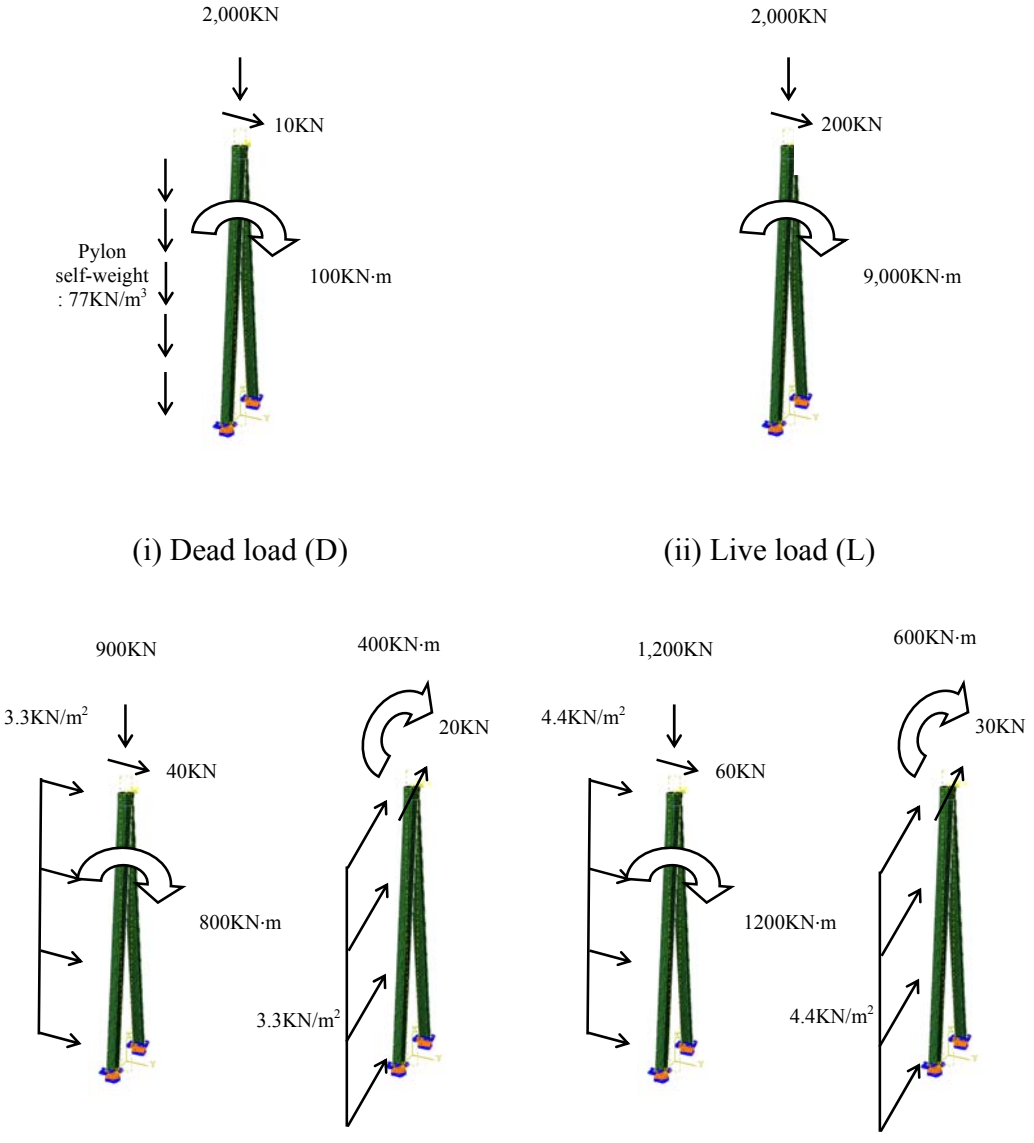

(i) Dead load (D)

(ii) Live load (L)

(iii) In-service wind load
(WL: In-plane & Out-of-plane)

(iv) Out-of-service wind load
(W: In-plane & Out-of-plane)

Figure 2.9 Loads considered during component and system reliability analysis

In this example, a total of 19 random variables are considered: 6 for Young's moduli, 6 for yield strengths, and 7 for the load scale factors. Table 2.8 lists the means, c.o.v.'s, and the distribution types for these variables.

		Mean	c.o.v.	Distribution Type
Young's modulus		2×10^8 (KN/m^2)	0.05	Normal
Yield strength		2.6×10^5 (KN/m^2)	0.05	
Load scale factor	Dead load	1.0	0.10	
	Live load	1.0	0.20	
	Wind load	1.0	0.40	

Table 2.8 Statistical properties of random variables in pylon system

Each of the two symmetric pylon arms is composed of one main body, 13 stiffeners, and 23 diaphragms. Based on findings from preliminary FE reliability analyses, a single random variable is assigned to represent the uncertainty of Young's modulus or yield strength for the whole set of diaphragms or stiffeners in each arm. This leads to 12 random variables representing Young's moduli and yield strengths of two main bodies, two groups of diaphragms, and two groups of stiffeners. To describe uncertainty in the load intensities, random load scale factors are introduced. Two random scale factors for dead load (self-weight and pre-stress), one for live load, and four for wind loads (in-plane and out-of-plane directions for W and WL load cases) are assigned. Figure 2.9 shows these load components that appear in the four types of loads that are considered. In this example, all the random variables are assumed to be statistically independent except for the following cases: First, it is assumed that all parts (i.e. bodies, stiffeners, and diaphragms) are made of the same steel from the same manufacturer, and thus they are highly correlated. The correlation coefficient between Young's moduli of different parts is assumed to

be 0.9. The same assumption is made for yield strengths of different parts. For the four load scale factors related to wind loads, i.e. W (in-plane), W (out-of-plane), WL (in-plane) and WL (out-of-plane), the correlation coefficients for the pairs of loads are assumed as follows:

(1) {W (in-plane), W (out-of-plane)} and {WL (in-plane), WL (out-of-plane)} : 0.8

(2) {W (in-plane), WL (in-plane)} and {W (out-of-plane), WL (out-of-plane)}: 0.6

(3) {W (in-plane), WL (out-of-plane)} and {W (out-of-plane), WL (in-plane)}: 0.48

Like the previous wing box example, it is assumed that the material used in the pylon structure shows linear elastic behavior until it reaches the yielding stress limit. For simplicity, this example also considers the yielding failures only. A component failure event, which can be defined for each combination of a selected physical component and a load case, is described as Eq. (2.9).

2.4.2. Analysis results

As done in the wing box problem, for efficient system reliability analysis, significant component events are identified as follows. By deterministic FE simulations using the mean values of the random variables, the locations with local maximum Von-Mises stresses, i.e. “hot spots” are first identified. Filtering hot spots with insignificant levels of stresses, component failure events are defined at two hot spots for each arm. Considering two symmetric arms and two load cases, i.e. LC1 and LC2, a total of eight component failure events E_i, $i = 1,\ldots,8$ are identified. See Table 2.9 for the identified component events and the failure probabilities computed by component reliability analyses.

Component events	Failure probability ($\times 10^{-3}$)
E_1 (LC1; hot spot on right body)	3.4342
E_2 (LC1; hot spot on left body)	3.4189
E_3 (LC1; hot spot on right stiffener)	0.1332
E_4 (LC1; hot spot on left stiffener)	0.1340
E_5 (LC2; hot spot on right body)	5.4255
E_6 (LC2; hot spot on left body)	5.4079
E_7 (LC2; hot spot on right stiffener)	0.2910
E_8 (LC2; hot spot on left stiffener)	0.2925

Table 2.9 Probabilities of component failure events by FORM analysis

After FORM analysis by use of FEUM-ABAQUS, the components are described by standard normal random variables and reliability indexes, i.e. $Z_i \le -\beta_i$, i = 1,…,8. The components E_3 and E_4 are neglected during the system reliability analysis because they are less than 5% of the probability of the most dominant component E_5. Using FORM, the sensitivities of the component event probabilities with respect to distribution parameters are also calculated. These component-level sensitivities in Eqs. (2.4a) and (2.4b) are used in calculating the sensitivities of the system failure probability in Eqs. (2.8a) and (2.8b) by use of the MSR method. In order to determine the statistical dependence between component events, the correlation coefficient matrix of Z_1, Z_2, Z_5, Z_6, Z_7 and Z_8 is constructed as given in Table 2.10.

Correlation	Z_1	Z_2	Z_5	Z_6	Z_7	Z_8
Z_1	1	0.9887	0.6129	0.6040	0.6032	0.6032
Z_2		1	0.6040	0.6129	0.6032	0.6032
Z_5			1	0.9929	0.9826	0.9826
Z_6				1	0.9826	0.9826
Z_7		Symmetric			1	0.9906
Z_8						1

Table 2.10 Correlation coefficient matrix of six component failure events

First, a series system event consisting of the six components is considered. The system failure probability is computed as 9.492×10^{-3}. Comparison with the MCS result (10^9 samplings, c.o.v. 3.25×10^{-4}), 9.404×10^{-3}, the MSR method turns out to provide a sufficiently accurate estimate. In addition, the event that at least one yielding failure occurs by the load combination 2 (LC2) while no failure occurs by LC1 is expressed as

$$E_{sys} = \overline{E}_1 \cap \overline{E}_2 \cap (E_5 \cup E_6 \cup E_7 \cup E_8) \tag{2.13}$$

The probability of this general system event is calculated as 5.633×10^{-3}, which is also sufficiently accurate, revealed by comparing against the results from the MCS (10^9 samplings, c.o.v. 4.30×10^{-4}), 5.368×10^{-3}. Furthermore, Table 2.11 shows the sensitivity-based importance measures of the general system event in Eq. (2.13) estimated by the MSR method.

Random variables		$\delta_j = \frac{\partial P_{sys}}{\partial \mu_j}\sigma_j$	$\eta_j = \frac{\partial P_{sys}}{\partial \sigma_j}\sigma_j$
Young's modulus	Diaphragm (Left)	-2.558×10^{-22}	-1.175×10^{-27}
	Diaphragm (Right)	-6.335×10^{-8}	1.422×10^{-9}
	Body (Left)	-3.552×10^{-22}	-2.279×10^{-27}
	Body (Right)	7.887×10^{-6}	-1.753×10^{-6}
	Stiffener (Left)	-4.140×10^{-25}	-1.049×10^{-27}
	Stiffener (Right)	-7.817×10^{-6}	-8.985×10^{-7}
Load scale factor	Dead load (Self weight)	2.709×10^{-4}	6.530×10^{-6}
	Dead load (Pre-stress)	6.319×10^{-4}	3.603×10^{-5}
	Live load	2.596×10^{-3}	1.919×10^{-3}
	In-service wind load (In-plane)	7.690×10^{-3}	1.812×10^{-2}
	In-service wind load (Out-of-plane)	1.452×10^{-3}	2.940×10^{-3}
	Out-of-service wind load (In-plane)	1.372×10^{-2}	3.279×10^{-2}
	Out-of-service wind load (Out-of-plane)	2.450×10^{-3}	5.235×10^{-3}
Yield strength	Body (Left)	-3.322×10^{-3}	3.009×10^{-3}
	Stiffener (Left)	-4.495×10^{-14}	8.093×10^{-5}
	Diaphragm (Left)	0	0
	Body (Right)	-3.710×10^{-3}	2.964×10^{-3}
	Stiffener (Right)	-2.333×10^{-14}	8.170×10^{-5}
	Diaphragm (Right)	0	0

Table 2.11 Sensitivity-based importance measures of the means and standard deviations of the random variables relative to series system probability

2.5. Summary

In summary, a new framework for finite element system reliability analysis (FE-SRA) was proposed using the matrix-based system reliability (MSR) method, and an interface code, FERUM-ABAQUS, was developed as a computational platform of the system reliability analysis. In the framework, the reliability analysis package FERUM repeatedly calls ABAQUS® to obtain structural responses during a component reliability analysis, and a system reliability analysis is performed by use of the results of the individual reliability analyses in the component level. The proposed framework allows us to compute the probabilities of general system events and their sensitivities with respect to design parameters based on the results of the component-level FE reliability analyses. These sensitivities are often useful; for example, they facilitate using gradient-based optimizer for reliability-based design optimization (Nguyen *et al*. 2010b) and reliability-based topology optimization (Nguyen *et al*. 2010a, 2011). Also, FERUM-ABAQUS is a more versatile computing platform than other existing FE-RA software. By employing ABAQUS® which is specialized in FE analysis, FERUM can perform reliability analysis most accurately based on sophisticated FE analysis. Finally, the proposed framework and FERUM-ABAQUS were successfully demonstrated through numerical examples of an aircraft wing torque box and a bridge pylon.

3. SYSTEM RELIABILITY ANALYSIS OF FATIGUE-INDUCED SEQUENTIAL FAILURES BY BRANCH-AND-BOUND METHOD EMPLOYING SYSTEM RELIABILITY BOUNDS

The development of an FE-SRA framework and interface code FERUM-ABQUS in Chapter 2 enables us to perform reliability analysis for complex system failure event in conjunction with sophisticated FE simulations. As discussed in Chapter 1, reliability analysis of sequential failures additionally requires a method to perform selective search schemes using event-trees of potential failure sequences. This chapter introduces a new branch-and-bound method to perform system reliability analysis of fatigue-induced sequential failures accurately and efficiently.

3.1. Literature Review

A variety of structural systems are often subjected to the risk of sequential failures caused by fatigue (Byers *et al*. 1997, Karamchandani *et al*. 1992). These structural systems should be designed to have an sufficient structural redundancy so that local fatigue-induced failures do not progress toward exceedingly large damage such as system collapse. For example, it was reported that the capsizing of the drill platform "Alexander L. Kielland" in 1981 was initiated by a brace failure caused by a fatigue crack starting from a hydrophone support. The initial brace failure was followed by failures of other braces and eventually system collapse (Almar-Naess 1985, Moan 2005). Thus, in risk-informed decision-making on design, maintenance and retrofit for robust structural systems, it is essential to quantify the risk of fatigue-induced sequential failures and identify critical sequences of local failures.

A challenge in such reliability analysis is that the definition of system-level failure is not determined a priori, but identified through structural analyses while following an event-tree of potential sequences of failures. For a complex structural system, one might need to explore a large number of local failure sequences to obtain an accurate definition of the system failure. Moreover, quantifying the likelihood of each failure sequence requires component and system reliability analyses in conjunction with structural analyses in order to account for the effect of the load re-distributions and various uncertainties. Therefore, system reliability analysis of sequential fatigue-induced failures may require overwhelming computational cost.

There have been several methodologies for performing system reliability analysis of sequential failures. Monte Carlo simulation (i.e. repeating computational simulations for many scenarios based on randomly-generated values of uncertain parameters) is the most straightforward and widely-used method (Ditlevsen and Bjerager 1989, Melchers 1994, Hu *et al*. 1998); however, when structural analysis demands time-consuming computational simulations or the failure probabilities are low, the computational and time costs required for converged results can be exceedingly large. Therefore, researchers have developed various non-sampling-based methods such as incremental load method (Moses 1982), truncated enumeration method (Melchers and Tang 1984), β-unzipping method (Thoft-Christensen and Murotsu 1986), and a method based on component importance factors (Gharaibeh *et al*. 2002). These methods perform selective search schemes using event-trees mostly based on the relative likelihoods of potential failure sequences. One of the most widely-used searching approaches is the so-called branch-and-bound method (Murotsu 1984, Guenard 1984) that was introduced to identify critical sequences with significant likelihood in an efficient manner. Although many research efforts have been made to develop risk analysis methods based on the branch-and-bound approach

(Karsan and Kumar 1988, Karamchandani *et al*. 1992, Wang *et al*. 2006), these methods are still either time-consuming or prone to miss critical failure sequences. In addition, the methods may underestimate the risk due to heuristic rules or assumptions that were introduced to enhance their efficiency.

According to Karamchandani *et al*. (1992), three techniques are commonly used to identify critical failure sequences: (1) deterministic search; (2) locally most-likely-to-fail-based search; and (3) branch-and-bound algorithm. First, the deterministic search approach (Thoft-Christensen and Murotsu 1986, Gharaibeh *et al*. 2002) performs a deterministic structural analysis using the mean values of the random variables to identify a sequence of failures leading to structure collapse. To get additional sequences, one can modify the values of some variables and repeat the deterministic analysis. For example, one can strengthen sections or members (termed the "members" hereafter) that were involved in the identified sequence to search for additional failure sequences. However, this deterministic approach is prone to missing critical failure sequences because the sequences identified by this approach may not have the highest likelihood.

The locally most-likely-to-fail-based search is a probabilistic extension of the deterministic search. The first step is to identify the member that is most likely to fail in the intact structure. A new structural analysis model is constructed to reflect the damage or failure of the identified member. Through component reliability analysis using the model, the most-likely-to-fail member under the damage scenario is identified. This process is repeated until a system failure such as collapse is observed. This method can identify additional sequences by modifying some random variables, e.g., increasing the mean strength of a member that is involved in identified sequences. However, the sequences identified by this local search approach may not be

the most critical ones overall. For example, there may exists a member whose failure probability is lower than that of the most-likely-to-fail member, but the conditional probability of structure collapse given its failure can be fairly high. This important sequence may not be identified by the locally most-likely-to-fail-based search because it focuses only on the most-likely-to-fail members at each step.

The branch-and-bound method (Murotsu 1984, Guenard 1984) is considered more accurate than the aforementioned methods. To identify system failure sequences that are "globally" most likely to occur, the method compares the probabilities of all the failure sequences that have been investigated during the search process and assumes further damage for the most likely sequence to continue the search. When the system failure of interest such as structural collapse is observed, the particular sequence is identified as a "system failure sequence." Unless heuristic rules are introduced to truncate apparently insignificant sequences, the branch-and-bound method can identify system failure sequences in the decreasing order of their likelihood. This enables us to terminate the search process without ignoring significant system failure sequences.

Although this selective search approach based on the probabilities of sequences helps reduce the number of sequences to explore, one still might need to explore a large number of sequences to obtain a reliable estimate on the structural system risk. This is due to the lack of reasonable criteria that would help terminate the search without underestimating the system-risk. The structural system failure event is often described as the union of the identified system failure sequences. During a search process, one can obtain a lower bound on the system failure probability by a system reliability analysis employing the identified failure sequences, which can be continuously updated as new failure sequences are identified. While the upper bound is

usually unknown, the trend of the lower bound updates alone cannot provide accurate termination criteria because the size of the updates on the lower bound caused by newly identified system failure sequences does not decrease monotonically due to the statistical dependence between identified failure sequences. This is the case even if the likelihood of identified sequences decreases monotonically. Therefore, a termination based on apparent convergence of the lower-bound may lead to underestimating the system risk. Moreover, one needs to perform a new system reliability analysis each time the lower-bound is updated.

3.2. Branch-and-Bound Method Employing System Reliability Bounds (B^3 method)

A new branch-and-bound method employing system reliability bounds (termed the B^3 method) is proposed to overcome the aforementioned challenges and to improve the efficiency and accuracy of risk analysis of a system with sequential failures. The search process of the B^3 method identifies *disjoint* failure sequences in order to (1) obtain both the lower and upper bounds of the system failure probability; (2) achieve monotonic decrease in the size of identified failure sequences as the search process proceeds; and (3) update the bounds of the system risk without performing additional system reliability analyses. The development of the B^3 method is two-folds: (1) formulating limit state functions for disjoint failure sequences that can account for the interdependence between multiple crack growths through stress re-distributions; and (2) developing a branch-and-bound search scheme to systematically update the bounds on the system failure probability with reasonable termination criteria.

3.2.1. Limit-state function formulations for disjoint failure sequences

First, let us consider the following crack-growth model, which is often termed the Paris equation (Paris and Erdogan 1963):

$$\frac{da}{dN} = C(\Delta K)^m \tag{3.1}$$

where a denotes the crack length, N is the number of load cycles, C and m are the material parameters, and ΔK denotes the range of the stress intensity factor. When considering cyclic *zero-to-tension* loading with constant amplitude, the range of stress intensity factor can be estimated by Newman's approximation (Newman and Raju 1981) as follows:

$$\Delta K = S \cdot Y(a) \cdot \sqrt{\pi a} \tag{3.2}$$

where S denotes the far-field stress "range" and $Y(a)$ is the "geometry" function. Other mathematical formulas such as the Walker equation (Walker 1970) and the Forman equation (Forman *et al*. 1967) can also be introduced to represent more general loading conditions. However, it is beyond the scope of this research, so the Paris equation in Eq. (3.2) is used for the following derivation. When substituting Eq. (3.2) into Eq. (3.1), one can obtain

$$\frac{1}{\left[Y(a)\sqrt{\pi a}\right]^m} da = C \cdot S^m dN \tag{3.3}$$

By integrating Eq. (3.3) from the initial condition to the current time point, the relationship between the time duration and the current crack length is derived as

$$\int_{a^0}^{a} \frac{1}{\left[Y(a)\sqrt{\pi a}\right]^m} da = C \cdot N \cdot S^m = C \cdot \nu_0 \cdot T \cdot S^m \tag{3.4}$$

where a^0 is the initial crack length, N is the total number of external loading applications with frequency ν_0, and T denotes the time duration. Suppose a crack failure is defined as the event that

the length of a crack exceeds the critical crack length a_i^c. In reality, it is a challenging issue to define the critical crack length, and one of the usual ways is to use the crack size measured when the stress intensity factor (K) reaches the fracture toughness (K_C). Then, for a structure consisting of n structural members, the time required for the crack growth from a_i^0 to a_i^c at the i-th member ($i = 1, \ldots, n$), T_i^0 is described as

$$T_i^0 = \frac{1}{C\nu_0 \left(S_i^0\right)^m} \int_{a_i^0}^{a_i^c} \frac{1}{\left[Y(a)\sqrt{\pi a}\right]^m} da \le T_s \tag{3.5}$$

where a_i^0 and S_i^0 are the initial crack length and far-field stress range of the i-th member, respectively. The superscripts "0" in T_i^0 and S_i^0 indicate that the structure has no preceding crack failures. Then, the limit-state function for the failure of the i-th member within an inspection cycle $[0, T_s]$ is given as

$$g_i(\mathbf{X}) = T_i^0 - T_s = \frac{1}{C\nu_0 \left(S_i^0\right)^m} \int_{a_i^0}^{a_i^c} \frac{1}{\left[Y(a)\sqrt{\pi a}\right]^m} da - T_s \tag{3.6}$$

where $\mathbf{X}$ denotes the vector of random variables representing uncertainties in the parameters of the problem such as material properties (C, m) and initial crack length (a_i^0). In structural reliability analysis, "$g_i(\mathbf{X}) \le 0$" generally indicates the occurrence of a failure event.

In order to identify the failure sequences as *disjoint* events (i.e. failure sequences that are mutually exclusive to each other) during the branch-and-bound search, let us first consider a scenario in which the i-th member fails before failures occur at any other members. This means that the time required to reach the critical crack length of the i-th member should be shorter than

those of the other members as well as the inspection cycle T_s. The probability of this scenario event is thus described as

$$P_i = P\left\{\left[\bigcap_{\forall l \neq i}\left(T_i^0 < T_l^0\right)\right] \cap \left(T_i^0 < T_s\right)\right\} \tag{3.7}$$

The event in Eq. (3.7) is a parallel system event consisting of n component events. The probability can be computed by a system reliability analysis employing the results by component reliability analyses of n individual events. Many existing methodologies mentioned in Section 2.2.2 are applicable to solve the parallel-system reliability problem.

Next, the probability that the j-th member fails following the failure of the i-th member is described as

$$P_j^i = P\left\{\left[\bigcap_{\forall l \neq i}\left(T_i^0 < T_l^0\right)\right] \cap \left(T_i^0 < T_s\right) \cap \left[\bigcap_{\forall m \neq i,j}\left(T_j^i < T_m^i\right)\right] \cap \left(T_i^0 + T_j^i < T_s\right)\right\} \tag{3.8}$$

where T_j^i denotes the inter-failure time required for the crack failure at the j-th member since the failure at the i-th. Since T_i^0 is always smaller than (T_i^0+ T_j^i), the second term in Eq. (3.8) can be eliminated, i.e.

$$P_j^i = P\left\{\left[\bigcap_{\forall l \neq i}\left(T_i^0 < T_l\right)\right] \cap \left[\bigcap_{\forall m \neq i,j}\left(T_j^i < T_m^i\right)\right] \cap \left(T_i^0 + T_j^i < T_s\right)\right\} \tag{3.9}$$

This can be generalized to failure sequences involving more than two member failures. For example, the probability of the progressive failure of the sequence $\{1 \rightarrow 2 \rightarrow \ldots \rightarrow (i-1) \rightarrow i\}$ is described as

$$P_i^{1,\ldots,(i-1)} = P\left\{\left[\bigcap_{\forall j\neq 1}\left(T_1^0 < T_j^0\right)\right]\bigcap\left[\bigcap_{\forall k\neq 1,2}\left(T_2^1 < T_k^1\right)\right]\bigcap\cdots\bigcap \left[\bigcap_{\forall l\neq 1,\ldots,i}\left(T_i^{1,\ldots,(i-1)} < T_l^{1,\ldots,(i-1)}\right)\right]\bigcap\left(T_1^0 + T_2^1 + \cdots + T_i^{1,\ldots,(i-1)} < T_s\right)\right. \tag{3.10}$$

where $T_i^{1,\ldots,(i\text{-}1)}$ denotes the time required for the failure at the i-th member since the sequential failure $\{1\rightarrow 2\rightarrow\ldots\rightarrow(i-1)\}$.

Unlike T_i^0 in Eq. (3.5), i.e. the time until the first local failure for an undamaged structure, the inter-failure time terms for damaged structures (such as $T_i^{1,\ldots,(i\text{-}1)}$ in Eq. (3.10)) should be computed with the effects of load re-distributions considered. For convenient derivation of such time terms in terms of random variables, a recursive formulation is developed as follows. Consider an auxiliary "damage" function

$$\Psi(a) = \int_{a^0}^{a} \frac{1}{\left[Y(a)\sqrt{\pi a}\right]^m} da \tag{3.11}$$

For example, let us consider the failure sequence $\{1\rightarrow 2\}$. From Eq. (3.4), it is seen that

$$\Psi(a_2^1) - \Psi(a_2^0) = C\cdot \nu_0 \cdot T_1^0 \cdot (S_2^0)^m \tag{3.12a}$$

$$\Psi(a_2^c) - \Psi(a_2^1) = C\cdot \nu_0 \cdot T_2^1 \cdot (S_2^1)^m \tag{3.12b}$$

where a_2^1 denotes the crack length at the member 2 at the moment the crack failure occurs at the member 1. Eqs. (3.12a) and (3.12b) respectively represent the growth of the crack at the member 2 before and after the crack failure occurs at the member 1. Summing up Eqs. (3.12a) and (3.12b), one obtains

$$\Psi(a_2^c) - \Psi(a_2^0) = C\nu_0 T_2^1 (S_2^1)^m + C\nu_0 T_1^0 (S_2^0)^m \tag{3.13}$$

Solving Eq. (3.13) for T_2^1,

$$\begin{aligned} T_2^1 &= \frac{1}{C\nu_0 (S_2^1)^m}\left[\Psi(a_2^c) - \Psi(a_2^0)\right] - \left(\frac{S_2^0}{S_2^1}\right)^m T_1^0 \\ &= \frac{1}{C\nu_0 (S_2^1)^m}\int_{a_2^0}^{a_2^c} \frac{da}{\left[Y(a)\sqrt{\pi a}\right]^m} - \left(\frac{S_2^0}{S_2^1}\right)^m T_1^0 \end{aligned} \tag{3.14}$$

It is noteworthy that the ratio of the far-field stress of the intact condition to that of the damaged state, S_2^0/S_2^1, incorporates the effect of the load re-distribution caused by the failure at member 1. Similarly, the time required for the crack failure at member 3 since the sequential failures {1→2} is derived as

$$T_3^{1,2} = \frac{1}{C\nu_0 (S_3^{1,2})^m}\int_{a_3^0}^{a_3^c} \frac{da}{\left[Y(a)\sqrt{\pi a}\right]^m} - \left(\frac{S_3^0}{S_3^{1,2}}\right)^m T_1^0 - \left(\frac{S_3^1}{S_3^{1,2}}\right)^m T_2^1 \tag{3.15}$$

Through mathematical induction, a recursive formulation is derived for a general failure sequence {1→2→… → $(i-1)$→ i} as follows:

$$T_i^{1,\ldots,i-1} = \frac{1}{C\nu_o (S_i^{1,\ldots,i-1})^m}\int_{a_i^0}^{a_i^c} \frac{da}{\left[Y\sqrt{\pi a}\right]^m} - \sum_{k=1}^{i-1}\left(\frac{S_i^{1,\ldots,k-1}}{S_i^{1,\ldots,k-1}}\right)^m T_k^{1,\ldots,k-1} \tag{3.16}$$

Using Eq. (3.16), the time terms in Eq. (3.10) can be described in terms of deterministic and random parameters for any failure sequence.

The system failure sequences identified by a search process based on the limit-state formulation in Eq. (3.10) are disjoint (or mutually exclusive to each other) because of the events describing the order of the failure events, e.g., $\bigcap_{\forall l \neq i} (T_i^0 < T_l^0)$. Therefore, the system failure probability can be calculated by summing up the probabilities of the identified failure sequences without additional system reliability analysis to account for the statistical dependence between the sequences, i.e.

$$P(E_{sys}) = P\left(\bigcup_{i=1}^{N_{fs}} C_i\right) = \sum_{i=1}^{N_{fs}} P(C_i) \tag{3.17}$$

where C_i (i=1,…,N_{fs}) denotes the identified system failure sequences and N_{fs} denotes the total number of the identified failure sequences. The probability of a system failure sequence, $P(C_i)$, is obtained by a system reliability analysis using Eq. (3.10). This disjoint-event-based formulation enables the aforementioned merits of the B^3 method. Although the formulation was derived based on the Paris equation and Newman's approximation, this framework can be applied to other analytical crack-growth models based on far-field stress, if necessary.

3.2.2. Systematic search scheme of the B^3 method

The proposed B^3 method uses a systematic search scheme that employs the aforementioned disjoint cut-set formulation and recursive limit-state functions. The search process is explained in detail as follows using an example in Figure 3.1.

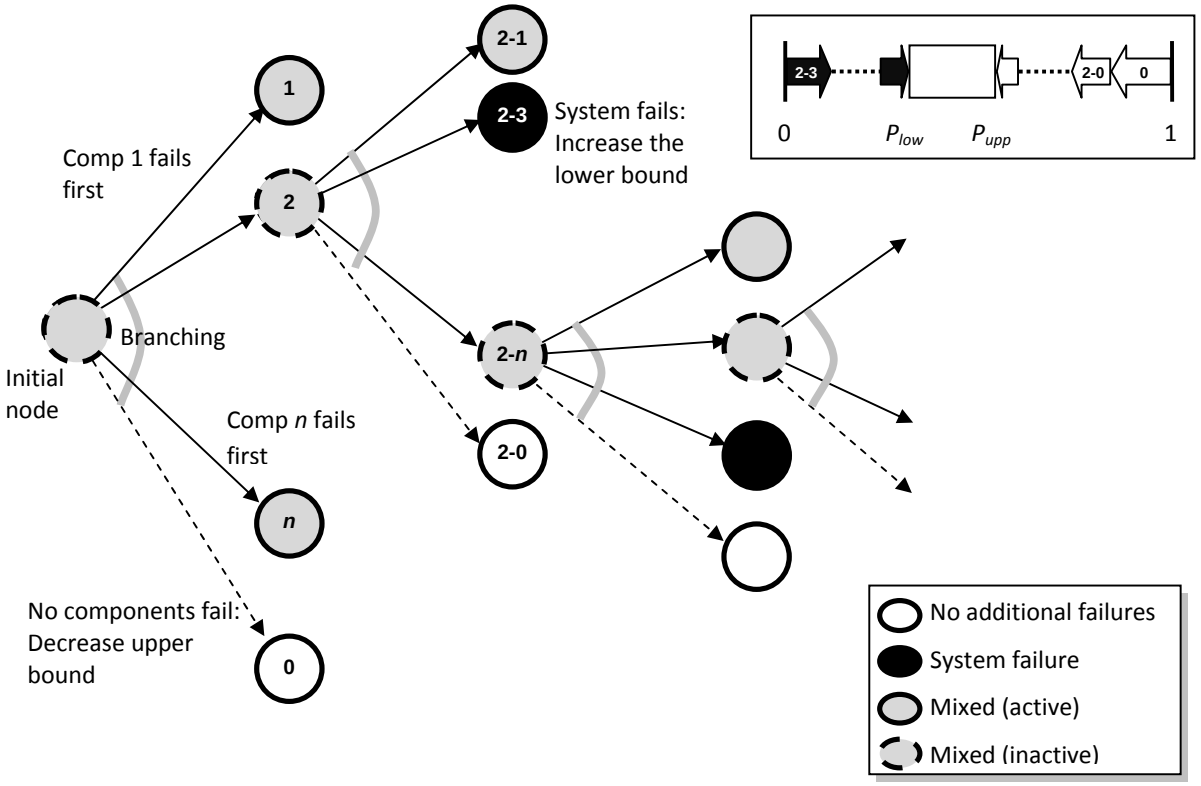

Figure 3.1 Search procedure by B^3 method

First, the lower and upper bounds of the system failure probability (denoted by P_{low} and P_{upp}) are set to be zero and one, respectively. These bounds are continuously updated as the search process identifies cases of system failures and non-failures and computes their probabilities. The search process starts with a node that contains all of the possible scenarios ("initial node", shown at the far left in the figure). This is considered one of the "mixed" nodes, which are given as gray nodes in Figure 3.1. Mixed nodes contain both system failure and non-failure cases. The stress distribution of the intact structure is obtained by a structural analysis.

Next, a "branching" process is performed to find the probabilities of individual member failures from the current structural condition, i.e. P_i in Eq. (3.7). If the structural condition

represented by a current node has n structural members (or locations) of potential crack failures, this branching process transfers the probability in the current "parent" node to the (n+1) "child" nodes as shown in the second column of the nodes in Figure 3.1. As a result, the current "parent" node becomes "inactive," i.e. stops contributing to the system probability calculations. Each of the first n child nodes, i.e. "1" through "n" in the figure, contains the probability that the corresponding member fails "first" (i.e. earlier than the others) during the given inspection cycle T_s. These are new "mixed" nodes and their probabilities are computed by system reliability analysis using Eq. (3.7). By contrast, the last "white" node, i.e. "0" in the figure, indicates the case that no further failure occurs during the inspection cycle. Since these (n+1) child nodes are mutually exclusive (or disjoint) and collectively exhaustive (MECE) events given the condition of their parent node, the probability of the white node is computed by the probability of the parent node minus the sum of the probabilities of all the other child nodes branching out from the parent node. The upper bound is now decreased by the probability of the white node. This is the "bounding" process to update the upper bound of the system failure probability.

The next step is to compare all the active mixed nodes and find the one with the highest probability. Then, a new structural analysis is performed using a structural model representing the damage scenario of the active mixed node with the highest probability. If the structural analysis reveals that the selected node represents a system failure case ("black" nodes in Figure 3.1), P_{low} is increased by the probability of the node, which is understood from Eq. (3.17). It is noted that the probability of the node has been already computed during the previous branching process. This is another "bounding" process to update the lower bound of the system failure probability. On the other hand, if the node with the highest probability does not represent a

system failure case, the aforementioned branching process is performed for the node to find the probabilities of the child nodes originating from the node.

For the example in Figure 3.1, suppose the node "2", i.e. the structure with member "2" damaged, has a higher probability than the other active mixed nodes and the structural analysis on the damage condition does not indicate a system failure. Then, a branching process is performed to find the probabilities of the sequences {2→1}, {2→3}, …, and {2→*n*} by system reliability analysis using Eq. (3.9). After the branching process, the upper bound is decreased by the probability of "2-0." Now, the probabilities of all the remaining active nodes "1", "3", …, "*n*", "2-1", "2-3", …, and "2-*n*" are compared. Suppose the node "2-3" has the highest probability and a structural analysis with members 2 and 3 failed identifies a system failure event. The node becomes a system failure ("black") node, and the lower bound of the system failure probability is increased by the probability of the current node, "2-3." Then, the next most likely active node (e.g., "2-*n*" in Figure 3.1) is selected to perform another structural analysis.

This iterative process of "branching" and "bounding" continues until the following termination criteria are satisfied. If finding the most critical paths is the main interest, one can stop the search process when the most recently identified system failure sequence has a probability lower than a given threshold, or when a desirable number of system failure sequences are identified. This is possible because the B^3 method guarantees finding the failure sequences in the decreasing order of their probabilities. On the other hand, if estimating the system failure probability is of interest, the process can be terminated when the width of the bounds is negligible compared to the overall risk level estimated from the bounds. The search procedure of the B^3 method is explained by a flow chart in Figure 3.2.

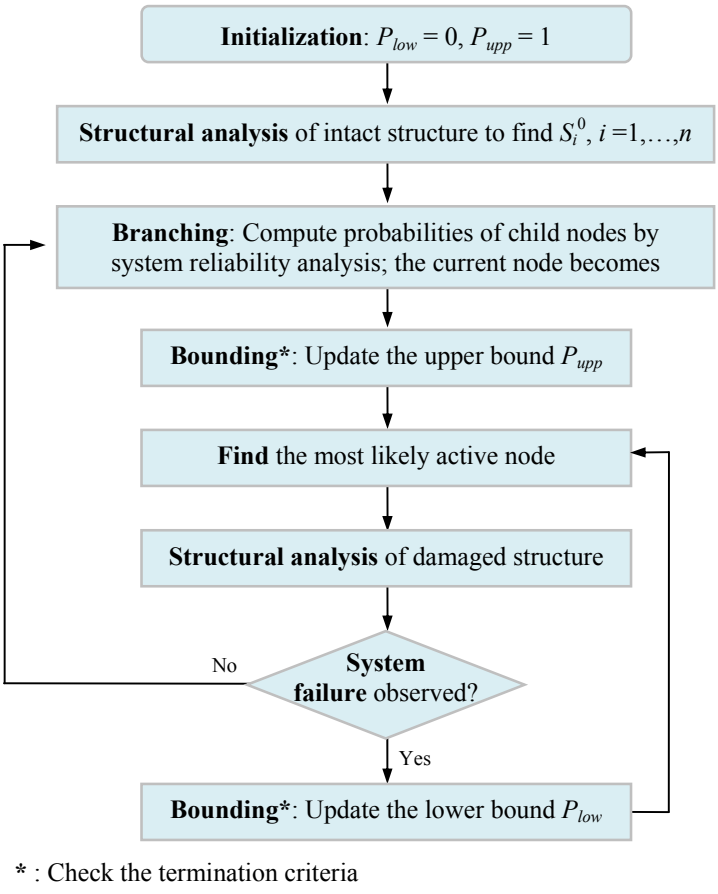

Figure 3.2 Flowchart of B^3 method search procedure

The B^3 method does not rely on an arbitrary definition of system failure such as "*x* number of member failures (at *y* location) constitute a system failure," (Karamchandani *et al*. 1992, Shabakhty *et al*. 2003), but identifies system failures during the search procedure with help of computational simulations. Unlike the deterministic search and locally most-likely-to-fail-based search methods, the B^3 method performs a global search and identifies critical paths in the decreasing order of their probabilities. This is because the proposed search scheme performs a new structural analysis for the most likely node among all active mixed nodes. Moreover, the

analytical search framework decreases the required number of structural analyses compared to Monte Carlo simulation approaches, especially for low-probability system risk.

The main difference between the B^3 method and existing branch-and-bound-based methods is that the proposed method describes a system event by use of mutually exclusive (or disjoint) failure modes. By contrast, when a branch-and-bound method uses a non-disjoint cut-set formulation, the probability of a failure sequence is computed without considering the likelihoods of specific orders. For example, the probability of a sequence $\{1\rightarrow 2\rightarrow \dots \rightarrow i-1\rightarrow i\}$ would be computed as

$$P_i^{1,\dots,i-1} = P\left\{\left(T_1^0 < T_s\right)\bigcap\left(T_1^0 + T_2^1 < T_s\right)\bigcap\cdots\bigcap\left(T_1^0 + T_2^1 + \cdots + T_i^{1,\dots,i-1} < T_s\right)\right\} \tag{3.18}$$

This is simplified as

$$P_i^{1,\dots,i-1} = P\left\{\left(T_1^0 + T_2^1 + \cdots + T_i^{1,\dots,i-1} < T_s\right)\right\} \tag{3.19}$$

Compared to the corresponding formulation of the B^3 method in Eq. (3.10), this probability is easier to obtain because one can compute this probability by a component reliability analysis rather than a system reliability analysis. However, the identified failure paths are non-disjoint and correlated, so the lower bound on the system failure probability should be computed by a system reliability analysis for the union of all identified failure paths, i.e.

$$P_{low} = P\left(\bigcup_{i=1}^{N_{id}} E_i\right) \tag{3.20}$$

where E_i is the occurrence of the i-th identified system failure sequence ($i = 1,\dots,N_{id}$) that appears in Eq. (3.19), and N_{id} is the total number of system failure modes identified by the

branch-and-bound search. By contrast, the B^3 method updates the lower bound just by adding the probability of newly identified system failure sequences to the current bound. Moreover, the B^3 method can provide the upper bound as well, which helps provide reasonable termination criteria for the search process.

In the existing methods, even though a branch-and-bound method can identify critical failure sequences in a decreasing order of their probabilities (unless heuristic or problem-dependent truncation rules are introduced), the increments of the bounds caused by newly identified system failure sequences are not decreasing monotonically. This is due to the statistical dependence between the failure sequences. However, in the B^3 method, the increments of the lower bound are the same as the probabilities of the identified system failure cases, which are found in the decreasing order. Therefore, the increments on lower bound are diminishing monotonically, which helps avoid continuing the search process unnecessarily.

To achieve the aforementioned merits of the disjoint-cut-set formulation, the B^3 method needs to perform more component and system reliability analyses than conventional branch-and-bound methods. Considering the efficiency in the search process and accuracy in system failure probability calculations, this additional task is worthwhile especially when the computational cost of the structural or finite element analysis is dominant. The component reliability analysis method used in the B^3 method should be able to identify the statistical dependence between the component events such that a system reliability analysis can be later performed with the dependence fully considered. The system reliability analysis method should be able to compute the probability of parallel systems accurately. In particular, the method should be able to handle parallel systems with a large number of component events because the number of component events quickly increases as the search process goes on. In this research, The First-Order

Reliability Method (FORM) and the Second-order Reliability Method (SORM) are employed. Both of them are widely-used component reliability analysis methods that can describe the dependence between component events using the normalized gradient vectors at the most probable failure points. A comprehensive review on these methods can be found in Der Kiureghian (2005). For the system reliability analysis, we use the multivariate normal integral method by Genz (1992) that can provide accurate estimation on the probabilities of large-size parallel systems using quasi-random integration points.

3.3. Illustrative Example: Multi-layer Daniels System

Daniels (1945) investigated the reliability of a bundle of ideally brittle wires that had identical and deterministic elastic moduli subjected to a deterministic load. In the example, wire strengths were assumed to be uncertain and statistically independent. It was also assumed that the deterministic load was equally distributed among the remaining wires. The system fails when all the members/wires fail. Based on these assumptions, the exact failure probability of the structural system was derived. This "Daniels system" is often used as a numerical example in developing and testing new system reliability analysis methods (Song and Der Kiureghian 2003, Straub and Der Kiureghian 2007, Kang *et al*. 2012, Gharaibeh *et al*. 2002, Lee and Song 2011a, b). The system failure event of a Daniels system is a complex system event because of the load re-distributions caused by member failures. In this chapter, the risk of fatigue-induced sequential failures of a multi-layer Daniels system (see Figure 3.3) is investigated to illustrate the proposed B^3 method. In this example, the system failure is defined as an event that all the wires in one of the three stories fail.

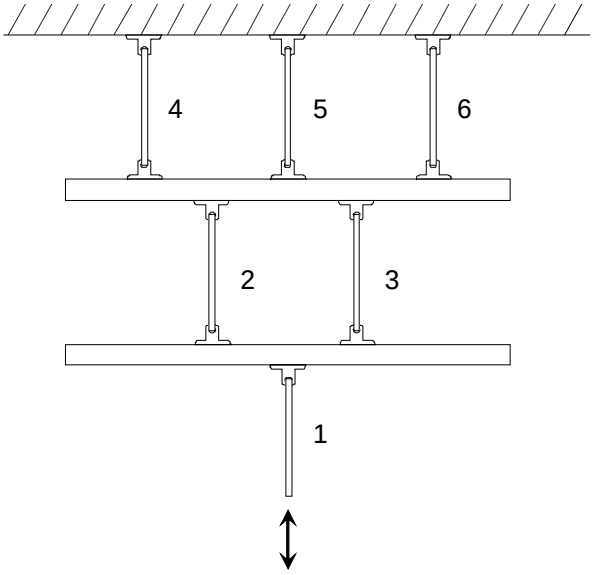

Figure 3.3 A multi-layer Daniels system

3.3.1. Problem description

As shown in Figure 3.3, the structure consists of six bars that are assumed to be perfectly brittle and to have identical, deterministic elastic moduli. The cross sectional areas of the bars are assumed to be A_1=0.03m^2, A_2=A_3=0.015m^2, and A_4=A_5=A_6=0.01mm^2. In this example, the uncertainties of C in Paris equation, initial crack length a_i^0, and external load are described by random variables with the mean values 1.202×10^{-13} (mm/cycle/(MPa·mm)^m), 0.11 (mm) and 1,200 (kN), respectively. For the sake of simplicity, all of the random variables are assumed to follow lognormal distribution with the coefficient of variation (c.o.v.) of 0.1 and to be statistically independent of each other. The following deterministic parameters are used: the loading frequency (v_0): 500,000 (cycle/year), the inspection cycle (T_s): 4 years, m=3, $Y(a)$=3, and the critical crack lengths: a_1^c=30mm, a_2^c=a_3^c=15mm, and a_4^c= a_5^c= a_6^c=10mm. Assuming the

load is equally distributed over remaining bars on each story, the stress in each bar is calculated by dividing the external load 1,200 (kN) by the sum of the cross sectional areas of the remaining bars. In this illustrative example for the B^3 method, these simple stress calculations constitute "structural analyses," which were aforementioned in describing the B^3 method. In applying the B^3 method to real-scale complex structural systems, the computational costs for structural analyses become dominant during the search process.

3.3.2. B^3 method application

As the first step, the lower bound P_{low} and upper bound P_{upp} values are initialized as 0 and 1, respectively. As shown in Figure 3.4, a branching is performed to compute the probability that the *i*-th member fails "first" in the intact structure during the inspection cycle [0, T_s] as in Eq. (3.7).

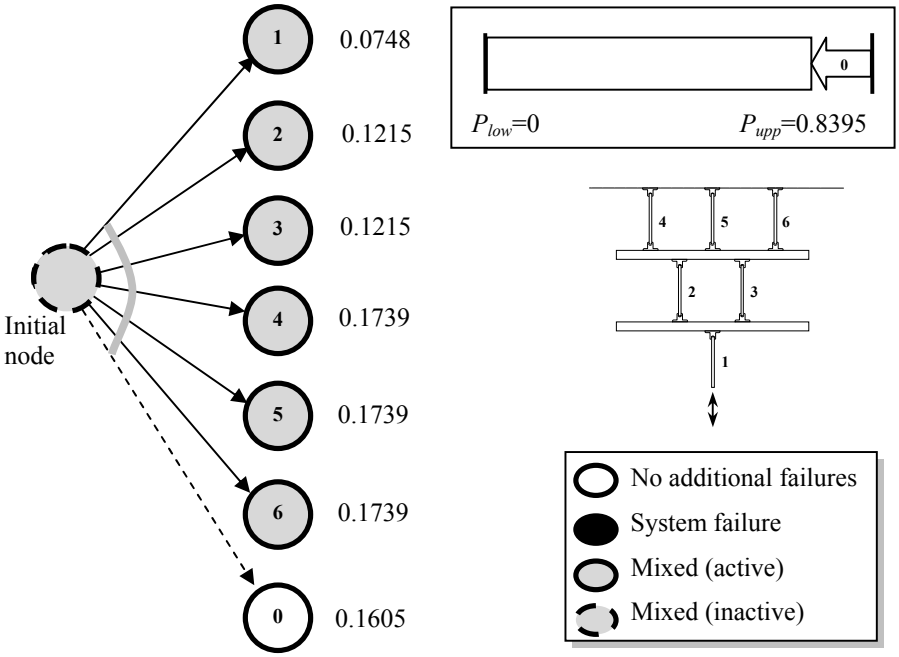

Figure 3.4 Results of the first branching

For example, the probability that the 6th member fails within the inspection cycle and earlier than the other members, i.e. the probability of the node "6" in Figure 3.4, is calculated by

$$P_6 = P\left\{\left[\bigcap_{\forall l \neq 6}\left(T_6^0 < T_l^0\right)\right] \cap \left(T_6^0 < T_s\right)\right\}, \text{ for } l = 1,...,5 \tag{3.21}$$

The component events in the parallel system in Eq. (3.22) are described as follows.

$$g_l(\mathbf{x}) = T_6^0 - T_l^0 = \frac{1}{C\nu_0\left(S_6^0\right)^m}\int_{a_6^0}^{a_6^c}\frac{1}{\left[Y(a)\sqrt{\pi a}\right]^m}da - \frac{1}{C\nu_0\left(S_l^0\right)^m}\int_{a_l^0}^{a_l^c}\frac{1}{\left[Y(a)\sqrt{\pi a}\right]^m}da \le 0 \tag{3.22a}$$

$$g_6(\mathbf{x}) = T_6^0 - T_s = \frac{1}{C\nu_0\left(S_6^0\right)^m}\int_{a_6^0}^{a_6^c}\frac{1}{\left[Y(a)\sqrt{\pi a}\right]^m}da - T_s \le 0 \tag{3.22b}$$

Preliminary analyses revealed that the nonlinearity of the limit-state functions in Eq. (3.22) may cause significant errors in component reliability analyses by FORM. Although SORM helps reduce the errors significantly, it is not desirable to use SORM for every component reliability analysis problem due to larger computational cost. Karamchandani *et al*. (1992) claimed the last component event in Eq. (3.21) (i.e. Eq. (3.22b)) governs the system probability and proposed to ignore the other components in evaluating the probability. To achieve reasonable accuracy without compromising computational efficiency, therefore, we employ FORM for all component events that do not involve T_s while we compute the probability of the last limit-state function, Eq. (3.22b), using SORM for accurate estimations. The results from this mixed approach will be presented and discussed in the following numerical examples through comparison with those by crude Monte Carlo simulations.

Next, using the first-order concept of system reliability (Hohenbichler and Rackwitz 1983), the probabilities of parallel systems such as the one in Eq. (3.21) are computed by evaluating a multi-variate normal integral. A parallel system with n component events is computed as follows.

$$P\left(\bigcap_{i=1}^{n} g_i(\mathbf{X}) \le 0\right) \cong \int_{\Omega} \varphi_n(\mathbf{z};\mathbf{R})\, d\mathbf{z} = \int_{\Omega} \frac{1}{(2\pi)^{n/2}\sqrt{\det \mathbf{R}}} \exp\left(-\frac{1}{2}\mathbf{z}^{\mathrm{T}}\mathbf{R}^{-1}\mathbf{z}\right) d\mathbf{z} \tag{3.23}$$

$$\text{where } \Omega = \left\{(z_1,...,z_n) \,|\, \bigcap_{i=1}^{n}(z_i \le -\beta_i)\right\}$$

where Ω is the domain of the parallel system event defined in the space of n standard normal random variables in $\mathbf{Z}$, $\varphi_n(\cdot)$ is the joint probability density function of $\mathbf{Z}$, $\mathbf{R}$ is the correlation

coefficient matrix of **Z**, and det **R** denotes the determinant of **R**. The component reliability indexes β_i, i=1,…,n are obtained by FORM and SORM. The correlation coefficient matrix **R** can be determined from the inner products of negative normalized gradient vectors (Der Kiureghian 2005) evaluated at the design points, which are again obtained by FORM. In this thesis, the multivariate normal integral method by Genz (1992) is used for evaluating these multi-variate normal integrals efficiently, even for the cases with a large number of component events. The MSR method is also applicable here. As previously stated, the B^3 method entails many parallel system analyses, which made the method by Genz optimal in the numerical examples in this paper.

Figure 3.4 shows the outcomes of the first branching, i.e. the probabilities of seven child nodes. Due to the given conditions and assumptions, the node numbers corresponding to the bars in the same layer show the same probabilities. The probability of the last white node is computed by the probability of the parent node (i.e. 1.0) minus the sum of the probabilities of the first six child nodes. The upper bound is decreased by this probability, i.e. P_{upp}=1−0.1605=0.8395. Now the probability of the initial node (i.e. 1.0) is transferred to its child nodes, which makes the initial node inactive. It is noted that only one structural analysis is required per branching regardless of the number of the child nodes.

For the second branching, the active mixed nodes with the highest probabilities are identified. In this example, nodes “4”, “5”, and “6” have the highest probability. Any of the nodes with the same probability can be selected for the next branching and this does not affect the final result. Suppose the node “6” is selected. The corresponding structural member (i.e. the bar “6”) is removed from the system. Since the structure still survives, a structural analysis is performed to find the stresses after the load re-distribution caused by the failure of the bar. The

second branching is performed based on the results of the structural analysis. The outcomes of this branching are shown in Figure 3.5.

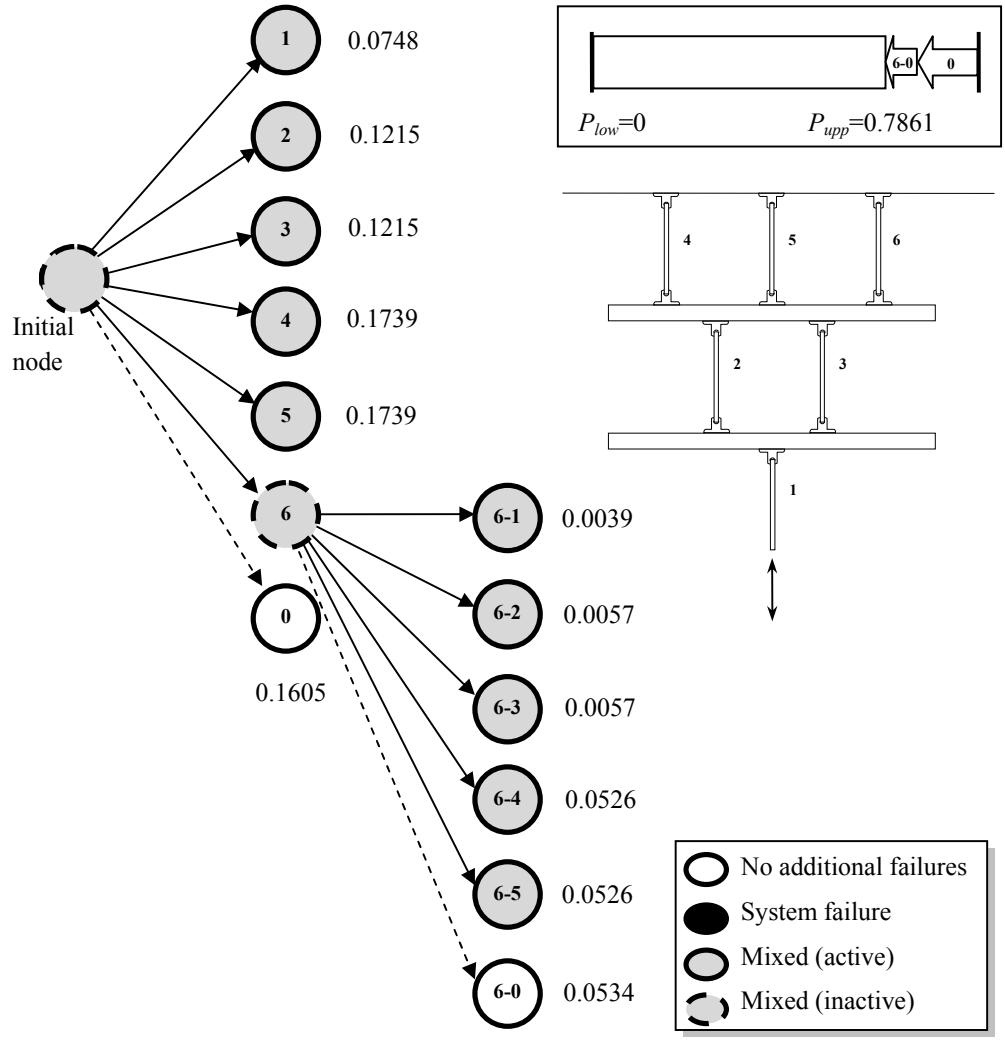

Figure 3.5 Results after the second branching

As a result of the second branching, node "6" becomes inactive, and the upper bound of system probability is further decreased by the probability of node "6-0." For the third branching, we need to find the active mixed node with the highest probability. With the local searching

technique discussed in Section 3.2, the next branching would start from node “6-4” or “6-5.” However, the branch-and-bound algorithm compares all active mixed nodes and chooses node “4” or “5” for the branching. After four more times of branching and four corresponding structural analyses, the event tree is expanded as shown in Figure 3.6.

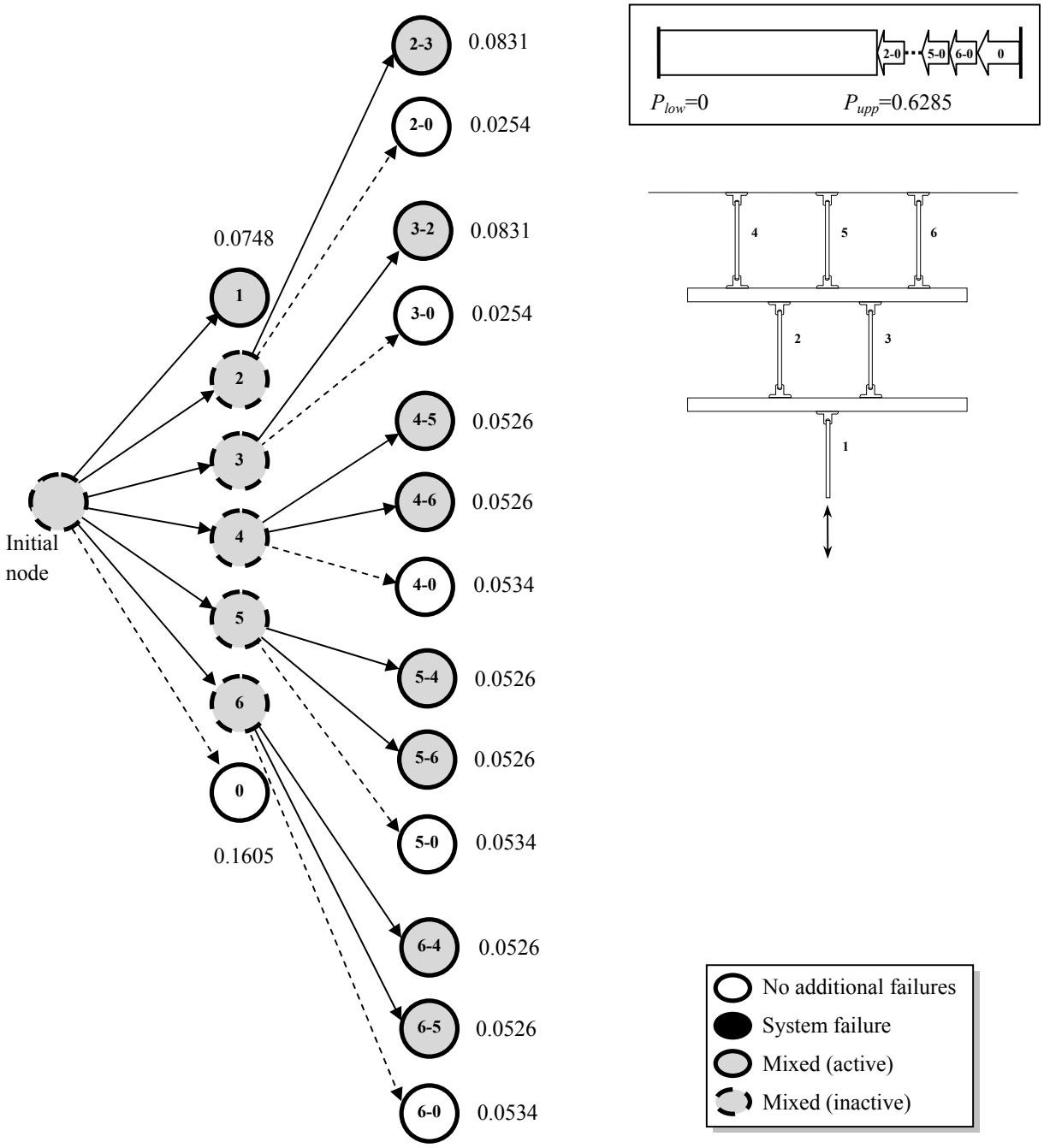

Figure 3.6 Results after six times of branching

In the figure, only some of the active mixed nodes with relatively higher probability are displayed. Nodes “2-3” and “3-2” have the highest probabilities, so the next branching starts from one of these nodes. Suppose node “2-3” is selected for the next branching. However, this case causes system failure because all the bars in the second layer are disconnected. Therefore, node “2-3” is identified as the system failure node and the lower bound is increased by its probability (see Figure 3.7).

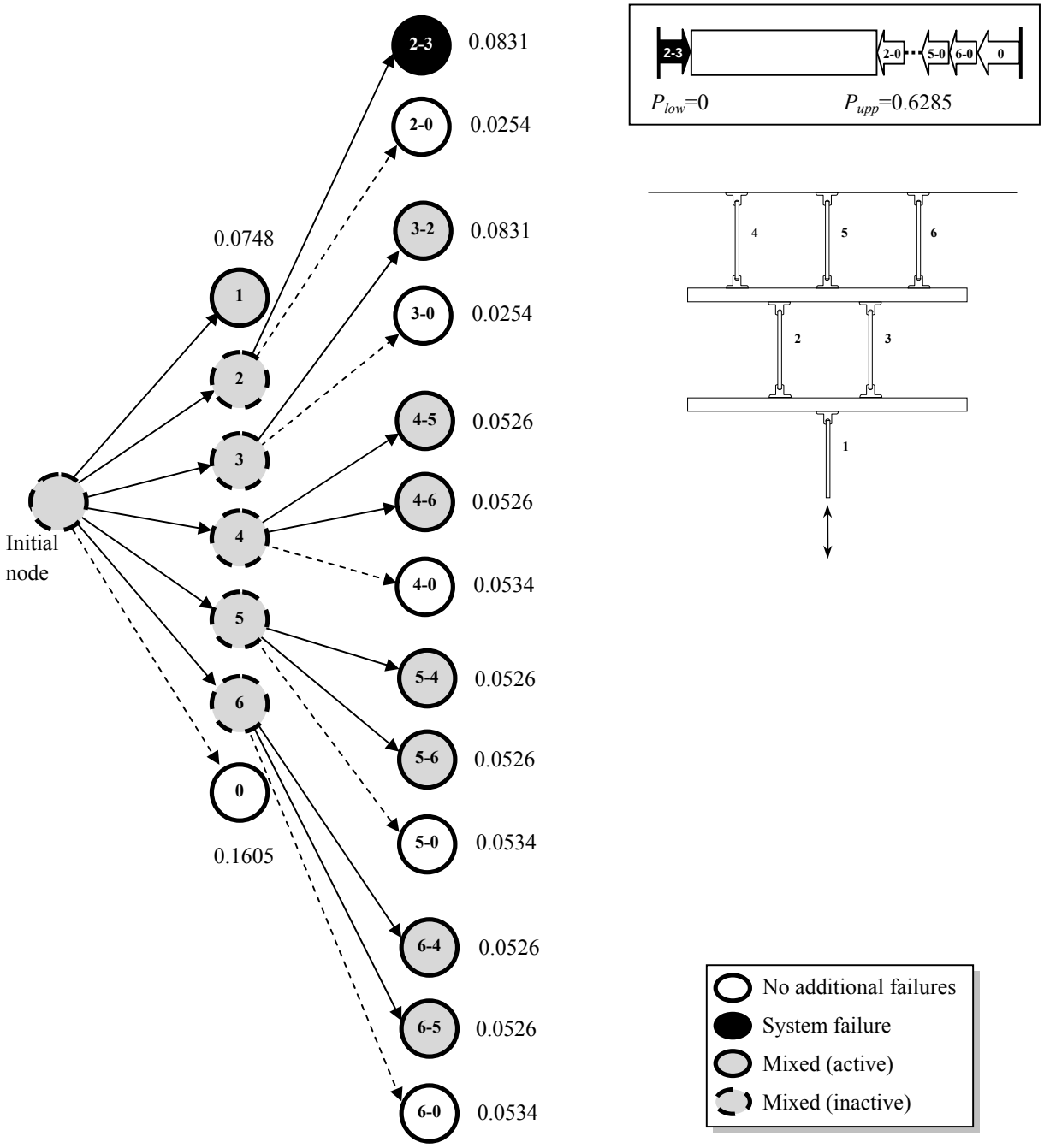

Figure 3.7 The first identification of system failure sequence

It is noteworthy that each structural analysis leads to either another branching or a system failure case identification, which decreases the upper bound or increases the lower bound. In other words, every structural analysis performed during the B^3-based search contributes to narrowing the bounds of the system failure probability. In this example, the iterative process is terminated when the gap of the bounds becomes smaller than a prescribed percentage of the upper bound. Figure 3.8 shows the updates of the bounds with the number of "structural analyses" during the search.

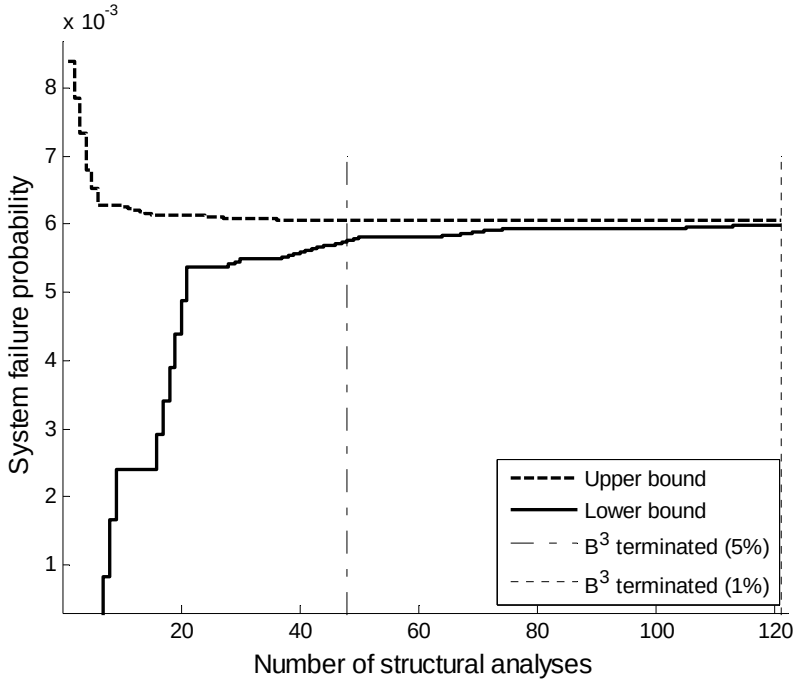

Figure 3.8 Updating of the bounds by the B^3 method

When the width of the bounds reaches 1% of the upper bound value, the lower and upper bounds of the system failure probability are estimated as 5.995×10^{-3} and 6.058×10^{-3} with 121

structural analyses. To verify this result, crude Monte Carlo simulations are performed. For each set of generated random variables, the system failure/non-failure is checked by performing structural analyses while following an event tree of load re-distributions. After 10^7 simulations, the system failure probability is estimated as 6.050×10^{-3} with a coefficient of variation (c.o.v.) of 4.053×10^{-3}, which belongs to the interval by the B^3 analysis. The average number of structural analyses for each Monte Carlo simulation is 1.017. Therefore, it is obvious that this sampling approach can be time-consuming or intractable especially when the computational cost of structural analyses are dominant.

It is noted that the upper bound curve becomes almost flat relatively early in the search, at a level fairly close to the exact system failure probability by Monte Carlo simulations. This is because, as the search proceeds, structural analyses are performed for systems with more damage and less redundancy, which lead to more "system failure" cases and thus most of the following updates are made on the lower bound. Even if non-failure is observed and thus branching is performed, the proportion of the white node decreases as the system loses its redundancy. Therefore, in most cases, it is not necessary to wait until the bounds converge to each other too closely. For example, the upper bound reaches 6.067×10^{-3} only after 48 structural analyses in this study. The corresponding lower bound is 5.772×10^{-3} and the gap of the bounds is 5% of the upper bound value. The bounds achieved at the 5% gap termination point (i.e. when the gap is 5% of the upper bound) show enough accuracy in predicting the level of the system failure probability when compared to those at the 1% gap termination point. This means further search beyond the 5% termination point may harm the efficiency of the analysis unnecessarily. In other words, the 5% gap seems to allow for an optimal trade-off between accuracy and efficiency, and

we experienced similar trends in other examples. Therefore, in the following numerical examples, the B^3 search will be terminated when the gap of the bounds reaches 5% of the upper bound.

Another important objective of the B^3 analysis is to identify critical system failure sequences efficiently. Table 3.1 shows the first twelve critical failure sequences identified by the B^3 method along with the probabilities of the sequences by the B^3 method and by crude Monte Carlo simulations. The entire set of critical failure paths identified until the 5% termination point is shown in Figure 3.9 following the order of their identification during the search. These results demonstrate that the B^3 method identifies critical failure sequences in the decreasing order of their probabilities, which allows us to terminate the search without missing critical failure sequences.

Failure sequence	Probability by B^3 method ($\times 10^{-4}$)	Probability by Monte Carlo simulation ($\times 10^{-4}$)
$2 \rightarrow 3$	8.31	7.90
$3 \rightarrow 2$	8.31	8.20
1	7.48	7.49
$4 \rightarrow 5 \rightarrow 6$	4.94	4.90
$4 \rightarrow 6 \rightarrow 5$	4.94	4.44
$5 \rightarrow 4 \rightarrow 6$	4.94	4.89
$5 \rightarrow 6 \rightarrow 4$	4.94	4.92
$6 \rightarrow 4 \rightarrow 5$	4.94	5.26
$6 \rightarrow 5 \rightarrow 4$	4.94	5.06
$4 \rightarrow 1$	0.39	0.37
$5 \rightarrow 1$	0.39	0.38
$6 \rightarrow 1$	0.39	0.39

Table 3.1 Identified critical system failure sequences and probabilities

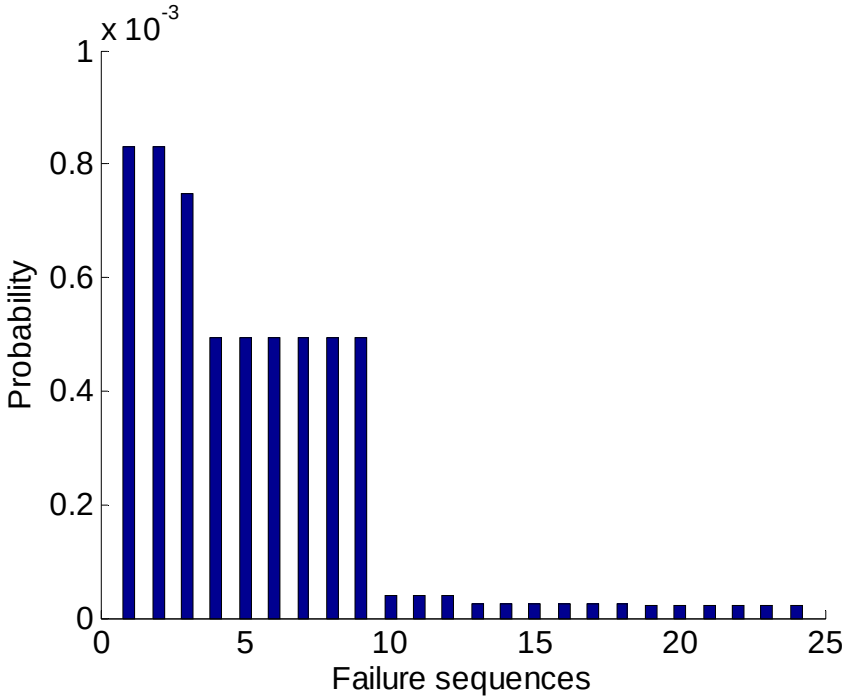

Figure 3.9 Probabilities of critical system failure sequences identified up to 5% termination point

3.4. Numerical Example: Three-dimensional Tripod Jacket Structure

In order to test the applicability of the proposed method to large-size complex structural systems, a three-dimensional tripod jacket structure consisting of 66 members in Figure 3.10 is considered. This type of offshore truss structures have been widely used in many research efforts for the system reliability analysis of fatigue-induced sequential failures. A benchmark structure of tripod offshore platform in Karamchandani *et al*. (1991) and (1992) is adopted in this example and slightly modified to facilitate testing the proposed method.

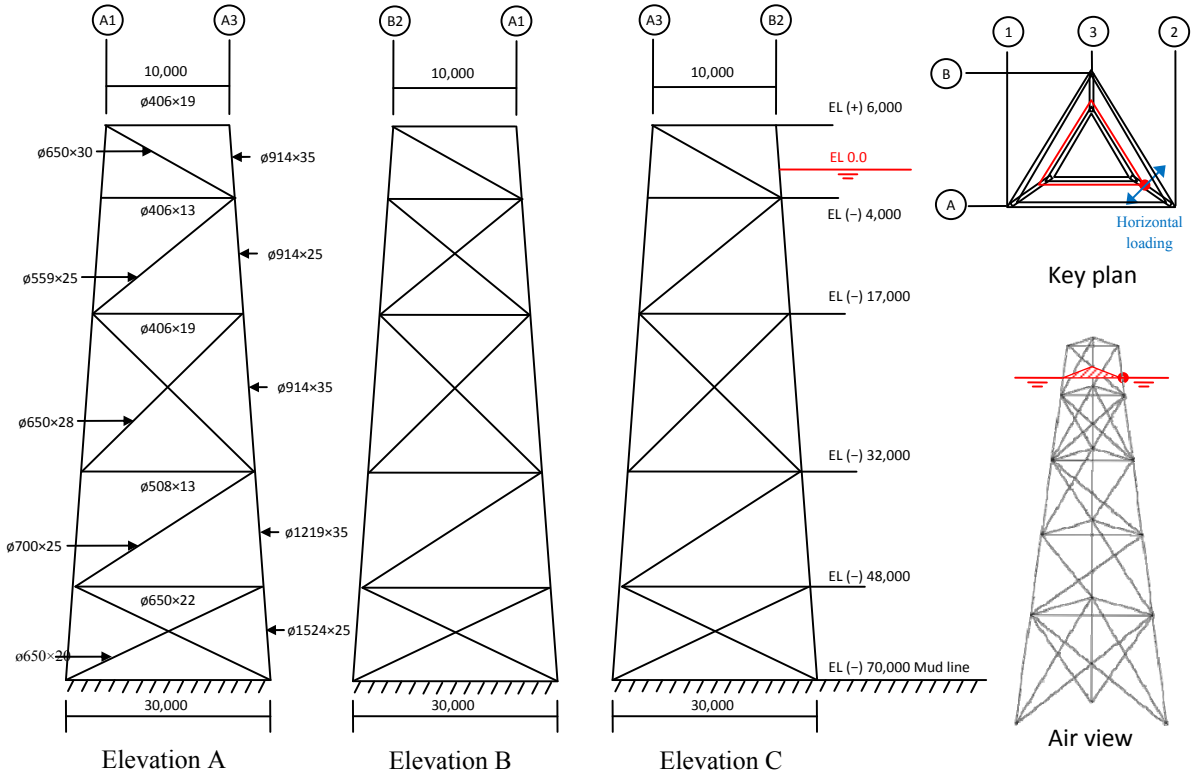

Figure 3.10 Three-dimensional tripod jacket structure

3.4.1. Structural configuration and loading

As shown in Figure 3.10, the target structure has a triangular plan with a height of 76 meters. The supports at the bottom are located at the corners of an equilateral triangle with sides of 30 meters. The lengths of the sides decrease linearly over the height and are finally reduced to 10 meters at the top. The structure has hollow section pipes with a variety of perimeter and thickness as shown in the figure. For example, "ϕ650×30" in the figure denotes a hollow section with a perimeter of 650 mm and a thickness of 30 mm. The cross sectional area of each member is calculated by the product of the perimeter and thickness. For the sake of simplicity, the

geometry function $Y(a)$ is assumed to be 3.0. Paris equation parameters C and m, and the initial crack lengths are described by random variables as described in the following section.

The 70-meter-long bottom portion of the structure is in the sea water. Single cyclic horizontal loading is applied at the sea level of the column "2" as illustrated in Figure 3.10. For the sake of simplicity, it is assumed that the dynamic loading has constant amplitude, and the uncertainty in the amplitude is described by a random load-scale factor I. It is also assumed that each steel truss member shows linear elastic behavior until a crack failure occurs. This assumption is apprehensible because most fatigue-induced failures are caused by relatively low-level stresses. Based on these assumptions, a deterministic structural analysis is performed for each damaged/undamaged condition considered during the search, and the calculated member stresses are multiplied by the uncertain load-scale factor I during the reliability analyses. The loading frequency (ν_0) and the inspection cycle (T_s) are given as 500,000/year and 4 years, respectively, and these parameters are assumed to be deterministic.

3.4.2. Statistical parameters

The uncertainties by random variables are described in a similar manner to the original example in Karamchandani *et al*. (1991, 1992) except for the Paris-equation parameters C and m. Kirkemo (1988) considered the following assumptions, i.e. (1) m and C are both deterministic, (2) m is deterministic, but C is uncertain, (3) C is deterministic, but m is uncertain, (4) m and C are both uncertain and described by uncorrelated random variables, and (5) m and C are both uncertain and described by negatively correlated random variables. It was recommended to use approaches (2) and (5) for a reasonable representation of the reality (Kirkemo 1988). Therefore, in this thesis, these two cases are considered as Case I and Case II, respectively. Case II considers uncertainties in both m and C whereas in Case I the given mean value of m will be

used as a deterministic parameter. Uncertainties in the initial crack lengths (a^0) and the load-scale factor (I) are also considered.

The statistical properties of the random variables are summarized in Table 2. The values of these statistical parameters were determined based on a comprehensive literature survey (Kirkemo 1988, Moan *et al*. 1993, Millwater *et al*. 1994, Moan and Song 2000, Shabakhty *et al*. 2003, Ayala-Uraga and Moan 2007, Moan and Ayala-Uraga 2008). In both cases, one random variable I is used to describe the uncertainty in the loading. Each of 66 members in Cases I and II has two (C and a^0) or three (C, m, and a^0) random variables, respectively. Therefore, a total of 133 and 199 random variables are used for Cases I and II, respectively. All random variables are assumed to be statistically independent of each other except for the following cases for which non-zero correlation coefficients are assigned: (1) between Paris equation parameters (C) of two different members (correlation coefficient 0.6); (2) between Paris equation parameters (m) of two different members (correlation 0.6); (3) between initial crack lengths (a^0) of two different members (correlation 0.6); and (4) between C and m of two different or the same members (correlation −0.2).

Random variables	Mean	c.o.v.	Distribution type	Number of random variables
C	1.202×10^{-13}	0.533	Lognormal	66
m	3.0	0.02	Lognormal	66
a^0 (mm)	0.11	1.0	Exponential	66
I	1.0	0.1	Lognormal	1

Table 3.2 Statistical properties of random variables

3.4.3. Component and system failure definition

It is assumed that a section fails when its crack length reaches the thickness of the section. Upon the occurrence of the section failure, the corresponding member is removed from the structural analysis model, which causes stress re-distribution. As for the system failure definition, most of the existing research employed some heuristic system failure criteria such as "the target structure collapses if any pair of members fail" or "the system fails if one leg member fails" (Karamchandani *et al*. 1992). As an attempt to accurately identify system failure cases via structural analyses instead of heuristic criteria, in this example, the following system failure criteria are checked after each structural analysis during a B^3-based search. The occurrence of any of these criteria constitutes system failure.

(1) Global statistical determinacy or instability condition: 3 × (number of nodes) – (number of members) – (number of reaction DOFs) > 0.
(2) Local instability condition: less than three members are connected to a non-supporting node.
(3) Condition of global stiffness matrix: the condition number of global stiffness matrix is exceedingly large compared to that of the intact structure.
(4) Unreasonably large displacement occurs.

It should be noted that this is an example of system failure criteria that can be used during a B^3 search. One can define a set of system failure criteria based on the objectives and safety concerns of a target structure of interest. For example, for many offshore structures, extreme loading is another important factor which may cause structural failures such as yielding (Karamchandani *et*

al. 1991). As stated above, the overloading failure can be introduced as a system failure definition in the B^3 method, which represents an apprehensible failure scenario that initial local failures occur from fatigue and the subsequent load re-distribution causes extreme loading and system failure. In order to introduce overloading failure as a criterion of local failure and consider the interaction between fatigue and overload failures, the B^3 formulations in Section 3.1 needs to be further developed to describe failures under extreme loading also as disjoint events, which will be an important future research topic.

3.4.4. Computational framework

Figure 3.11 illustrates the computational framework of the B^3 analysis for the three-dimensional tripod jacket structure. As shown in the figure, the B^3 framework consists of three elements: branch-and-bound algorithm, structural analysis, and (component and system) reliability analysis. For the target truss structure, a structural analysis code for linear elastic behavior was made in MATLAB®. Computer codes for the branch-and-bound process and reliability analysis were also developed in MATLAB®. The methods employed for component and system reliability analysis (i.e., FORM, SORM, and a method by Genz) were discussed in Section 3.4.2.

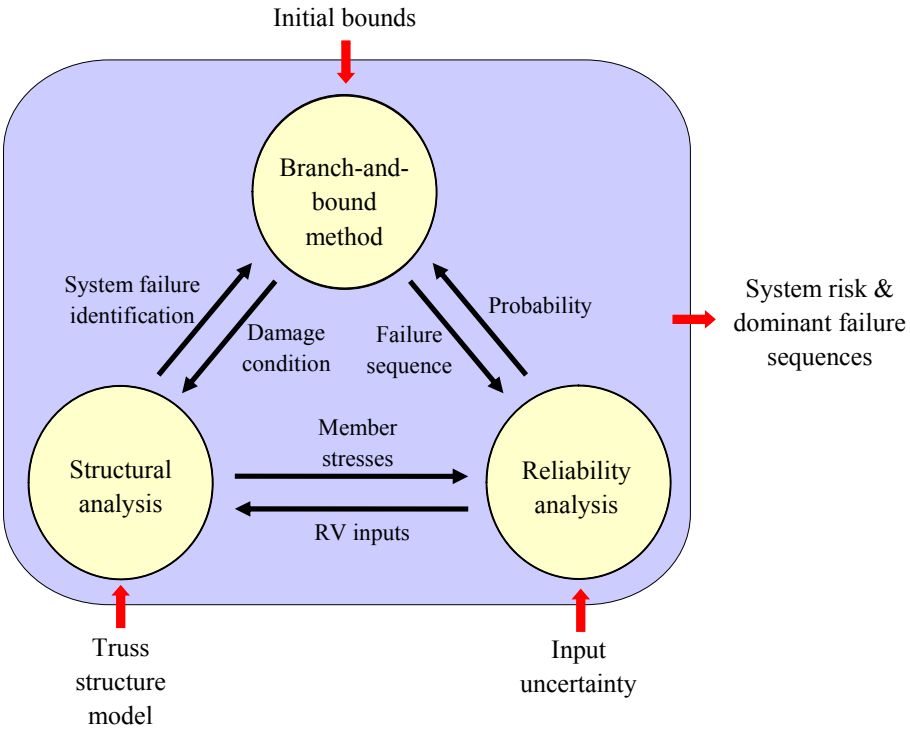

Figure 3.11 Computational framework of B^3 analysis for tripod jacket structure

During the B^3 analysis, the main part in charge of branching and bounding repeatedly requires structural analysis and reliability analysis. If a damage condition is identified as a system failure case through structural analysis, the lower bound increases. If it is identified as a non-failure case, branching is made from the node representing the damage condition, and the member stresses obtained from the structural analysis are provided to the reliability analysis so that the probabilities of the new failure sequences can be calculated.

3.4.5. Analysis results

This section presents the results of B^3 analyses for Cases I and II. The results are compared to those by conventional branch-and-bound approach (i.e. based on non-disjoint failure sequences)

in both cases. First of all, Figure 3.12 shows the updates of the upper and lower bounds by the B^3 method and those of the lower bound by the conventional branch-and-bound-based approach (i.e. Eq. (3.20)) with the number of structural analyses.

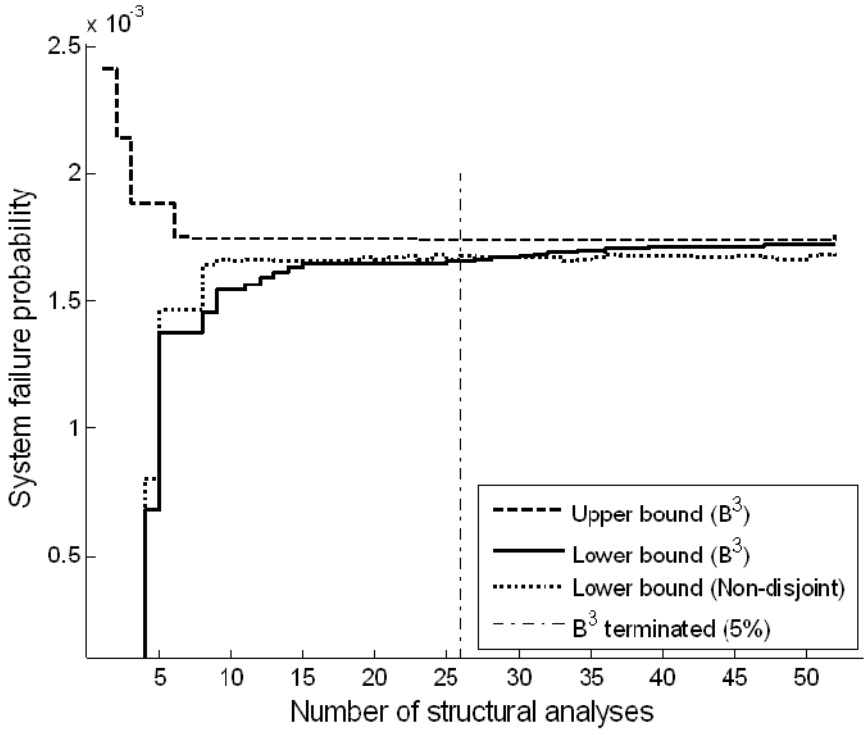

Figure 3.12 Bounds by B^3 method and conventional approach (Case I)

The lower and upper bound by the B^3 method at 5% gap termination point are 1.656×10^{-3} and 1.739×10^{-3} respectively with only 26 FE analyses. The system failure probability estimated by crude Monte Carlo simulation with one million samples is 1.734×10^{-3}, with a c.o.v. of 2.40×10^{-2}, which belongs to the interval by the B^3 method and is close to the upper bound as observed in the multi-layer Daniels system example.

At the same termination point, the lower bound by the conventional method is 1.676×10^{-3}, which is a seemingly good result. However, as the trend in the figure shows, the approach has a couple of drawbacks in terms of search termination. First, it is not guaranteed that the updates in the lower bound diminish monotonically even though the system failure sequences are identified in the decreasing order of their likelihoods. This is because of the impact of the statistical dependence between the failure sequences on the system failure probability in Eq. (3.20). For example, the curve of the lower bound becomes almost flat after 10 structural analyses. Since the upper bound is usually not available for the conventional approach, the search procedure is often terminated when the lower bound converges. Therefore the flat trend may result in underestimation of system failure probability. Second, the lower bound of the conventional approach requires more structural analyses for the convergence than the bounds by the B^3 method. For example, even after 50 structural analyses, the lower bound does not increase much from an earlier flat trend. By contrast, the lower bound by the B^3 method increases monotonically and converges to the upper bound at around the exact solution after 50 structural analyses. Sometimes, the incremental amount of lower bound is even negative due to the numerical error from simulation which is introduced to solve the general cut-set system in Eq. (3.21). These two issues are more clearly shown in Case II.

Figure 3.13 shows the probabilities of critical system failure sequences identified until the 5% termination point of the B^3 analysis. This once again confirms that the failure modes are identified in the decreasing order of their probabilities. Furthermore, Figure 3.14 displays the first four system failure sequences that satisfy the system failure criteria described in Section 3.4.3. In the figure, each thick bar indicates a failed member. The probability of each sequence is

also verified by a comparison with crude Monte Carlo simulations (one million samples). Only 9 structural analyses were required to identify these failure sequences.

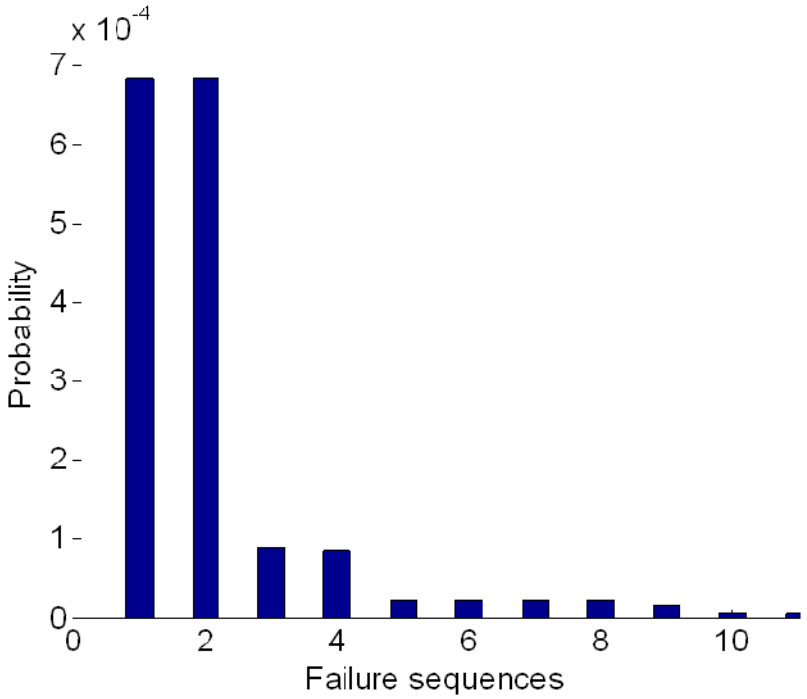

Figure 3.13 Critical system failure sequences identified until 5% termination point (Case I)

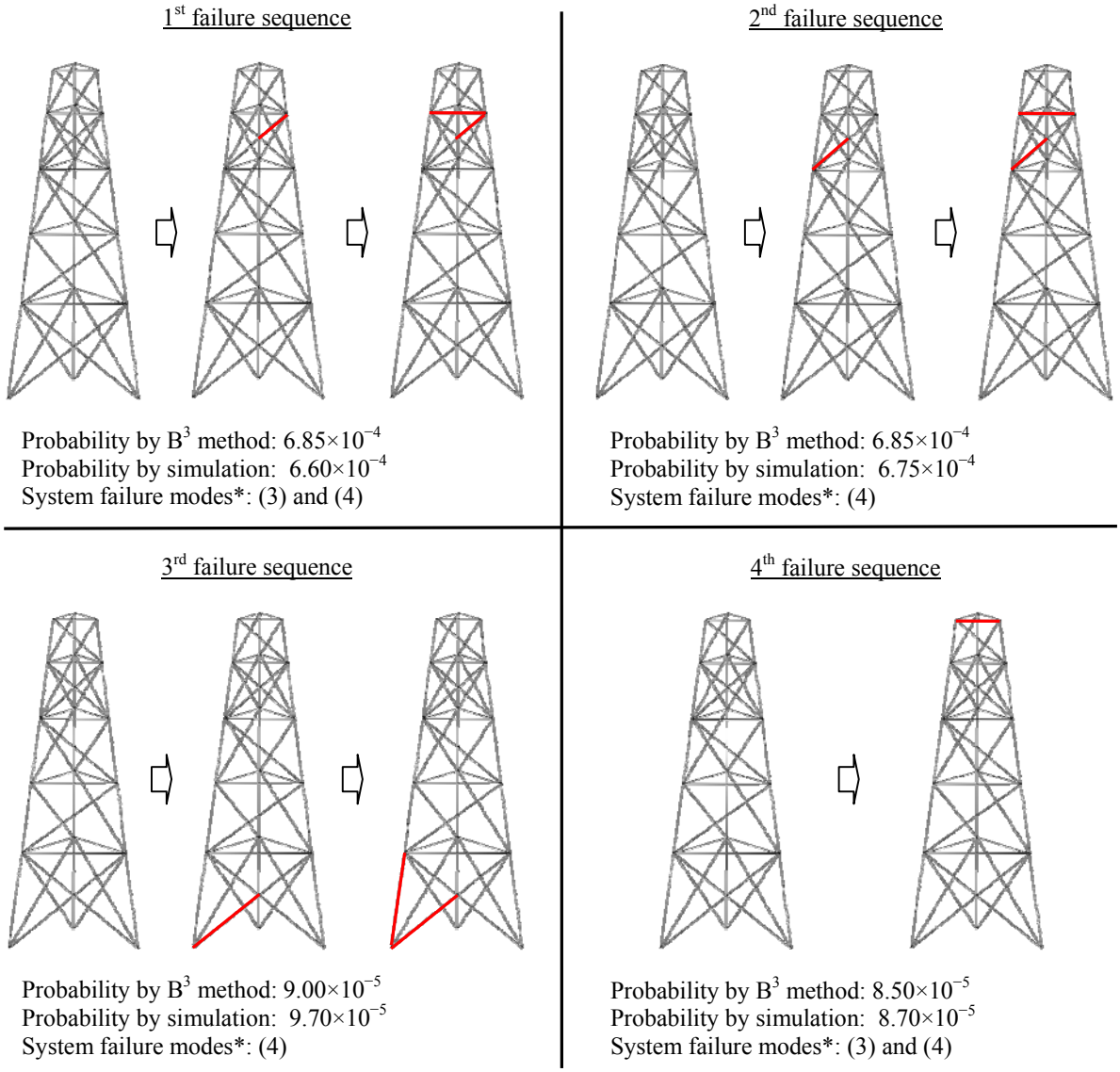

* See Section 3.4.3.

Figure 3.14 Four major system failure sequences (Case I)

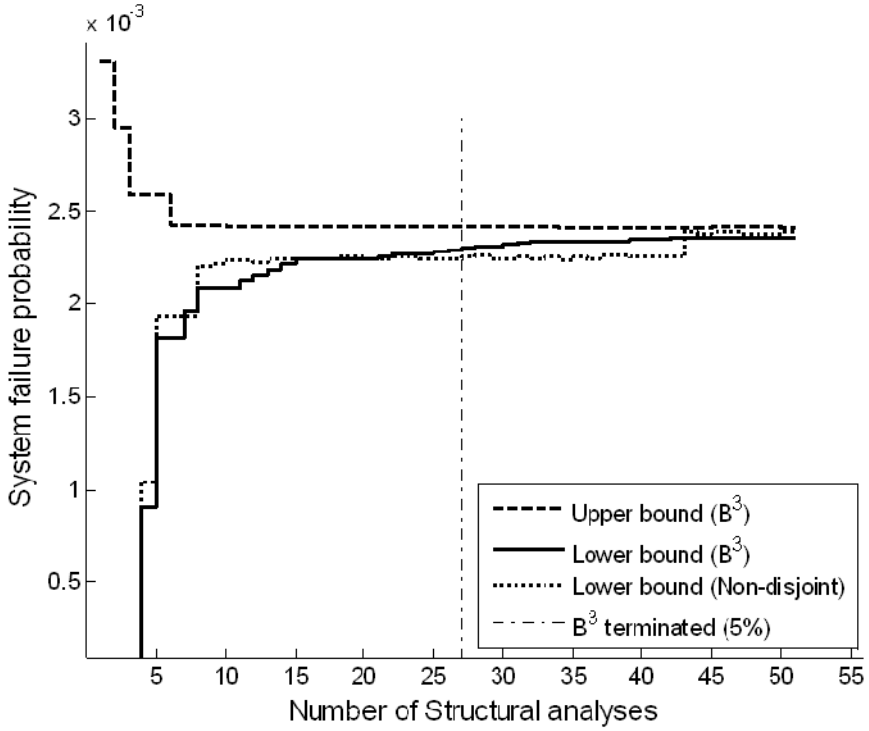

Figure 3.15 Bounds by B^3 method and conventional approach (Case II)

Figures 3.15-3.17 show the bounds and critical failure sequences for Case II. As shown in Figure 3.15, the lower and upper bounds by the B^3 method at 5% gap termination point are estimated as 2.302×10^{-3} and 2.416×10^{-3} respectively with only 27 structural analyses of the truss. The system failure probability is estimated as 2.392×10^{-3} by Monte Carlo simulation (one million samples, c.o.v. 2.04×10^{-2}), which belongs to the interval by the B^3 analysis, and is fairly close to the upper bound as observed in the previous examples. The aforementioned limitations of the conventional approach are more clearly seen in this example. There is a long flat trend of the lower bound (between 10 and 43 structural analyses), which may lead to early termination of the search. By contrast, in the B^3 approach, the existence of the upper bound and the continuous

increase in the lower bound help avoid the risk of inaccurate estimation of the system failure probability.

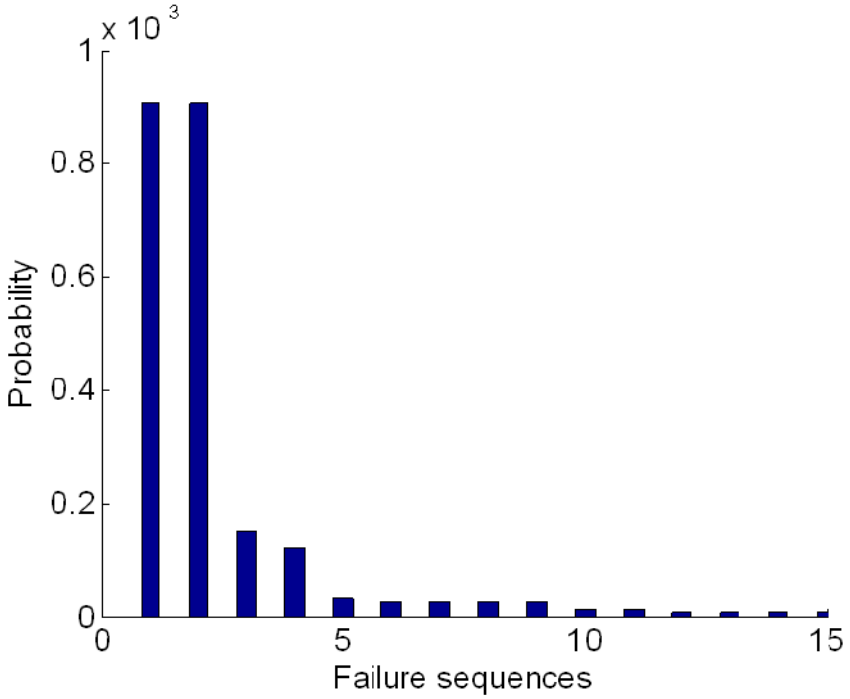

Figure 3.16 Critical system failure sequences identified until 5% termination point (Case II)

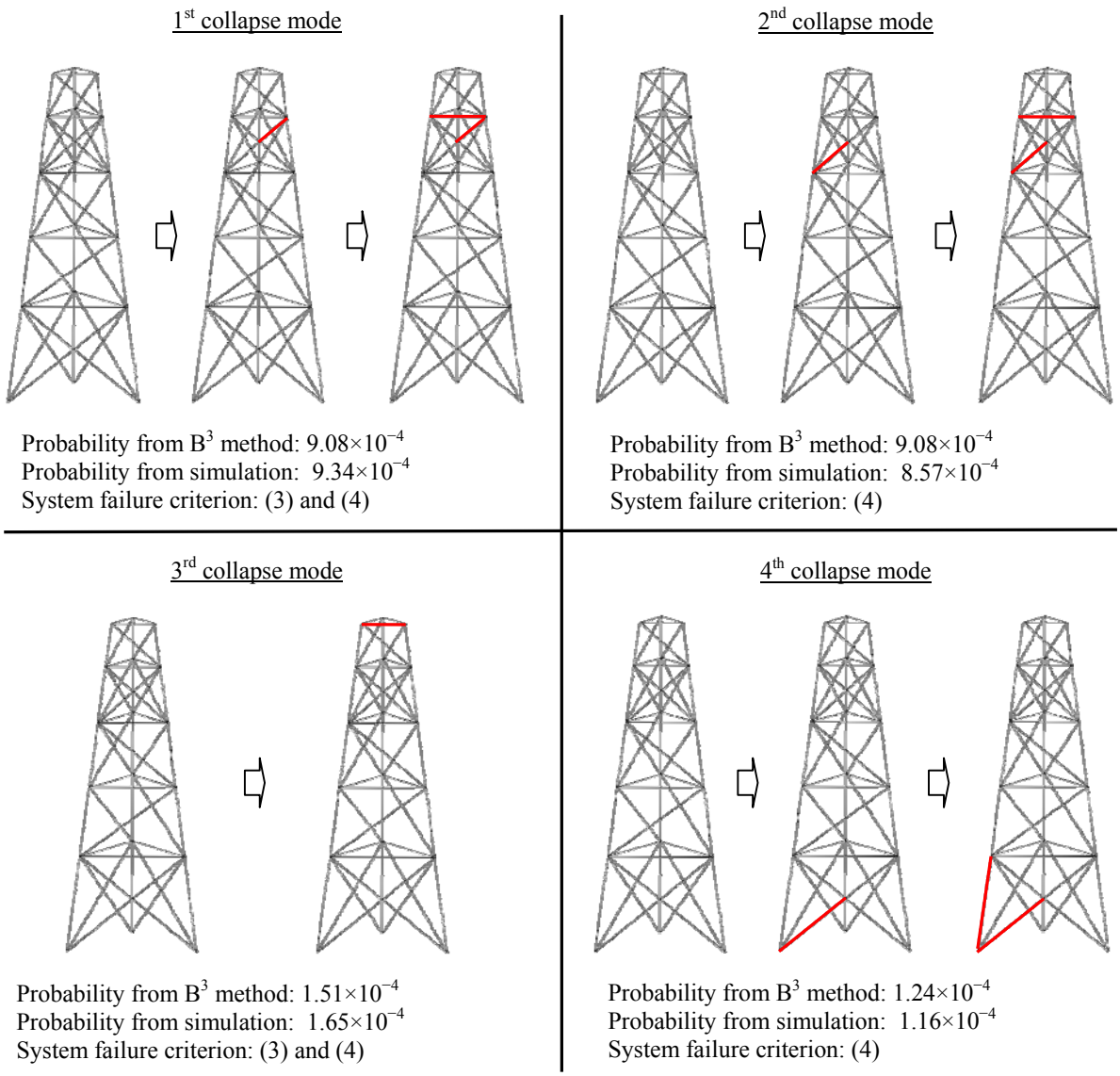

Figure 3.17 Four major system failure sequences (Case II)

Figure 3.16 shows the probabilities of the critical failure sequences identified until the 5% termination point of the B^3 analysis, and Figure 3.17 displays the four major system failure sequences along with their probabilities. It is also noted that the different assumptions on the

uncertainties by Cases I and II lead to different orderings in the identified system failure sequences.

3.5. Summary

A new Branch-and-Bound method employing system reliability Bounds (termed the B^3 method) was developed in order to estimate the probability of system failure caused by fatigue-induced sequential failures by identifying critical system failure sequences efficiently and accurately. Due to the proposed disjoint cut-set formulation employing a recursive formulation of limit-states and systematic search procedure, the B^3 method can identify critical sequences of fatigue-induced failures causing a system failure in the decreasing order of their likelihood. Unlike existing branch-and-bound approaches, the proposed method provides both lower and upper bounds on the system failure probability while the size of the updates on each bound is diminishing monotonically. Every structural analysis performed during the search contributes to updating either lower or upper bound, i.e. narrowing the bounds. This significantly reduces the computational time required for accurate results especially when computational cost for structural analyses is dominant. The updated bounds provide reasonable criteria for terminating a branch-and-bound search without missing critical sequences. After a demonstration by a multi-layer Daniels system, the method was tested by a three-dimensional offshore structure with 66 members. The results by the B^3 method are verified by crude Monte Carlo simulations. The merits of the proposed approach are successfully demonstrated through comparison with the results by a conventional branch-and-bound approach.

4. FE-BASED SYSTEM RELIABILITY ANALYSIS OF FATIGUE-INDUCED SEQUENTIAL FAILURES OF CONTINUUM STRUCTURES

In Chapter 3, the B^3 method was developed for system reliability analysis of fatigue-induced sequential failure. The method quantifies the risk of fatigue-induced sequential failure at the system level and identifies critical failure sequences in the decreasing order of likelihood. The B^3 method was originally developed for reliability analysis of discrete structures such as truss. Therefore, the method is not readily applicable to continuum structures, which are often represented by finite element (FE) models. In particular, the method has limitations in describing general stress distributions in limit-state formulations, evaluating stress intensity range based on crack length, and dealing with slow convergence of the upper and lower bounds for structures with high redundancy. In this chapter, the B^3 method (in Chapter 3) is integrated with the FE-SRA framework (in Chapter 2) and further developed to perform FE-based system reliability analysis of fatigue-induced sequential failures of continuum structures.

4.1. Literature Review

As discussed in Chapter 3, fatigue is one of the main causes of failures in various structural systems. Therefore, an adequate level of structural redundancy should be provided to prevent fatigue-induced structural failure, and some studies have been undertaken to quantify the likelihood of system-level failure caused by fatigue-induced sequential failures, especially for offshore structures, which are often modeled as discrete (truss) structures (Almar-Naess 1985, Moan 2005, Karamchandani 1992, Moan and Song 2000, Shabakhty *et al*. 2003). However, it is noted that fatigue-induced sequential failure is an important failure mechanism not only to

discrete structures, but also to continuum structures such as subsystems in aircraft structures. For example, according to the "Damage Tolerance" design philosophy adopted by the U.S. Air Force in early 1970s, an aircraft structure with some cracks is still considered safe as long as the structure can resist further damage and system failure, and can accomplish the mission for a given period of time (Tiffany 1978, Millwater and Wieland 2010). Therefore, for risk-based design, maintenance, and retrofit of robust structural systems from truss to continuum, it is essential to quantify the likelihood of fatigue-induced sequential failures and identify the critical sequences of local failures.

However, it is noted that most of the existing studies about the reliability analysis of fatigue-induced sequential failure (reviewed in Section 3.1) focus on relatively simple discrete structures such as truss. There have been few studies on such reliability analysis of more complex structures (such as continuum), and the applications using sophisticated FE simulations are limited (Alford *et al*. 1992, Shi and Mahadevan 2001). Even though the aforementioned merits of the B^3 method have been successfully demonstrated through numerical examples in Chapter 3, the method was originally developed for system reliability analysis of truss-type structures, and thus not readily applicable to continuum structures due to the following limitations as discussed in Lee and Song (2011b): (1) the far-field stress, which is a main parameter in the fatigue crack-growth formulation of the B^3 method, is not generally conspicuous for a continuum structure; (2) it is not always feasible to derive an analytical relationship between the stress intensity range and the crack length using the so-called geometry function for a continuum which has a complex stress distribution; and (3) the structural complexity of a continuum often results in many dominant failure sequences having a similar level of likelihood, which prevents fast convergence of the lower and upper bounds during a B^3 analysis.

In order to take advantage of the merits of the B^3 method for FE-based system reliability analysis of continuum structures, the method is further developed as follows (Lee and Song 2011b): (1) the limit-state function formulation is modified to incorporate the general stress distribution instead of using a far-field stress assumption; (2) an external computer program is integrated with the B^3 computational framework to estimate the stress intensity range with the general stress distribution without relying on analytical geometry function $Y(a)$; and (3) an additional search termination criterion is introduced to facilitate efficient system reliability analysis of a continuum that has many failure sequences with similar probabilities. Hereafter, the B^3 method further developed in this chapter for continuum structures is referred to as *the B^3 method for continuum*, while the method described in Chapter 3 is called *the B^3 method for truss*.

4.2. Branch-and-Bound Method Employing System Reliability Bounds for Continuum (B^3 Method for Continuum)

4.2.1. Development I: limit-state function formulations for general stress distribution

The limit-state function formulation of the B^3 method for continuum also starts with Paris equation in Eq. (3.1), to characterize the speed of the crack growth. In the B^3 method for truss, the stress intensity range (ΔK) was evaluated by use of Newman's approximation, i.e. by using an analytical function of far-field stress and crack length, as shown in Eq. (3.2). In order to incorporate general stress distribution rather than analytical functions based on Newman's approximation, the limit-state function formulations have been modified as follows. Integrating Eq. (3.1) from the initial condition to the current time point, the relation between the time duration T and the corresponding crack length a is derived as

$$\int_{a^0}^{a} \frac{1}{[\Delta K]^m} da = C \cdot N = C \cdot \nu_0 \cdot T \tag{4.1}$$

At the *i*-th member, a crack failure is assumed to occur when the crack exceeds a critical length a_i^c. Then, the limit-state function for the member's failure within an inspection cycle [0, T_s] is described as

$$g_i(\mathbf{X}) = T_i^0 - T_s = \frac{1}{C\nu_0} \int_{a_i^0}^{a_i^c} \frac{1}{[\Delta K]^m} da - T_s \tag{4.2}$$

The difference between this and the limit-state function in Eq. (3.6) is that the stress intensity factor K is not evaluated by Newman's approximation. Similarly to Eq. (3.11), an auxiliary "damage" function is then determined as

$$\Psi(a) = \int_{a^0}^{a} \frac{1}{[\Delta K]^m} da \tag{4.3}$$

Consider the failure sequence {1→2} for example, using the damage function, one can derive the followings:

$$\Psi(a_2^1) - \Psi(a_2^0) = C \cdot \nu_0 \cdot T_1^0 \tag{4.4a}$$

$$\Psi(a_2^c) - \Psi(a_2^1) = C \cdot \nu_0 \cdot T_2^1 \tag{4.4b}$$

Summing up Eqs. (4.4a) and (4.4b), one obtains

$$\Psi(a_2^c) - \Psi(a_2^0) = C\nu_0 T_2^1 + C\nu_0 T_1^0 \tag{4.5}$$

Solving Eq. (4.5) for T_2^1, one can derive

$$
\begin{aligned}
T_2^1 &= \frac{\left[\Psi(a_2^c) - \Psi(a_2^0)\right]}{C\nu_0} - T_1^0 \\
&= \frac{1}{C\nu_0} \int_{a_2^0}^{a_2^c} \frac{da}{\left[\Delta K\right]^m} - T_1^0 \\
&= \frac{1}{C\nu_0} \int_{a_2^0}^{a_2^1} \frac{da}{\left[\Delta K_2^0\right]^m} + \frac{1}{C\nu_0} \int_{a_2^1}^{a_{c2}} \frac{da}{\left[\Delta K_2^1\right]^m} - T_1^0
\end{aligned}
\tag{4.6}
$$

where $\Delta K_2{}^0$ and $\Delta K_2{}^1$ respectively denote the range of the stress intensity factors at member 2 in the intact structure and in the damaged structure with the first failure at member 1. The time until the failure, i.e. T_i^0 in Eq. (4.2) can be described in terms of the crack length at a different member. For example, the time until the failure in member 1 is

$$
T_1^0 = \frac{1}{C\nu_0} \int_{a_1^0}^{a_1^c} \frac{1}{\left[\Delta K_1^0\right]^m} da = \frac{1}{C\nu_0} \int_{a_2^0}^{a_2^1} \frac{1}{\left[\Delta K_2^0\right]^m} da \tag{4.7}
$$

Substituting Eq. (4.7) into Eq. (4.6), one can derive

$$
T_2^1 = \frac{1}{C\nu_0} \int_{a_2^1}^{a_2^c} \frac{1}{\left[\Delta K_2^1\right]^m} da \tag{4.8}
$$

Considering Eq. (4.4a), Eq. (4.8) is further derived as follows to describe $T_2{}^1$ in terms of the previous time term in the sequence, $T_1{}^0$:

$$T_2^1 = \frac{1}{C\nu_0}\int_{a_2^0}^{a_2^c}\frac{1}{\left[\Delta K_2^1\right]^m}da - \frac{1}{C\nu_0}\int_{a_2^0}^{a_2^1}\frac{1}{\left[\Delta K_2^1\right]^m}da$$
$$= \frac{1}{C\nu_0}\int_{a_2^0}^{a_2^c}\frac{1}{\left[\Delta K_2^1\right]^m}da - T_1^0 \cdot \frac{\displaystyle\int_{a_2^0}^{a_2^1}\frac{1}{\left[\Delta K_2^1\right]^m}da}{\displaystyle\int_{a_2^0}^{a_2^1}\frac{1}{\left[\Delta K_2^0\right]^m}da} \tag{4.9}$$

In the case of a truss structure, ΔK can be estimated by use of Newman's approximation in Eq. (3.2), and the ratio of two integrals in Eq. (4.9) is simply $(S_2^0/S_2^1)^m$ where S_2^0 and S_2^1 are the far-field stresses at member 2 in the intact structure and in the structure with member 1 damaged, respectively. It is important to note that in such a case, T_2^1 can be calculated without estimating a_2^1. However, Newman's approximation employing far-field stress is not generally available. In such a general case, a_2^1 is needed to use Eq. (4.9). One could try to solve Eq. (4.7) for a_2^1 each time, but it would seriously harm the efficiency of the analysis which requires solving the equation a large number of times.

For this reason, in the B^3 method for continuum, Eq. (4.9) is approximated by performing both integrals in the ratio up to a_2^c instead of a_2^1, i.e.

$$T_2^1 \approx \frac{1}{C\nu_0}\int_{a_2^0}^{a_2^c}\frac{1}{\left[\Delta K_2^1\right]^m}da - T_1^0 \cdot \frac{\displaystyle\int_{a_2^0}^{a_2^c}\frac{1}{\left[\Delta K_2^1\right]^m}da}{\displaystyle\int_{a_2^0}^{a_2^c}\frac{1}{\left[\Delta K_2^0\right]^m}da} \tag{4.10}$$

Through mathematical induction, the following recursive formulation is derived for a general failure sequence $\{1\rightarrow 2\rightarrow\ldots\rightarrow(i-1)\}$:

$$T_i^{1,\ldots,i-1} \approx \frac{1}{C\nu_o}\int_{a_i^0}^{a_i^c}\frac{1}{\left[\Delta K_i^{1,\ldots,i-1}\right]^m}da - \sum_{k=1}^{i-1}\frac{\displaystyle\int_{a_i^0}^{a_i^c}\frac{1}{\left[\Delta K_i^{1,\ldots,i-1}\right]^m}}{\displaystyle\int_{a_i^0}^{a_i^c}\frac{1}{\left[\Delta K_i^{1,\ldots,k-1}\right]^m}}T_k^{1,\ldots,k-1} \tag{4.11}$$

The impact of the approximation in computing the ratio is examined by a numerical example in Chapter 3. The B^3 method for truss (i.e. the B^3 method that does not employ this approximation) is also applicable to the example, which enables us to assess the impact of the approximation accurately.

4.2.2. Development II: evaluating stress intensity range using an external computer program

The generalized formulation of time terms in Eq. (4.11) makes it essential to compute the range of the stress intensity factor (ΔK) along the crack length (a) for a complex stress distribution which cannot be generally described by a far-field stress. Among a variety of existing computer programs and methods for crack-growth analysis, AFGROW® (Harter 2006) is chosen for finding the a-ΔK relation without relying on Newman's approximation.

AFGROW® provides a variety of crack-growth models which allow users to predict crack growth for various geometries, materials, and stress distributions. AFGROW® provides not only closed-form stress intensity solutions for simple cases, but also non-closed-form solutions for general cases based on the results of the FE analysis. Another advantage of AFGROW® is that the software provides Component Object Model (COM) Automation interface, which allows other Windows applications such as MS Excel® to communicate with AFGROW®. This feature is particularly useful because the proposed system reliability analysis

method of fatigue-induced sequential failures requires a large number of deterministic crack-growth analyses.

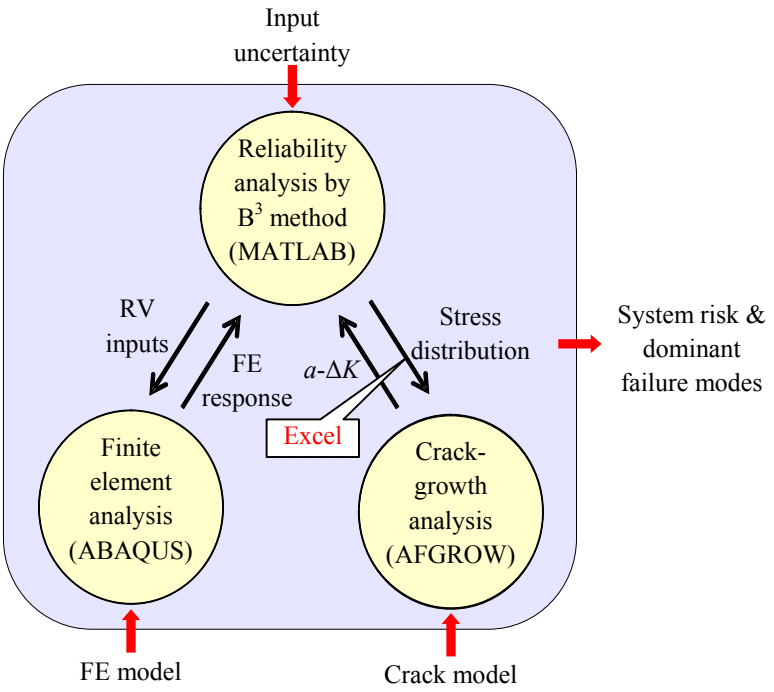

Figure 4.1 Computational framework of the B^3 method for continuum

Figure 4.1 illustrates the computational framework of the B^3 method for FE system reliability analysis of a continuum. The main B^3 analysis code in MATLAB® repeatedly calls ABAQUS® to obtain the stress distribution from the finite element (FE) analysis for given Random Variables (RVs) and damage conditions during the search procedure, and the stress distribution is transferred to AFGROW® for estimating the corresponding stress intensity range along the crack length, which is the basic information needed for estimating the time term in Eq. (4.11). The computational framework in Figure 4.1 performs successfully in the numerical

examples in this chapter. However, AFGROW® and ABAQUS® can be replaced by other computer programs for crack-growth and FE analysis if necessary.

4.2.3. Development III: additional termination criterion for systematic search scheme

The flow chart in Figure 4.2 illustrates the search procedure of the B^3 method for continuum. After performing the first FE analysis and crack-growth analysis respectively using ABAQUS ® and AFGROW®, the first set of child nodes are branched out from the initial node and their probabilities are calculated through component and system reliability analyses. For the numerical examples in this thesis, the First-Order Reliability Method (FORM) and the Second-order Reliability Method (SORM) are used for component reliability analysis (Der Kiureghian 2005). A multivariate normal integral method by Genz (1992) is used for system reliability analysis. Based on the probability calculations, the first bounding is made and P_{upp} is decreased by the probability of the newly-identified non-failure case. The next step is to compare all the nodes except for system-failure, non-failure, and "parent" nodes to select the one with the highest probability. Then, a new FE analysis is performed using an FE model representing the damage scenario of the selected node. If the FE analysis reveals that the selected node represents a system failure case, P_{low} is increased by the probability of the node. On the other hand, if the FE analysis reveals that a system-level failure does not occur, another crack-growth analysis and branching process are performed to find the probabilities of child nodes originating from the selected node.

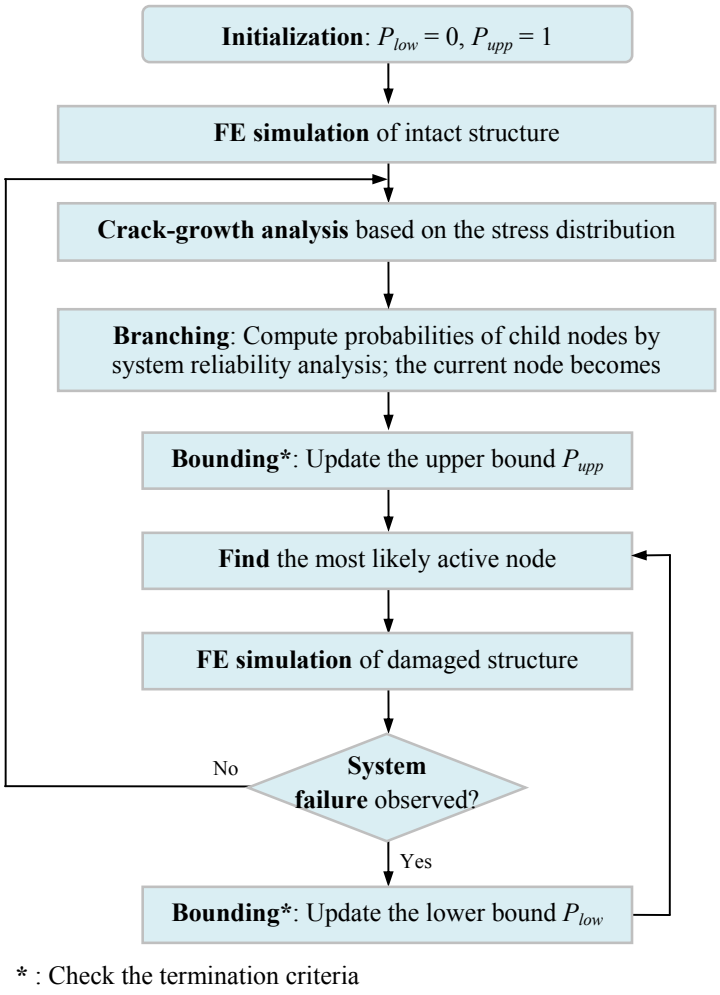

Figure 4.2 Flow chart of the B^3 method for continuum

This search process repeating "branching" and "bounding" is continued until the termination criteria are satisfied. If finding the most critical paths is the main interest, one can terminate the search process when the most recently identified system failure sequence has a probability lower than a given threshold or a desirable number of critical failure sequences is identified. On the other hand, if estimating the system failure probability is of interest, one could terminate the process when the updates on the bounds made by the newly-identified failure

sequence become negligible compared to the overall risk level identified by the bounds. When the system failure probability of a three-dimensional truss structure was calculated in Chapter 3, the search was terminated when the ratio of the gap of the bounds to the upper bound becomes smaller than a given threshold value. However, more complex structures with a higher level of structural redundancy including continuum structures tend to have many competing failure sequences with similar likelihood. In this case, the termination rule based on the gap of the bounds may result in spending large computational time in identifying many competing failure sequences with negligible probabilities and making very small updates on the lower bound. In order to avoid making unnecessary computational efforts on negligible updates on the lower bound, in the B^3 method for continuum, it is suggested to terminate if the updates on the lower bound become negligible. In summary, the search process is terminated if *any* of the following conditions is satisfied:

1) (the gap of two bounds) / (the upper bound) $< \varepsilon_1$
2) (the lower bound increment) / (the upper bound) $< \varepsilon_2$

where ε_1 and ε_2 are predetermined values that are fairly small compared to 1.0, which define the convergence level of a particular analysis. For the numerical examples in this chapter, ε_1=0.05 and ε_2=0.001 are used. The performance of the newly-suggested termination criteria will be tested and compared to that of the criteria proposed in the B^3 method for truss (in Chapter 3).

4.3. Numerical Example I: FE Multi-layer Daniels System

In this section, the multi-layer Daniels system which was introduced in Chapter 3 is considered again as a numerical verification example of the B^3 method for continuum. This is because 1) the structure is simple and widely used as a numerical example to test a new system reliability

analysis method (as discussed in Section 3.3); and 2) since the system consists of discrete members (bars) and far-field stress is available, the B^3 method for truss is also applicable to this example, which enables us to investigate the impact of the approximation of the limit-state function formulation in Eq. (4.11).

4.3.1. Problem description

The structural behavior is the same as the one in Chapter 3, and the component and system failure definitions are also identical with Chapter 3. As shown in Figure 4.3 (left), the multi-layer Daniels system consists of six bars that are assumed to be perfectly brittle and to have identical and deterministic elastic moduli. The cross sectional areas of the bars are given as A_1=100mm^2, A_2=A_3=50mm^2, and A_4=A_5=A_6=33.33mm^2, and their widths are W_1=38.1mm, W_2=W_3=19.05mm, and W_4=W_5=W_6=12.7mm. In this example, the uncertainties of initial crack length a_i^0, external load I, and C and m in Paris equation are considered as random variables with the mean values 0.11 (mm), 17.2 (kN), 1.36×10^{-13} (mm/cycle/(MPa·mm)^m), and 3.0, respectively. It is assumed that the initial crack length follows exponential distribution and the other random variables follow lognormal distribution. The coefficients of variation (c.o.v.) of a_i^0, I, C, and m are 1.0, 0.1, 0.533, and 0.02, respectively. For the sake of simplicity, all random variables are assumed to be statistically independent of each other. In addition, the following deterministic parameters are used: the loading frequency (v_0): 100 (cycle/hour), the inspection cycle (T_s): 2,000 hours, and the critical crack lengths: a_1^c=30.48mm, a_2^c= a_3^c=15.24mm, and a_4^c= a_5^c= a_6^c=10.16mm.

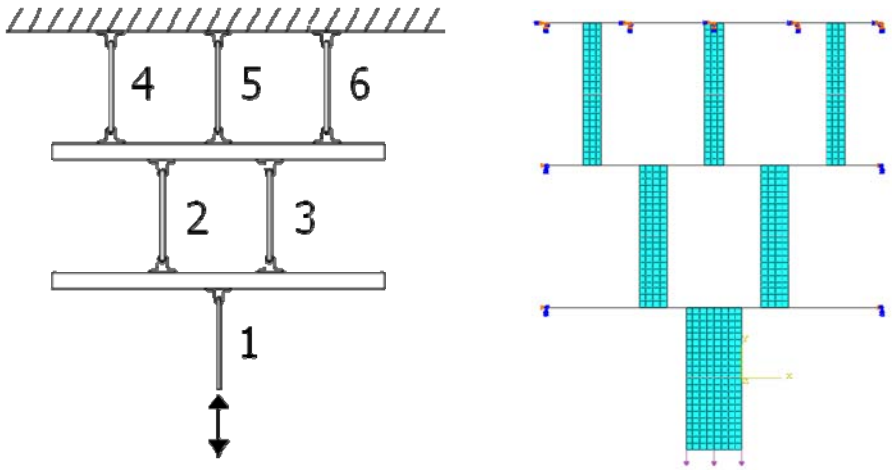

Figure 4.3 Multi-layer Daniels system (left); and its FE model in ABAQUS® (right)

Compared to the example in Chapter 3, some deterministic and random parameters are changed. Although most of the changes are not significant for the system reliability analysis of the structure, it is noticeable that the constant geometric function (i.e. $Y(a)$=3 in Section 3.3.1) is not employed to make the example more realistic. The specific geometric function will be provided in the following section.

Based on the above conditions, a finite element (FE) model is constructed for ABAQUS® as shown in Figure 4.3 (right). Figure 4.4 shows the FE responses of the intact structure and the damaged structure with member 2's failure (circle) for example. As stated in Section 3.2, the stress distribution estimated by the FE analysis is transferred to AFGROW®, and the corresponding a-ΔK relation is returned for calculating the time terms in Eq. (4.11).

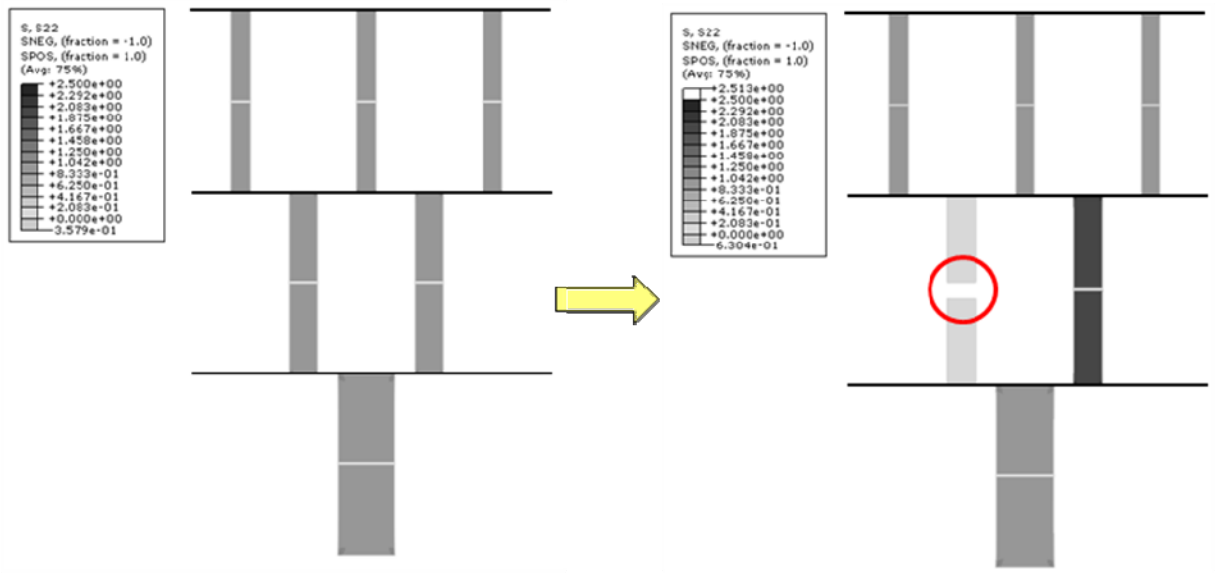

Figure 4.4 The stress distribution of the intact structure (left); and the damaged structure after the failure of the member 2 (right)

4.3.2. Analysis results

Figure 4.5 shows the updates of the upper and lower bounds of system failure probability with the number of "FE simulations" during the analysis employing the B^3 method for continuum. It is noteworthy from Figure 4.2 that each of FE simulations leads to either a branching or a system failure case identification, which decreases the upper bound or increases the lower bound, respectively. When the analysis is terminated, the upper and lower bounds are estimated as 1.010×10^{-2} and 9.608×10^{-3} for 30 FE simulations.

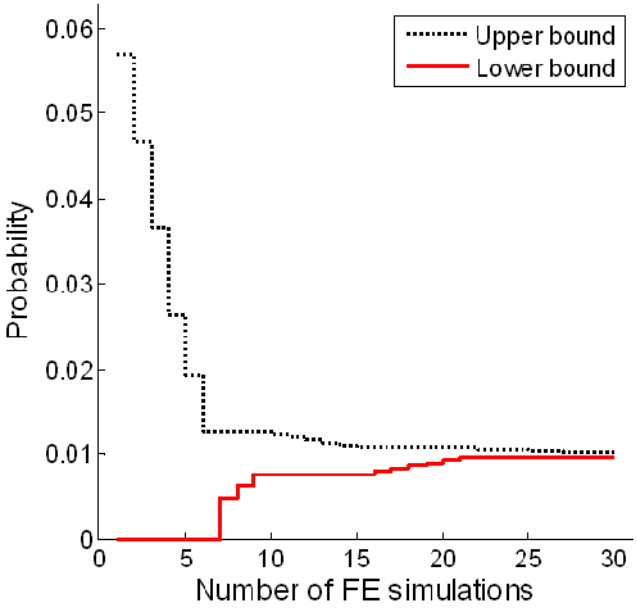

Figure 4.5 Bounds on the system failure probability by the B^3 method for continuum

Since the load is assumed to be equally distributed to the remaining bars on each story, the far-field stress in each bar is easily calculated by dividing the external load by the sum of the cross sectional areas of the remaining bars in this example. Therefore, this problem can be also solved by the B^3 method for truss (i.e. the B^3 method in Chapter 3 before further developments described in this chapter) as well. Based on the far-field stress, we are able to estimate ΔK by use of Newman's approximation in Eq. (3.2) and the following geometry function (Harter 2006, Tada *et al*. 1985):

$$Y(a)=\frac{\left\{0.752+2.02\frac{a}{W}+0.37\left[1-\sin\left(\frac{\pi a}{2W}\right)\right]^3\right\}}{\cos\left(\frac{\pi a}{2W}\right)}\times\sqrt{\frac{2W}{\pi a}\tan\left(\frac{\pi a}{2W}\right)} \tag{4.12}$$

where $Y(a)$ is the geometry function, a is the crack length, and W is the width of a plate.

By the B^3 method for truss, the bounds are estimated as 9.767×10^{-3} and 9.299×10^{-3} after 32 structural analyses. From Monte Carlo simulations (MCS) with 3×10^5 sets of generated random variables, the system failure probability is estimated as 9.807×10^{-3} (c.o.v.=1.83%), which requires 3.163×10^5 structural analyses. In addition, the B^3-based methods and MCS can also identify the critical failure sequences in the decreasing order of their probabilities. For the nine most critical failure sequences, which can be categorized into three failure patterns, all three methods provide the exact same order of patterns as shown in Table 1. Due to the symmetry, the second and third failure patterns respectively have two and six failure sequences with the same likelihoods. It is noted that MCS does not provide us with such symmetric results due to its random-sampling nature. All the results from three different approaches match well, and the slight difference between the results from the B^3 method for truss and the B^3 method for continuum is mainly due to the approximation introduced in Eq. (4.11).

Identified failure sequence	Probability by the B^3 method for truss ($\times 10^{-3}$)	Probability by the B^3 method for continuum ($\times 10^{-3}$)	Probability by Monte Carlo simulation ($\times 10^{-3}$)
1	4.871	4.869	4.660
2 → 3	1.332	1.408	1.263
3 → 2	1.332	1.408	1.353
4 → 5 → 6	0.294	0.321	0.320
4 → 6 → 5	0.294	0.321	0.307
5 → 4 → 6	0.294	0.321	0.335
5 → 6 → 4	0.294	0.321	0.363
6 → 4 → 5	0.294	0.321	0.341
6 → 5 → 4	0.294	0.321	0.322

Table 4.1 Identified critical failure sequences in the continuum Daniels system

Lastly, in Figure 4.5, it is noted that the upper bound curve becomes almost flat relatively early in the search, at a level fairly close to the actual system risk confirmed by MCS. This is because, as the search proceeds, FE analyses are performed for systems with more damage and less redundancy. Most of the updates are thus made on the lower bound. Therefore, in most cases, it is not necessary to wait until the bounds converge to each other too closely, which is the motivation for introducing an additional termination criterion on the lower bound in Section 4.2.3.

4.4. Numerical Example II: Longeron in Aircraft Structure

In order to test the applicability of the proposed method to continuum structures, an aircraft longeron system is considered, which is a non-discrete structural system with a higher level of structural complexity compared to truss-type structures. A longeron is a thin strip of metal, wood, or carbon fiber, to which the skin of the aircraft is fastened, and has been widely used as a target structure of verification examples (Heida and Grooteman 1998, Gooteman 2008, Taylor 1998)

due to the following advantages: (1) Despite their structural complexity, it is easy to identify "hot spots" which have relatively high stresses and are generally located around fasteners; (2) Local failure of a fastener can be described as the event that its crack length exceeds a critical level; and (3) It is relatively simple to reflect the damage or failure of the identified member in the FE model.

4.4.1. Structural configuration and loading

Figure 4.6 shows an FE model of longeron system developed in ABAQUS® and the numbering choices of 40 fastener holes, which are considered as possible locations of crack failures. A big plate on the bottom is a part of the aircraft skin, and the assembled structure on the skin represents the longeron. Figure 4.7 displays how parts in the longeron are assembled. Two long T-shaped parts are overlapped in the middle, and then fastened with two small plates. It is assumed that the main material of the skin and longeron is aluminum. All the parts are attached together by 6.35mm (0.25-inch) diameter fasteners made of steel, i.e. D=6.35mm. The fasteners are simulated by spring elements. Around the fasteners, the edge of each part has $3\times D$ distance from the center of the first fastener, and the pitch between fasteners has a $6\times D$ distance. Assuming the longeron system is located in an upper fuselage under bending caused by vertical acceleration, the system is subjected to pure tension/compression loads, which cause an initial crack of around each fastener hole to grow from hole to the nearest edge. Figure 4.8 shows the load re-distribution caused by a local crack failure (circle).

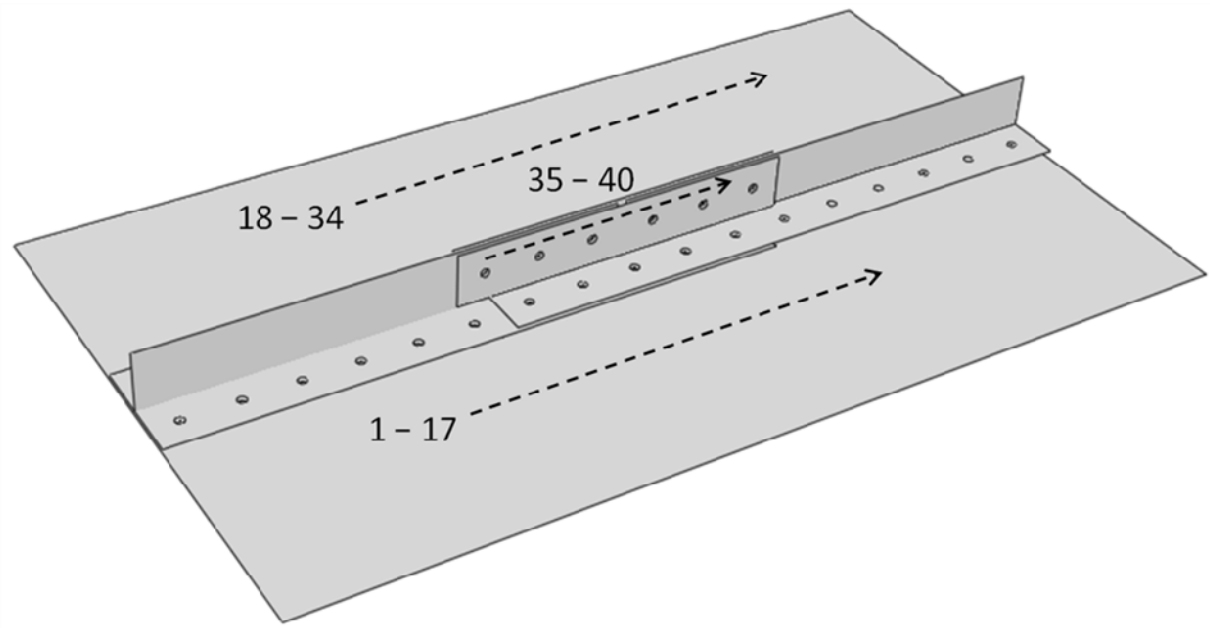

Figure 4.6 Longeron FE model and fastener hole numbers

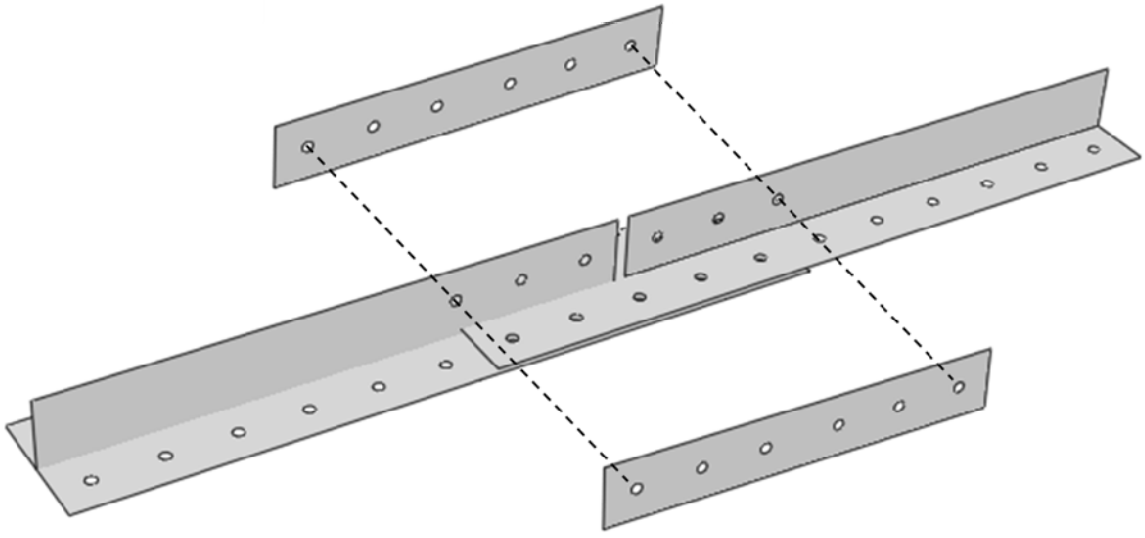

Figure 4.7 Assembly of longeron FE model

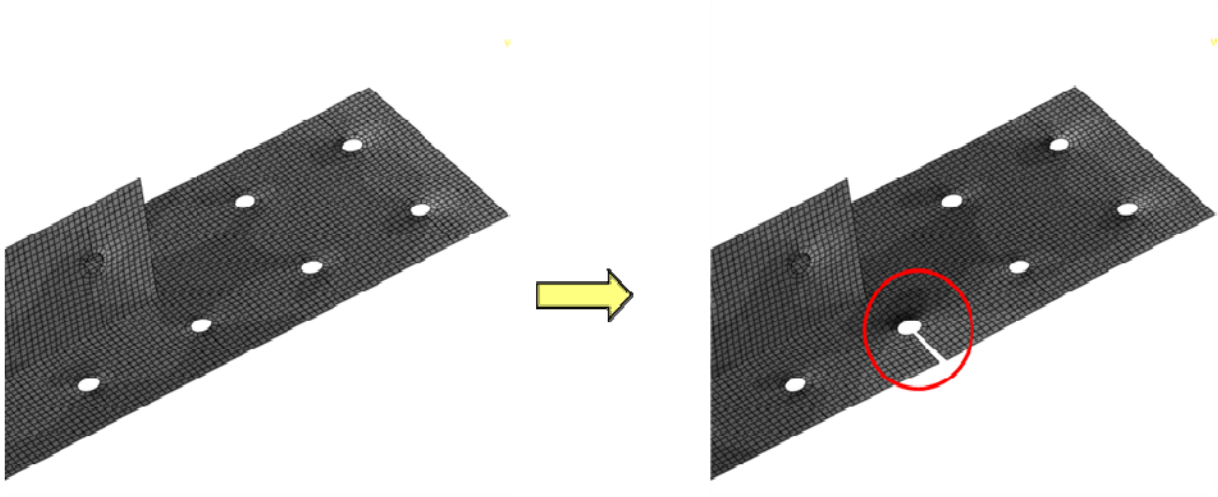

Figure 4.8 Load re-distribution after a local failure by an FE simulation

The loading intensity, the loading frequency (ν_0), the inspection cycle (T_s), and the critical crack lengths are given as 206.8 Mpa, 15/hour, 2,000 hours, and 12.7mm, respectively. These parameters are assumed to be deterministic. The uncertainty in the loading amplitude is described by a random load-scale factor I as explained in the following section.

4.4.2. Statistical parameters

The statistical properties of the random variables are summarized in Table 4.2. The values of the statistical parameters in the table were determined based on a comprehensive literature survey performed in Chapter 3. In this example, one random variable I is used to describe the uncertainty in the loading intensity (i.e. the loading intensity 206.8 Mpa is scaled by this random variable), and each of 40 fastener holes has one random variable of a^0. In addition, based on findings from preliminary deterministic FE analysis, hot spots are identified around all fastener holes on the two T-shaped parts. For that reason, two random variables are assigned to represent

C and m of each of the two parts. Therefore, a total of 45 random variables are used. All random variables are assumed to be statistically independent of each other except the following cases for which non-zero correlation coefficients are assigned: (1) between Paris equation parameters (C) of two different parts (correlation coefficient: 0.6); (2) between Paris equation parameters (m) of two different parts (correlation: 0.6); (3) between initial crack lengths (a^0) of two different fastener holes (correlation: 0.6); (4) between C and m of the same parts (correlation: −0.97); and (5) between C and m of two different parts (correlation: −0.6).

Random variables	Mean	c.o.v.	Distribution type	Number of random variables
C	1.202×10^{-13}	0.533	Lognormal	2
m	3.0	0.02	Lognormal	2
a^0 (mm)	0.11	1.0	Exponential	40
I	1.0	0.1	Lognormal	1

Table 4.2 Statistical properties of random variables

The correlation coefficients in cases (1), (2), (3), and (5) can be changed depending on how closely the manufacture processes of two different parts are related to each other. However, it is noted the strong negative correlation between C and m in case (4) has been presented in several studies reported in the literature (Yarema 1980, Borrego *et al*. 2001).

4.4.3. Component and system failure definitions

In this example, it is assumed that the section around a fastener hole fails when its crack length reaches the 80% of the distance between the fastener hole and the edge; however, one can use another component failure definition of interest. Upon the occurrence of such a section failure,

the corresponding crack is embodied in the FE model, which causes stress re-distribution as shown in Figure 4.8 (right).

As an attempt to accurately identify system failure cases via FE analyses instead of introducing heuristic system failure criteria, in this example, it is assumed that the structural system fails if net-section yielding occurs around any hole in the system (i.e. the average stress of the area excluding a hole and a crack reaches the yielding stress limit). The yield strengths of aluminum and steel are given as 496.4 and 517.1 MPa, respectively. It should be noted that this is an example of system failure criteria that can be used during a B^3 search. Like the component failure criteria, one can introduce a set of his/her own system failure criteria (e.g., the occurrence of a local yielding and the observation of a large displacement) based on the objectives and safety concerns of a target structure.

4.4.4. Analysis results

Figure 4.9 shows the updates of the upper and lower bounds made by the B^3 method for continuum. With the new termination criteria described in Section 3.3, the lower and upper bounds are respectively 1.192×10^{-3} and 1.321×10^{-3} after only 156 FE simulations. With the old criteria (i.e. the first one only), however, both bounds are respectively 1.209×10^{-3} and 1.273×10^{-3} for 406 FE simulations. In the previous multi-layer Daniels system and the numerical examples in Lee and Song (2011a), it was noted that the actual system risk was closer to the upper bound rather than the lower bound. Without no significant update in the upper bound, the old termination criteria requires 7 more days to perform 250 more FE simulations using a general personal computer (2.61 GHz CPU and 3.25 GB RAM). These additional costs are consumed mostly for identifying many negligible failure sequences and making slight updates on the lower

bound. This is because the longeron system has many failure sequences which have a similar level of likelihood.

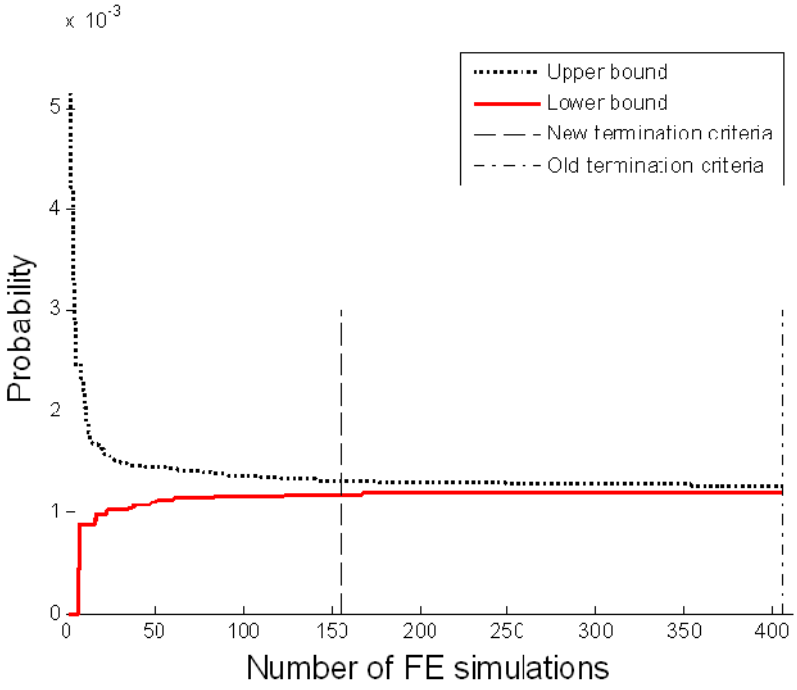

Figure 4.9 Bounds by the B^3 method with old and new termination criteria

In addition, the critical failure sequences are identified in the decreasing order of their likelihood. The eight most critical failure sequences, which can be grouped into four major patterns, are listed in Table 4.3. As shown in the table, we can observe various system failure sequences on different locations and materials. It is noteworthy that the results of the B^3 analysis reflect the symmetry of the longeron, which can be easily confirmed from Figure 4.6.

Identified failure sequence	Probability by the B^3 method ($\times 10^{-3}$)	Yielding material	Yielding location
11	4.448	aluminum	around #11 hole
28	4.448	aluminum	around #28 hole
22 → 5	0.480	steel	#35 fastener
5 → 22	0.480	steel	#35 fastener
23 → 11	0.282	aluminum	around #11 hole
6 → 28	0.282	aluminum	around #28 hole
6 → 22 → 4	0.109	steel	#35 fastener
23 → 5 → 21	0.109	steel	#35 fastener

Table 4.3 Identified critical system failure sequences in the aircraft longeron structure

Lastly, it should be also noted that the B^3 method for truss is not applicable to this continuum problem, and MCS would not be a feasible option due to the computational cost. The minimum number of samples (N_δ) to achieve a target level of c.o.v.(δ) can be calculated by $N_\delta = (1-P_f)/(\delta^2 P_f)$ where P_f is the probability of the event of interest (Haldar and Mahadevan 2000). For 5% c.o.v., therefore, it would be required to explore 3×10^5 samples with a similar number of FE simulations. However, it is impossible to perform such a huge number of FE analyses even though each analysis takes only a few minutes. Furthermore, the computational cost will significantly increase if a lower level of probability is expected or one aims to achieve a high-level of convergence (i.e. low c.o.v. value). On the other hand, the proposed method allows us to perform system reliability analysis for only 156 FE simulations.

4.5. Summary

In this chapter, the Branch-and-Bound (B&B) method employing system reliability Bounds (proposed in Chapter 3) is further developed for FE-based system reliability analysis of fatigue-induced sequential failures of continuum structures. Despite merits over existing branch-and-

bound approaches, the B^3 method which was originally developed for truss is not readily applicable to continuum structures because of its limitations in (1) describing general stress distributions in limit-state formulations; (2) evaluating stress intensity range based on the crack length; and (3) dealing with slow convergence of the bounds for continuum. In order to overcome these limitations, (1) the limit-state function was modified to incorporate general stress distribution instead of using far-field stress assumption; (2) an external computer program such as AFGROW® was incorporated into the B^3 computational framework to estimate the stress intensity range for the given stress distribution; and (3) the termination criteria of B^3 analysis was modified to avoid performing unnecessary simulations that would make insignificant updates on the lower bound. The B^3 method for continuum was demonstrated by a numerical example of multi-layer Daniels system, and the results were verified by the B^3 method for truss and Monte Carlo simulation. Furthermore, the proposed method was applied to a numerical example of aircraft longeron system. It was successfully shown that the proposed method enable us to perform system reliability analysis of fatigue-induced sequential failures using a large-scale FE models.

5. INSPECTION-BASED SYSTEM RELIABILITY UPDATING FOR FATIGUE-INDUCED SEQUENTIAL FAILURE

As discussed in Chapters 3 and 4, fatigue-induced sequential failure is one of the major failure modes of a structural system, and an adequate level of structural redundancy should be provided to avoid the disastrous collapse of the structural system. Such structural safety can be guaranteed through not only proper structural design, but also structural maintenance such as inspection. For efficient risk-based maintenance, it is thus essential to estimate the reliability of a structure against fatigue-induced sequential failures and update the original reliability based on the observations from inspections. The development of the B^3 method enables us to perform system reliability analysis of fatigue-induced sequential failures of discrete structures (Chapter 3) and continuum structures (Chapter 4). This chapter introduces a new system reliability updating method employing the B^3 method. The new method allows us to update the original system-level reliability of a structure based on inspection results in an accurate and efficient way.

5.1. Literature Review

Much research effort has been dedicated to the inspection-based reliability updating of structures, and several approaches have been developed as a result. These approaches are categorized as "parameter updating" (or "model updating") and "reliability updating" (Moan and Song 2000). In parameter updating, the distribution parameters of random variables (such as mean and standard deviation) are updated using the inspection results to reduce statistical uncertainties in the random variables by the additional information from the inspection. Updating statistical parameters naturally leads to updated reliability estimates of the structure. There has been

increasing interest in solving this challenging problem, especially by the use of a Bayesian approach (Box and Tiao 1992, Sivia 1996), and a comprehensive review of parameter updating (model updating) can be found in Beck and Au (2002). By contrast, in reliability updating, the new information obtained from inspections is used directly to update the original reliability which was calculated during the design process to the conditional probability given inspection results. In either approach, if the updated reliability reveals that the structure does not have an adequate level of safety, additional structural members or repair efforts can be introduced.

The choice of an updating approach depends mainly on the nature of additional information available from inspections and the structural details. If the original statistical data of the random variables are not reliable and need to be more robust, they can be updated through inspection and the reliability can be further updated using the updated statistical parameters. The original reliability can be updated directly if the statistical parameters are reliable. In this thesis, the focus will be on reliability updating.

There have been many studies about inspection-based reliability updating. Many of the previous studies focused on updating the original reliability of the structural members (Madsen 1985, Jiao and Moan 1990, Zhao *et al*. 1994). In these studies, the sources of uncertainty in structural inspections were defined and the types of inspection event were classified. However, both initial reliability analysis and updating were limited to component events. In a variety of structures, however, the system aspects need to be considered for accurate risk estimation and inspection-based reliability updating (Moan and Song 2000). In particular, the structural reliability against fatigue-induced sequential failures needs to be analyzed at the system level as discussed in Chapters 3 and 4, and it is the same with inspection-based reliability updating. However, system reliability updating is a challenging task because the common or correlated

random variables involved with fatigue crack growth may result in significant statistical dependence among the failures of different structural members or among inspected and uninspected members. Furthermore, due to the nature of fatigue-induced sequential failure, each structural member generally contributes to multiple important failure sequences.

It is noted that simulation techniques have been employed in some previous studies. Because there is a challenge in treating "reliability updating" using simulation techniques, most of the studies employing simulation techniques dealt with "parameter updating." In order to overcome the challenge, Straub (2011) developed a method to make various reliability analysis methods including simulation techniques applicable to reliability updating. (The challenge and the method proposed by Straub (2011) will be discussed in more details, in Section 4.1.2.) In addition, Beck and Au (2002) also employed a simulation approach to obtain updated reliability estimates of a structure. These simulation-based-approaches are straightforward and help account for system effects in structural behavior and inspections. However, due to the nature of simulation-based techniques, they may require exceedingly large cost for converged results, especially when the level of the updated probability is low.

The existing simulation- and non-simulation-based studies on reliability updating have a couple of important points in common. First, the original probability can be updated whether an inspection detects a crack or not, which allows for the full usage of the inspection results during the update. Second, reliability updating is affected by uncertainty in detection, which is often characterized by the probability of detection (POD). In reality, a crack may not be detected due to an error by the detection device. Of course, POD increases if a crack-detection device with a high resolution is used. Much effort has been devoted in various industries to evaluate the quality of non-destructive techniques (NDT) for inspection for cracks in metals, and the likelihood that a

crack is detected is expressed by a POD curve for the NDT used for inspection. A detailed literature review of POD can be found in Moan and Ayala-Uraga (2008).

Since these studies on reliability updating methodologies, several further studies have been conducted on optimal inspection strategies. In general, strategies are categorized as risk based inspection (RBI) or cost based inspection (Soares 2000). According to Straub (2004), the research about RBI began in the early 1970's, and quantitative inspection models were first investigated to update deterioration models using Bayes' rule (Tang 1973). Yang and Trapp (1974) presented a sophisticated procedure that allowed for the computation of the probability of fatigue failure for aircraft under periodic inspections, taking into account the uncertainty in the inspection performance. Based on this procedure, Yang and Trapp (1975) introduced a method for optimizing inspection frequencies. A more detailed literature review can be found in Straub (2004).

On the other hand, Toyoda-Makino and Tanaka (1998) proposed a cost-based optimal inspection strategy for random fatigue crack growth. Their results showed that using reliability as the only criterion was contrary to engineering reality, since structural system availability is being degraded while inspection cost is increasing. It is also considered that periodical inspections are not always effective for fatigue failure because the fatigue crack growth rate gradually accelerates as the fatigue damage grows. For these reasons, the authors proposed an optimal inspection schedule minimizing cost for fatigue failure. There have been several other studies about cost-based inspection planning, and a detailed review is presented in Soares (2000).

Another noticeable point of previous studies about inspection-based reliability updating is the types of structure that have been considered. The most common are offshore structures because, in reality, the offshore industry often requires that the structural integrity of fixed

offshore platforms be ensured by periodic inspection. For this reason, several authors have dealt with offshore structures in their research, e.g., Wirching *et al*. (1990), Baker and Descamps (1999), and Jiao and Moan (1990). The authors first derived formulations describing fatigue-induced failure to perform an initial fatigue reliability analysis and then discussed optimal inspection planning and maintenance strategies. In their formulations, however, the stress of structural members was mostly assumed to have uniform distribution because offshore platforms can be considered as truss. The approaches based on this assumption cannot deal with continuum structures that usually show non-uniform stress distribution. Although there have been several studies for other types of structures, such as aircraft structures by Yang and Trapp (1974), Itagaki and Ito (1998), and Deodatis *et al*. (1992), and bridges by Zhao *et al*. (1994), the formulations were all based on uniformly-distributed stress.

In spite of the aforementioned research efforts about reliability updating and further applications, there have been few studies about fatigue-induced sequential failure. In addition, most of the existing studies focus on marine structures (Moan and Song 2000, Moan and Ayala-Uraga 2008) and bridges (Zhao *et al*. 1994, Zhu and Wu 2011) modeled by discrete structural models, and there is a lack of research for other structural types such as continuum. These motivated the development of a new system reliability updating method for fatigue-induced sequential failure over truss and continuum. This chapter proposes a new system reliability updating method employing the B^3 method.

5.2. Reliability Updating through Inspection Events

In many previous studies about inspection-based reliability updating, researchers have constructed the basic formulations starting from conditional probability. First, let us describe the probability of an event as

$$P_i = P\left(E_i\right) \tag{5.1}$$

where E_i stands for a general event of interest at the i-th structural member. Although a component event is introduced in Eq. (5.1) and used in the following derivation, it can be replaced by a system event if one aims to update the system reliability. The probability P_i in Eq. (5.1) is updated to the following conditional probability based on an inspection result at the j-th member:

$$P_{i,up} = P\left(E_i \mid IE_j\right) \tag{5.2}$$

where IE_j stands for an inspection event at the j-th member. Reliability updating can be made whether the member of interest was actually inspected (i.e. $i = j$) or not (i.e. $i \neq j$).

Eq. (5.2) can be extended to utilize multiple available inspection results for reliability updating. The updated probability at the i-th member is

$$P_{i,up} = P\left[E_i \mid IE_j \bigcap IE_k \bigcap \cdots \bigcap IE_l\right] \tag{5.3}$$

where IE_j, IE_k, …, IE_l denote the inspection events observed at multiple structural members. The impact of using several inspection events to reliability updating will be discussed in the following numerical examples.

Inspection results are normally categorized into two types of events: "equality" and "inequality" types, depending on whether a crack is detected or not. Since inspections are generally made at multiple locations, there are three possible combinations of the inspection results, inequality, equality, and mixed cases (Jiao and Moan 1990), as explained in detail below.

5.2.1. Inequality case

Suppose no crack is detected from inspection at single or multiple members. There are two possible explanations for the inspection result. First, a crack is too small to be detected. Second, although a relatively large crack actually exists at the inspected location, it may be missed due to human error or the limitations of the detecting device. In either case, this event can be described as an "inequality" event, i.e.

$$IE_j : g_{j,no}(\mathbf{X}) = T_I - T_j^d(\mathbf{X}) < 0 \tag{5.4}$$

where $\mathbf{X}$ denotes the vector of random variables including detectable crack size, T_j^d denotes the required time for the crack growth to a detectable crack size at the j-th member, and T_I denotes the time that the member is inspected. The detectable crack size is related to a specific inspection method and modeled as a random variable reflecting the actual probability of detection (POD) curve. Among several stochastic formulations of POD available, numerical examples in this study use the exponential distribution, which is commonly used in the literature (Moan and Song 2000).

The conditional probability given the event in Eq. (5.4), i.e. single inequality event, may be calculated as

$$P_{i,up} = P\left(E_i \mid IE_j\right) = \frac{P\left(E_i \cap IE_j\right)}{P\left(IE_j\right)} = \frac{P\left[E_i \cap \left(g_{j,no}\left(\mathbf{X}\right) < 0\right)\right]}{P\left(g_{j,no}\left(\mathbf{X}\right) < 0\right)} \tag{5.5}$$

Likewise, the conditional probability given multiple inequality events is calculated as

$$\begin{aligned} P_{i,up} &= P\left(E_i \mid IE_j \cap \cdots \cap IE_k\right) = \frac{P\left(E_i \cap IE_j \cap \cdots \cap IE_k\right)}{P\left(IE_j \cap \cdots \cap IE_k\right)} \\ &= \frac{P\left[E_i \cap \left(g_{j,no}\left(\mathbf{X}\right) < 0\right) \cap \cdots \cap \left(g_{k,no}\left(\mathbf{X}\right) < 0\right)\right]}{P\left[\left(g_{j,no}\left(\mathbf{X}\right) < 0\right) \cap \cdots \cap \left(g_{k,no}\left(\mathbf{X}\right) < 0\right)\right]} \end{aligned} \tag{5.6}$$

5.2.2. Equality case

If a crack is detected and measured, this inspection event is described as an "equality" event and formulated as

$$IE_j : g_{j,yes}\left(\mathbf{X}\right) = T_I - T_j^m\left(\mathbf{X}\right) = 0 \tag{5.7}$$

where T_j^m denotes the required time for the crack growth to the measured crack size at the j-th member. In the equation, it should be noted that T_j^m is equal to the inspection time T_I, which makes the formulation different from the limit-state formulations in Eq. (5.4).

The conditional probability given the equality event in Eq. (5.7) is calculated as

$$P_{i,up} = P\left(E_i \mid IE_j\right) = \frac{P\left(E_i \cap IE_j\right)}{P\left(IE_j\right)} = \frac{P\left[E_i \cap \left(g_{j,yes}\left(\mathbf{X}\right) = 0\right)\right]}{P\left[g_{j,yes}\left(\mathbf{X}\right) = 0\right]} \tag{5.8}$$

The updated probability $P_{i,up}$ in Eq. (5.8) cannot be easily calculated using existing structural reliability methods because both numerator and denominator are close to zero. In order to

facilitate the calculation, the following alternative formulation is used. First, Eq. (5.8) can be alternatively described as

$$P_{i,up} = \lim_{\theta \to +0} \frac{P\left[E_i \cap \left(-\theta < g_{j,yes}\left(\mathbf{X}\right) \le 0 \right) \right]}{P\left(-\theta < g_{j,yes}\left(\mathbf{X}\right) \le 0 \right)} \tag{5.9}$$

In the equation, infinitesimal is θ introduced to eliminate the equal signs in Eq. (5.8). Eq. (5.9) is equal to

$$P_{i,up} = \lim_{\theta \to +0} \frac{P\left[E_i \cap \left(g_{j,yes}\left(\mathbf{X}\right) \le 0 \right) \right] - P\left[E_i \cap \left(g_{j,yes}\left(\mathbf{X}\right) \le -\theta \right) \right]}{P\left(g_{j,yes}\left(\mathbf{X}\right) \le 0 \right) - P\left(g_{j,yes}\left(\mathbf{X}\right) \le -\theta \right)} \tag{5.10}$$

Finally, Eq. (5.10) can be transformed to the ratio of the sensitivities with respect to the parameter θ, i.e.

$$P_{i,up} = \left[\frac{\frac{\partial}{\partial \theta} P\left[E_i \cap \left(g_{j,yes}\left(\mathbf{X}\right) + \theta \le 0 \right) \right]}{\frac{\partial}{\partial \theta} P\left[\left(g_{j,yes}\left(\mathbf{X}\right) + \theta \le 0 \right) \right]} \right]_{\theta = 0} \tag{5.11}$$

This formulation is the same as shown in Moan and Song (2000), and the updated probability can be calculated via numerical differentiation of the results of reliability analysis performed by use of an existing reliability analysis method.

Likewise, the conditional probability given multiple equality events is formulated as follows.

$$P_{i,up} = P\left(E_i \mid IE_j \cap \cdots \cap IE_k\right) = \frac{P\left(E_i \cap IE_j \cap \cdots \cap IE_k\right)}{P\left(IE_j \cap \cdots \cap IE_k\right)}$$
$$= \frac{P\left[E_i \cap \left(g_{j,yes}(\mathbf{X}) = 0\right) \cap \cdots \cap \left(g_{k,yes}(\mathbf{X}) = 0\right)\right]}{P\left[\left(g_{j,yes}(\mathbf{X}) = 0\right) \cap \cdots \cap \left(g_{k,yes}(\mathbf{X}) = 0\right)\right]} \tag{5.12}$$

The equation is transformed to the ratio of sensitivities with respect to the parameters $\theta_1, \ldots, \theta_n$, that is,

$$P_{i,up} = \left[\frac{\dfrac{\partial^n}{\partial\theta_1 \cdots \partial\theta_n} P\left[E_i \cap \left(g_{j,yes}(\mathbf{X}) + \theta_1 \le 0\right) \cap \cdots \cap \left(g_{k,yes}(\mathbf{X}) + \theta_n \le 0\right)\right]}{\dfrac{\partial^n}{\partial\theta_1 \cdots \partial\theta_n} P\left[\left(g_{j,yes}(\mathbf{X}) + \theta_1 \le 0\right) \cap \cdots \cap \left(g_{k,yes}(\mathbf{X}) + \theta_n \le 0\right)\right]} \right]_{\theta_1 = \cdots = \theta_n = 0} \tag{5.13}$$

where n is the number of the observed "equality" events. The updated probability $P_{i,up}$ in Eq. (5.13) can also be calculated using the n-th order numerical differentiation. However, this equation needs to be used with a caution, because such a high-order numerical differentiation can create significant error unless the probability calculations in numerator and denominator are extremely accurate. This may give rise to the research needs for new methods to evaluate component and system reliability estimate more precisely than the existing methods. However, this is out of the scope of this thesis, and multiple equality events will not be handled in the numerical examples.

5.2.3. Mixed case

In most practical situations, inspections are made at multiple locations at a given time, which often results in a mixed set of inequality and equality events. To derive the formulation for such

"mixed cases," the simplest case involved with single inequality event and single equality event is first considered. From Eq. (5.3), the updated failure probability is formulated as

$$P_{i,up} = P\left[E_i \mid IE_j \cap IE_k \right] \tag{5.14}$$

where IE_j and IE_k denote the inequality event and equality event, respectively. Using Eqs. (5.5) and (5.8), Eq. (5.14) is further derived as follows.

$$P_{i,up} = \frac{P\left(E_i \cap IE_j \cap IE_k \right)}{P\left(IE_j \cap IE_k \right)} = \frac{P\left[E_i \cap \left(g_{j,no}\left(\mathbf{X}\right) < 0 \right) \cap \left(g_{k,yes}\left(\mathbf{X}\right) = 0 \right) \right]}{P\left[\left(g_{j,no}\left(\mathbf{X}\right) < 0 \right) \cap \left(g_{k,yes}\left(\mathbf{X}\right) = 0 \right) \right]} \tag{5.15}$$

Based on the same derivation as Eqs. (5.8) - (5.11), Eq. (5.15) can be transformed to

$$P_{i,up} = \left[\frac{\dfrac{\partial}{\partial \theta} P\left[E_i \cap \left(g_{j,no}\left(\mathbf{X}\right) < 0 \right) \cap \left(g_{k,yes}\left(\mathbf{X}\right) + \theta \le 0 \right) \right]}{\dfrac{\partial}{\partial \theta} P\left[\left(g_{j,no}\left(\mathbf{X}\right) < 0 \right) \cap \left(g_{k,yes}\left(\mathbf{X}\right) + \theta \le 0 \right) \right]} \right]_{\theta=0} \tag{5.16}$$

Finally, this formulation can be generalized for a mixed case involved with multiple inequality and equality inspection events as

$$\begin{aligned} P_{i,up} = \Bigg\{ & \frac{\partial^n}{\partial \theta_1 \cdots \partial \theta_n} P\Big[E_i \cap \left(g_{j,no}\left(\mathbf{X}\right) < 0 \right) \cap \cdots \cap \left(g_{k,no}\left(\mathbf{X}\right) < 0 \right) \cap \\ & \left(g_{l,yes} + \theta_1 \le 0 \right) \cap \cdots \cap \left(g_{m,yes} + \theta_n \le 0 \right) \Big] / \\ & \frac{\partial^n}{\partial \theta_1 \cdots \partial \theta_n} P\Big[\left(g_{j,no}\left(\mathbf{X}\right) < 0 \right) \cap \cdots \cap \left(g_{k,no}\left(\mathbf{X}\right) < 0 \right) \cap \\ & \left(g_{l,yes} + \theta_1 \le 0 \right) \cap \cdots \cap \left(g_{m,yes} + \theta_n \le 0 \right) \Big] \Bigg\}_{\theta_1 = \cdots = \theta_n = 0} \end{aligned} \tag{5.17}$$

where n is the number of equality events. Furthermore, it can be easily seen that Eq. (5.17) is the combination of Eqs. (5.6) and (5.13). For the aforementioned difficulty in high order numerical differentiation, the mixed case with multiple equality events will not be discussed in this thesis.

5.3. System Reliability Updating Method Employing B^3 Method

To update the probability of a system failure caused by fatigue-induced sequential failures based on inspection results, a system reliability updating method is developed using the B^3 method. As explained in Chapters 3 and 4, the B^3 method identifies system failure and non-failure cases (i.e. black and white nodes in the event tree, see Figure 3.1) as disjoint events and obtains the upper and lower bounds of system failure probability. From Eq. (3.17), the conditional probability of the system failure is derived as the sum of conditional probabilities of the failure sequences given inspection events, i.e.

$$P(E_{sys} \mid IE) = \frac{P\left(\bigcup_{i=1}^{N_{fs}} (C_i \cap IE)\right)}{P(IE)} = \frac{\sum_{i=1}^{N_{fs}} P(C_i \cap IE)}{P(IE)} = \sum_{i=1}^{N_{fs}} P(C_i \mid IE) \tag{5.18}$$

where IE denotes an equality or inequality event observed during the inspection or the intersection of multiple observed events. Therefore, one can obtain bounds on the updated system failure probability by replacing the probabilities of the failure and non-failure cases identified by the B^3 analysis by the updated ones.

Therefore, the system reliability updating is a two-step procedure. First, B^3 analysis is performed to identify system failure and non-failure cases as well as to calculate upper and lower bounds on system failure probability. Second, the probabilities of the identified system failure cases (black nodes in the event tree) and non-failure cases (white nodes) are updated using Eqs.

(5.6), (5.13), and (5.17), and the updated upper and lower bounds on the updated system reliability are obtained. For example, Figure 5.1 shows the event tree in Figure 3.1 after updated by a given inspection event IE_i.

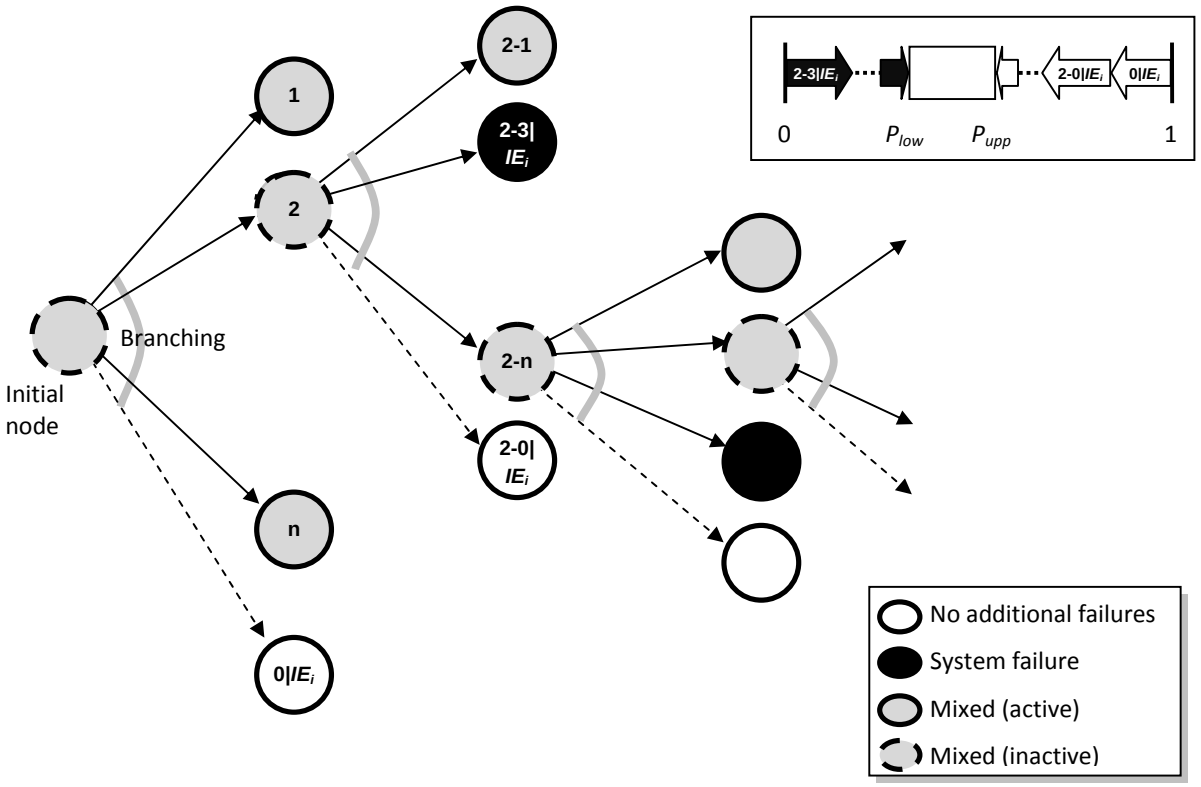

Figure 5.1 Probability updates for failure and non-failure cases

The mixed nodes (i.e. grey nodes) do not need to be updated because those are not used to compute the bounds, which helps achieve the updated bounds efficiently. Another advantage of this method is that the second step does not require additional structural analyses (or FE simulations). However, it is also important to note that the system failure sequences identified as critical ones for the original system failure probability may not be critical for the updated

(conditional) failure probability. Therefore, the bounds may get wider during the updating process.

For inequality cases, using Eqs. (3.4) and (4.1), the required time for the crack growth to a detectable crack size at the *j*-th member (T_j^d) in Eq. (5.4) can be derived as

$$T_j^d = \begin{cases} \dfrac{1}{C\nu_0\left(S_i^0\right)^m}\displaystyle\int_{a_i^0}^{a^d}\frac{1}{\left[Y(a)\sqrt{\pi a}\right]^m}da & \text{for truss} \\ \dfrac{1}{C\nu_0}\displaystyle\int_{a_i^0}^{a^d}\frac{1}{\left[\Delta K\right]^m}da & \text{for continuum} \end{cases} \tag{5.19}$$

where a^d is the detectable crack size during the inspection process.

For truss and continuum structures, therefore, the limit-state function for an inequality event in Eq. (5.4) is described as

$$IE_j : g_{j,no}\left(\mathbf{X}\right) = \begin{cases} T_I - \dfrac{1}{C\nu_0\left(S_i^0\right)^m}\displaystyle\int_{a_i^0}^{a^d}\frac{1}{\left[Y(a)\sqrt{\pi a}\right]^m}da < 0 & \text{for truss} \\ T_I - \dfrac{1}{C\nu_0}\displaystyle\int_{a_i^0}^{a^d}\frac{1}{\left[\Delta K\right]^m}da < 0 & \text{for continuum} \end{cases} \tag{5.20}$$

Likewise, for equality cases, the limit-state function in Eq. (5.7) is described as

$$IE_j : g_{j,yes}\left(\mathbf{X}\right) = \begin{cases} T_I - \dfrac{1}{C\nu_0\left(S_i^0\right)^m}\displaystyle\int_{a_i^0}^{a^m+\varepsilon^m}\frac{1}{\left[Y(a)\sqrt{\pi a}\right]^m}da = 0 & \text{for truss} \\ T_I - \dfrac{1}{C\nu_0}\displaystyle\int_{a_i^0}^{a^m+\varepsilon^m}\frac{1}{\left[\Delta K\right]^m}da = 0 & \text{for continuum} \end{cases} \tag{5.21}$$

where a^m is the measured crack size and ε^m is the measuring error. Lastly, for mixed case, Eq. (5.17) can be used with the Eqs. (5.20) and (5.21). The proposed method of system reliability updating for fatigue-induced sequential failures is tested and verified by the multi-layer Daniels system and aircraft longeron structure, both of which were already introduced in Chapters 3 and 4.

5.4. Numerical Example I: Multi-layer Daniels System

5.4.1. Problem description

In order to test the proposed method, a multi-layer Daniels system is considered as the first numerical example. Most of the details are exactly same as for the one in Section 4.3. Table 5.1 lists the hypothetical inspection scenarios investigated in the numerical example.

Case	Scenario number	Scenario description
Inequality	1	No crack is detected at member 1 (T_I = 2,000 hours & mean of a^d = 1.0 mm).
	2	No crack is detected at member 1 (T_I = 2,000 hours & mean of a^d = 0.5 mm).
	3	No crack is detected at member 1 (T_I = 4,000 hours & mean of a^d = 1.0 mm).
	4	No crack is detected anywhere (T_I = 2,000 hours & mean of a^d = 1.0 mm).
Equality	5	0.1mm crack is found at member 1 (T_I = 2,000 hours).
	6	0.3mm crack is found at member 1 (T_I = 2,000 hours).
	7	0.5mm crack is found at member 1 (T_I = 2,000 hours).
	8	0.5mm crack is found at member 1 (T_I = 4,000 hours).
Mixed	9	0.5mm crack is found at member 1, but nowhere else (T_I = 2,000 hours & mean of a^d = 1.0 mm).

Table 5.1 Inspection scenarios for generalized Daniels system

5.4.2. Statistical properties

As in Section 4.3, for the sake of simplicity, it is assumed that all the random variables are statistically independent. Their statistical properties including detectable crack size (a^d) and measuring error (ε^m) are shown in Table 5.2. The statistical information of the new random variables is determined based on a literature review (Moan and Song 2000).

Random variables	Mean	c.o.v.	Distribution type	Number of random variables
C	1.202×10^{-13}	0.533	Lognormal	6
m	3.0	0.02	Lognormal	6
a^0 (mm)	0.11	1.0	Exponential	6
a^d (mm) (inequality cases)	1.0 (0.5 for Scenario 2)	1.0	Exponential	Number of inspected members
ε^m (mm) crack sizing error (equality cases)	0	0.1 (standard deviation)	Normal	Number of inspections
I	1.0	0.1	Lognormal	1

Table 5.2 Statistical properties of random variables

It should be noted that the detectable crack size (a^d) and the crack sizing error (ε^m) in Table 5.2 are used only for inequality and equality cases, respectively, which means each instance of crack detection or non-detection brings an additional random variable. In mixed cases, both of the random variables are introduced, and the number of them is the same as the number of inspections regardless of crack-detection.

5.4.3. Analysis results

For a verification purpose, the updated reliability by the proposed method is compared to that by Monte Carlo simulation (MCS). For inequality case, it is straightforward to compute the updated

reliability using existing simulation techniques. However, if one or more observations are of the equality type, both numerator and denominator in Eq. (5.7) are very close to zero and the updated reliability cannot be evaluated directly using MCS. In order to overcome this challenge, a new method using a likelihood function has been developed (Straub 2011). In the method, equality information is transformed into inequality information, which enables reliability updating by use of a general MCS technique.

As explained in Section 5.2.2, for equality events, the reliability updating based on the proposed method has to be done carefully because it requires numerical differentiation using infinitesimal θ and the corresponding result is often sensitive to θ. In the numerical examples of this thesis, it was decided through numerical tests to use one percent of the limit-state function (i.e. $g_{j,yes}(\mathbf{X})$ in Eq. (5.17)) evaluated with the mean values of random variables as θ. Figure 5.2 shows the probabilities at multiple time points from the B^3 method and MCS. As shown in the figure, the failure probability increases with the increasing service time of the structure, and the results from the B^3 method and MCS match well.

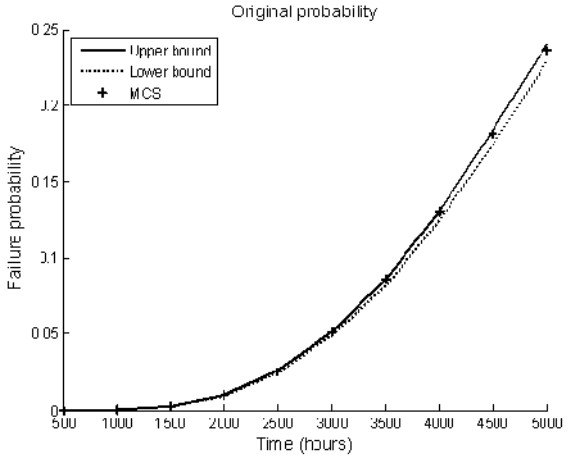

Figure 5.2 Original system failure probabilities by B^3 method and MCS

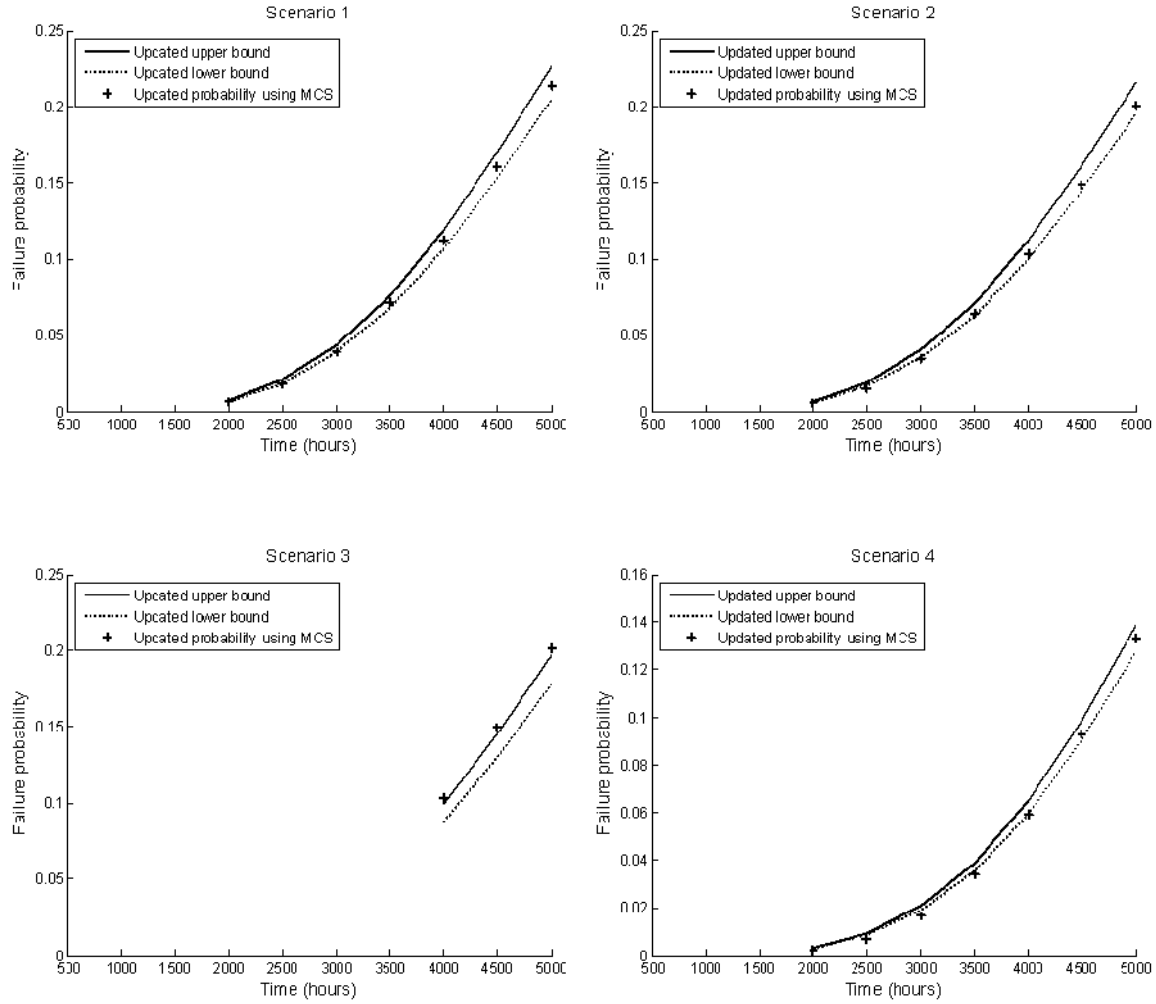

Figure 5.3 Updating results by the proposed method and MCS for inequality cases (Scenarios 1-4 in Table 5.1)

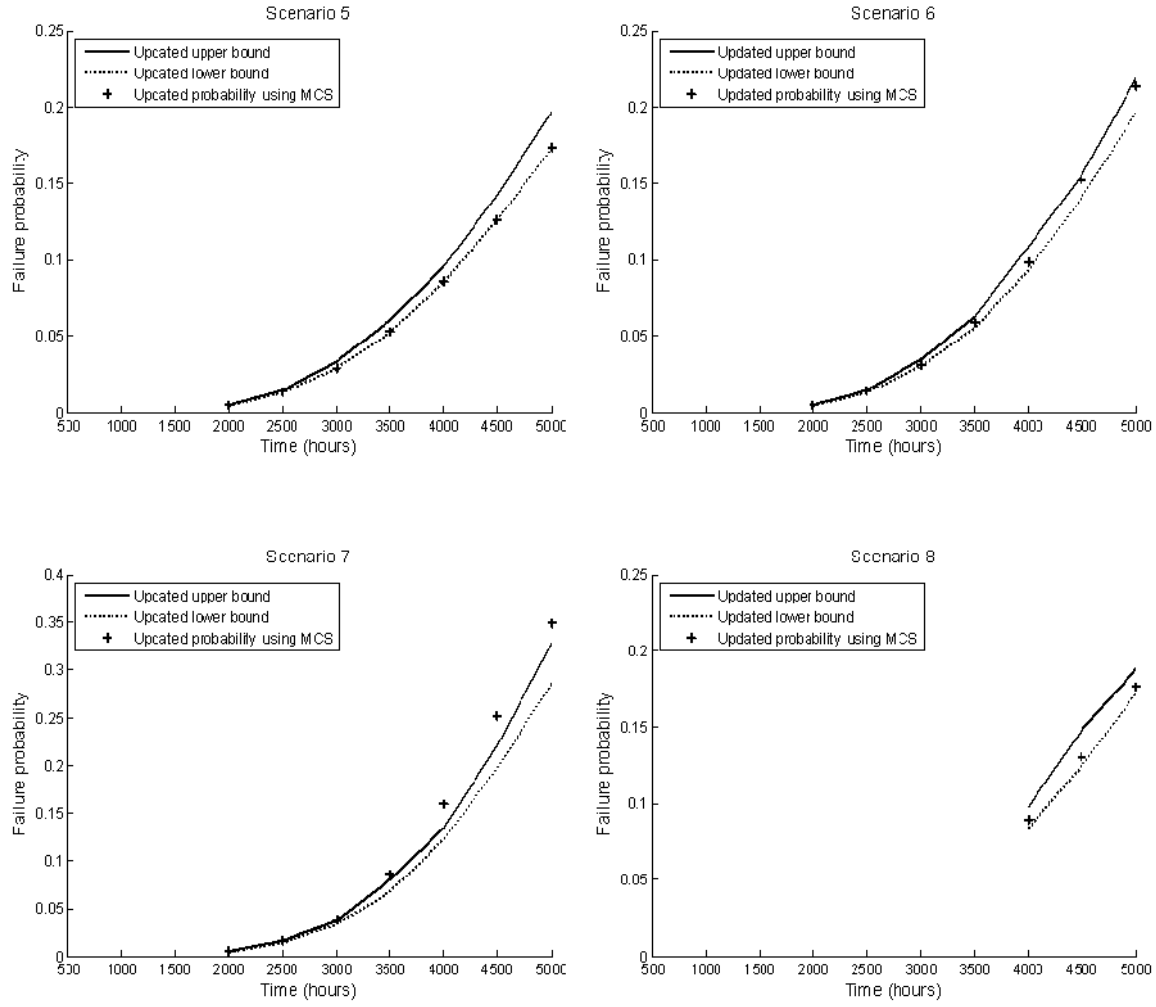

Figure 5.4 Updating results by the proposed method and MCS for equality cases (Scenarios 5-8 in Table 5.1)

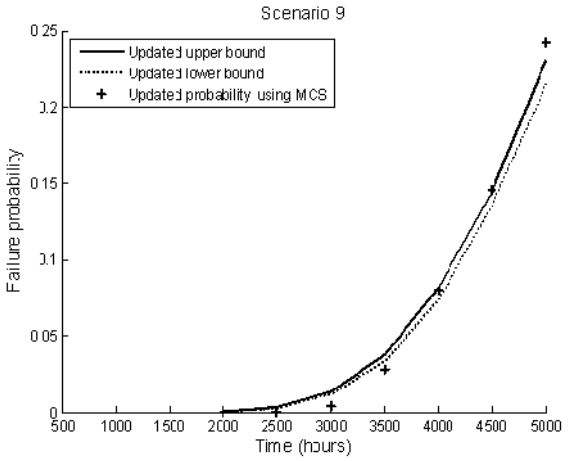

Figure 5.5 Updating results by the proposed method and MCS for mixed case (Scenario 9 in Table 5.1)

Figures 5.3-5 compare the results by the proposed method to those by MCS. As shown in the figures, the updated failure probabilities estimated by the proposed method and MCS show good agreement.

Next, the updated probabilities of different scenarios are compared with each other to investigate the impact of various inspection conditions on the reliability updating, such as the number of inspections, crack detecting resolution, an inspection interval, and measured crack length. As observed in Chapters 3 and 4, the actual system failure probability is fairly close to the upper bound from B^3 analysis. Therefore, only the upper bounds are provided in the plots to facilitate clear comparison.

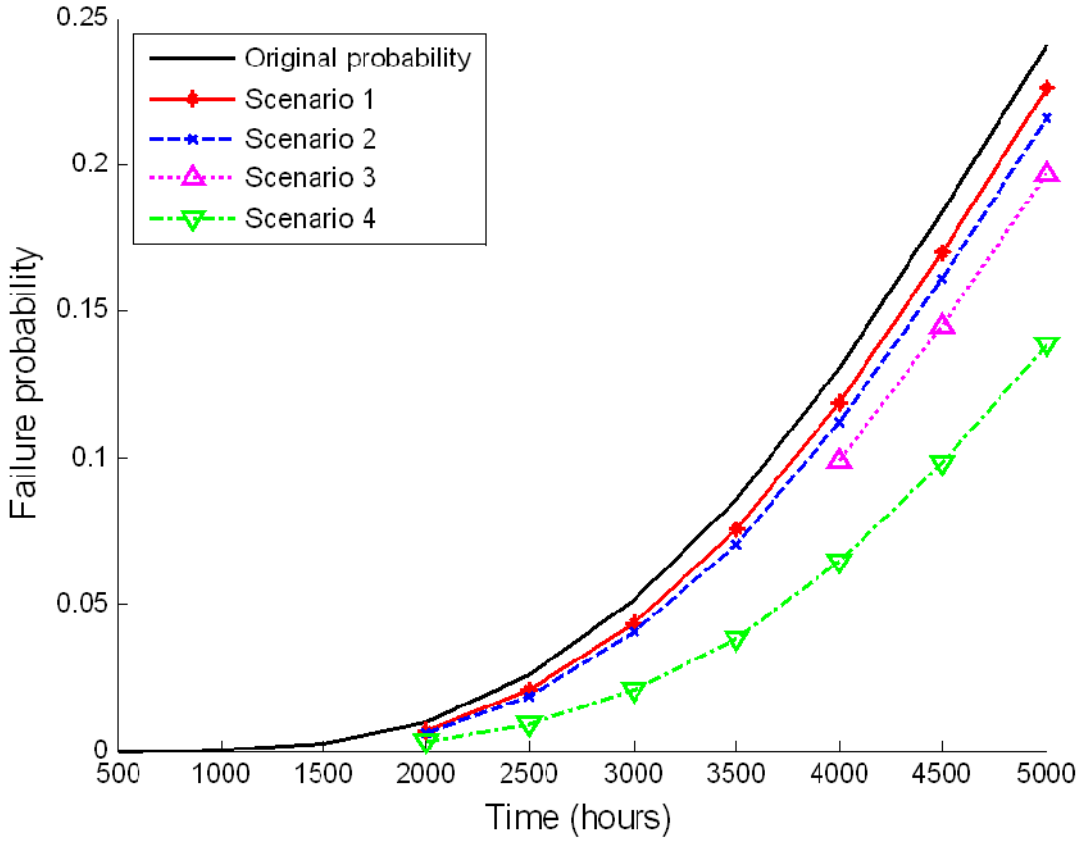

Figure 5.6 Comparison of updated probabilities for inequality cases (Scenarios 1-4 in Table 5.1)

Figure 5.6 compares the original system failure probability and the probabilities updated by inequality cases (Scenarios 1-4). In Scenario 1, the reliability updating decreases the failure probability because no crack has been detected even after 2,000 hours. The updated failure probability decreases further in Scenario 2 because no crack is detected even when a better crack-detecting device is used (with a smaller mean of detectable crack size a^d). In Scenario 3, no crack is detected even though an inspection is made at a later time (4,000 hours) than in

Scenario 1, which further reduces the system failure probability. In Scenario 4, it is assumed that crack is not observed at any of the members. Since the structure consists of six members, the inspection event described as the intersection of six inequality events, as shown in Eq. (5.6). Compared to Scenario 1, we have five additional signs indicating the better safety of the structure, which further reduces the system failure probability as shown in Figure 5.6.

To further investigate the performance of the proposed method, the update of the probability of each system failure sequence in Scenario 1 is shown in Table 5.3. The original probabilities are the same as those in Table 4.1.

Failure sequence	Original probability ($\times 10^{-3}$)	Updated probability ($\times 10^{-3}$)	
		Proposed method	MCS
1	4.871	0.196	0.188
$2 \rightarrow 3$	1.332	1.299	1.281
$3 \rightarrow 2$	1.332	1.299	1.320
$4 \rightarrow 5 \rightarrow 6$	0.294	0.285	0.305
$4 \rightarrow 6 \rightarrow 5$	0.294	0.285	0.311
$5 \rightarrow 4 \rightarrow 6$	0.294	0.285	0.263
$5 \rightarrow 6 \rightarrow 4$	0.294	0.285	0.283
$6 \rightarrow 4 \rightarrow 5$	0.294	0.285	0.279
$6 \rightarrow 5 \rightarrow 4$	0.294	0.285	0.293

Table 5.3 Updated probabilities of critical system failure sequences in Scenario 1 (in Table 5.1)

Since the inspection was made at member 1 only and no crack was found, the probability of the failure sequence including member 1 decrease significantly while the others experience small updates. It is noted that the reliability of uninspected members also can be updated, because they are correlated with the inspected ones (i.e. member 1 in this case) by sharing common random variables in their limit-state functions.

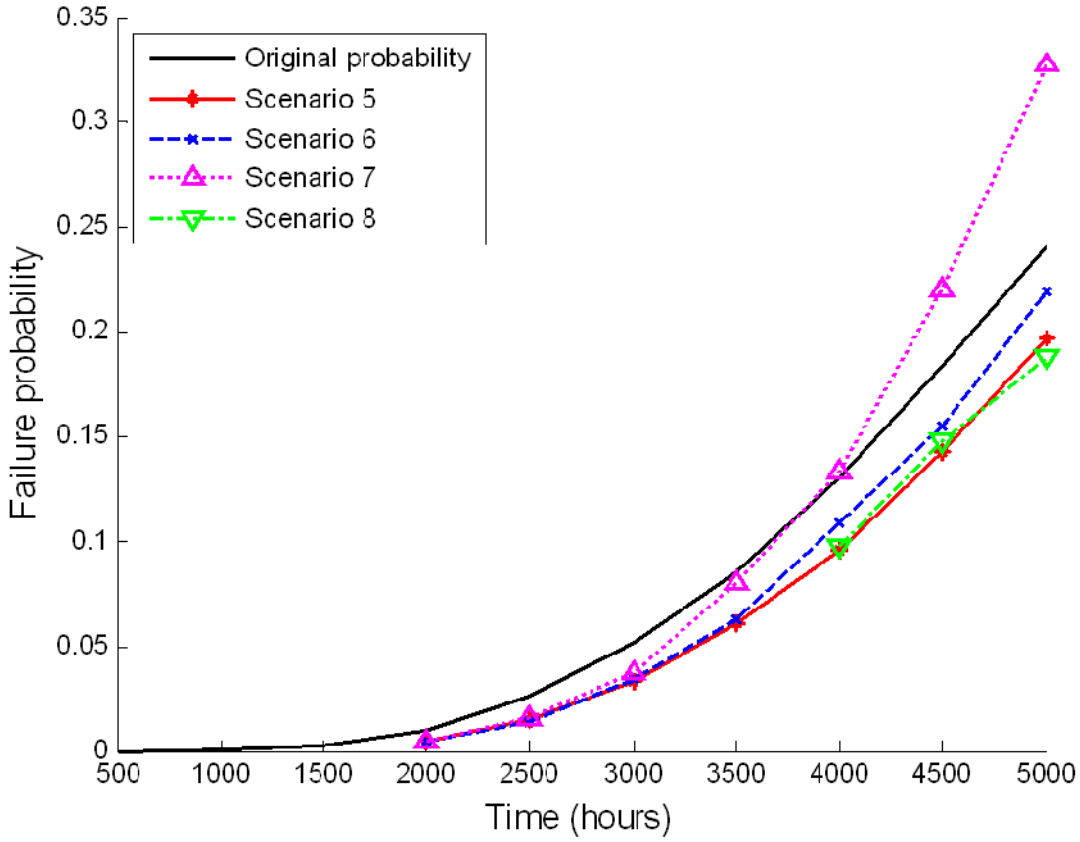

Figure 5.7 Comparison of updated probabilities for equality cases (Scenarios 5-8 in Table 5.1)

For equality cases, Figure 5.7 shows the updated failure probabilities of Scenarios 5-8. From Scenario 5 to Scenario 7, the measured crack size increases from 0.1mm to 0.5mm. It is clearly seen that the longer crack size is measured, the more likely the system is to fail. In Scenarios 8, the same size of crack as Scenario 7 is measured later time, which reduces the updated system failure probability.

Failure sequence	Original probability ($\times 10^{-3}$)	Updated probability ($\times 10^{-3}$)	
		Proposed method	MCS
1	4.871	0.062	0.000
2 → 3	1.332	1.220	1.285
3 → 2	1.332	1.220	1.266
4 → 5 → 6	0.294	0.265	0.288
4 → 6 → 5	0.294	0.265	0.280
5 → 4 → 6	0.294	0.265	0.244
5 → 6 → 4	0.294	0.265	0.231
6 → 4 → 5	0.294	0.265	0.248
6 → 5 → 4	0.294	0.265	0.243

Table 5.4 Updated probabilities of critical system failure sequences in Scenario 5 (in Table 5.1)

Table 5.4 shows the updated probabilities of the critical failure sequences in Scenario 5. As observed in the inequality scenarios, the probabilities of the failure sequences involving member 1 significantly decrease in Scenario 5, and the other probabilities also decrease slightly. This is because the observed crack length (0.1mm) is small considering the inspection time (2,000 hours), and the failures of the inspected and uninspected members are correlated through common random variables in the limit-state functions. It is also noteworthy that the proposed reliability updating method show relative errors around 5-10%. This is because of the numerical differentiation that is introduced to calculate the derivative terms in Eq. (5.11).

As previously stated, traditional reliability updating methods employing numerical differentiation can cause errors, even in a simple reliability problem whose limit-state function is expressed analytically with a few random and deterministic variables (Straub 2011). In this thesis, the First-Order Reliability Method (FORM) and Second-order Reliability Method (SORM) are employed for component reliability analysis. Both of them are widely-used reliability analysis methods that can describe the statistical dependence between component events effectively.

However, they are based on the first- and second-order approximations of a limit-state surface. This concept may cause some errors in component reliability analysis, and the error may be propagated to the system reliability analysis. The errors are due to the complexity of the reliability problem, which is characterized as follows: (1) system failure is defined by a large number of failure sequences; (2) many random variables are non-normal; and (3) limit-state functions are nonlinear. As shown in the results of the updated probabilities, the error is not critical for inequality cases. On the contrary, the error may increase to a noticeable level in the equality cases, whose updated probabilities can be sensitive numerically. It is necessary to develop new component and system reliability analysis methods that can overcome this challenge and provide more precise component and system reliability estimates than the existing methods. However, it is out of the scope of this research.

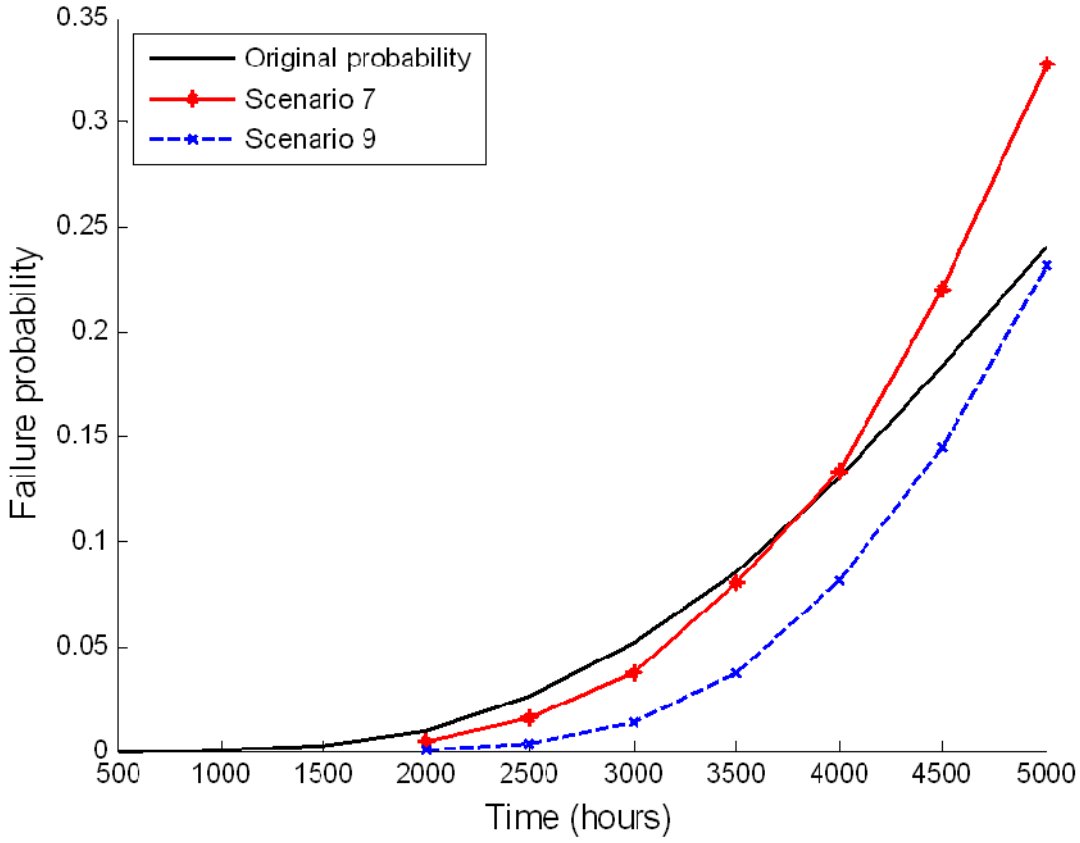

Figure 5.8 Comparison of updated probabilities for mixed case (Scenario 9 in Table 5.1)

Lastly, Figure 5.8 compares the updated probabilities for Scenarios 7 and 9. It is seen that the updated failure probability becomes much smaller in Scenario 9 than in Scenario 7 even though the same size of crack was observed at the same inspection time point. This is due to the additional inequality events, "no more cracks are detected at other locations (i.e. members 2-6)" observed in the mixed case for Scenario 9.

5.5. Numerical Example II: Longeron in Aircraft Structure

5.5.1. Problem description

As another numerical example to test the proposed system reliability updating method, the aircraft longeron system in Chapter 4 is considered. Most of the details are the same as those in Section 4.4. Table 5.5 lists the inspection scenarios considered for reliability updating.

Case	Scenario number	Scenario description
Inequality	1	No crack is detected at member 5 (T_I = 2,000 hours & mean of a^d = 1.0 mm).
	2	No crack is detected at member 5 (T_I = 2,000 hours & mean of a^d = 0.5 mm).
	3	No crack is detected at member 5 (T_I = 4,000 hours & mean of a^d = 1.0 mm).
	4	No crack is detected anywhere (T_I = 2,000 hours & mean of a^d = 1.0 mm).
Equality	5	0.1mm crack is found at member 5 (T_I = 2,000 hours).
	6	0.3mm crack is found at member 5 (T_I = 2,000 hours).
	7	0.5mm crack is found at member 5 (T_I = 2,000 hours).
	8	0.5mm crack is found at member 5 (T_I = 4,000 hours).
Mixed	9	0.5mm crack is found at member 5, but nowhere else (T_I = 2,000 hours & mean of a^d = 1.0 mm).

Table 5.5 Inspection scenarios for longeron system

5.5.2. Statistical properties

The statistical properties of the random variables given in Table 5.2 are used for this example. Unlike the Daniels system example, non-zero correlation coefficients are assigned for the following cases to make the example realistic: (1) between Paris equation parameters (C) of two different parts (correlation coefficient: 0.6); (2) between Paris equation parameters (m) of two

different parts (correlation: 0.6); (3) between initial crack lengths (a^0) of two different fastener holes (correlation: 0.6); (4) between C and m of the same parts (correlation: −0.97); (5) between C and m of two different parts (correlation: −0.6); and (6) between the same kind of inspections (correlation: 0.6). In the other cases, it is assumed that the random variables are independent.

The correlation coefficients in cases (1) through (5) are the same as for Section 4.4, and (6) represents the correlation between inspections at multiple locations with the same device. The correlation coefficients in cases (1), (2), (3), (5), and (6) can change depending on how closely the manufacturing and inspection processes of two different parts are related to each other. Lastly, the strong negative correlation between C and m in case (4) is based on a literature review (Yarema 1980, Borrego *et al*. 2001), as discussed in Section 4.4.2.

5.5.3. Analysis results

Let us compare the updated probabilities from the scenarios given in Table 5.5. The overall trend in the updated probabilities is similar to that of the Daniels system example in Section 5.4. First, as shown in Figure 5.9, the updated probability in Scenario 1 is smaller than the original probability because no crack is detected. In addition, the updated probability decreases further in Scenarios 2 and 3, in which a better crack-detection device and a later inspection are respectively assumed. In Scenario 4, it is assumed that no cracks are detected at any locations. Since the longeron structure has a total of 40 possible cracking locations, the inspection event includes 40 inequality cases. Obviously, the inspection result indicates that the structure is much more reliable than Scenario 1, as shown in the figure.

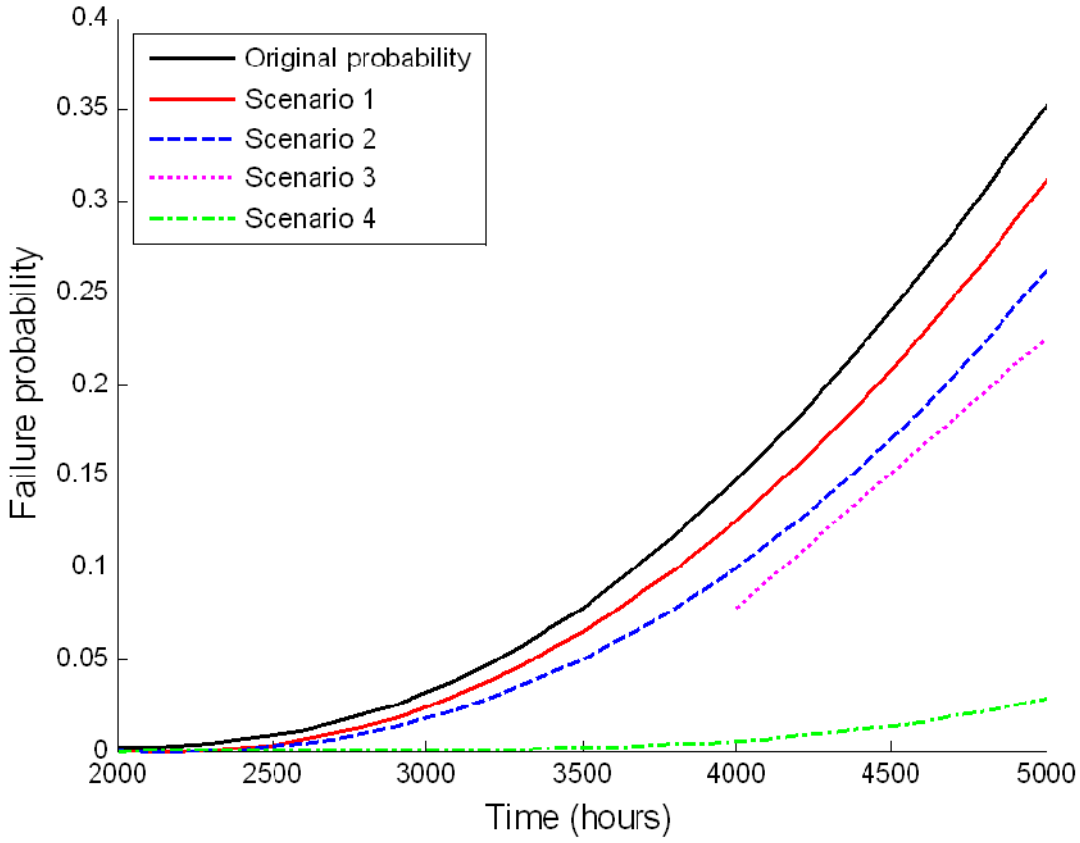

Figure 5.9 Comparison of updated probabilities for inequality cases (Scenarios 1-4 in Table 5.5)

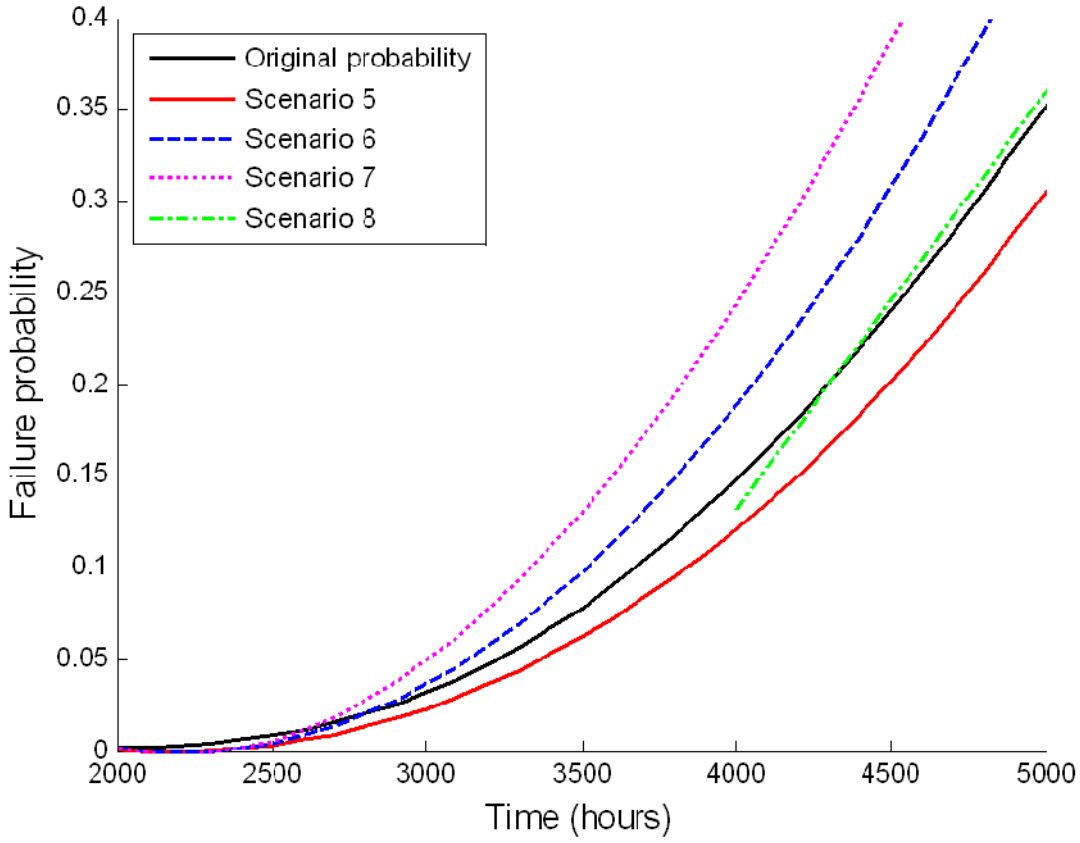

Figure 5.10 Comparison of updated probabilities for equality cases (Scenarios 5-8 in Table 5.5)

For equality cases, Figure 5.10 shows the updated failure probabilities for Scenarios 5-8. The updated probabilities in Scenarios 5-7 show how they increase with the increasing measured size of a crack. When comparing the results from Scenarios 7 and 8, it is observed that the updated probability for Scenario 8 is much smaller, which is because the same size crack is detected from an inspection at a later time.

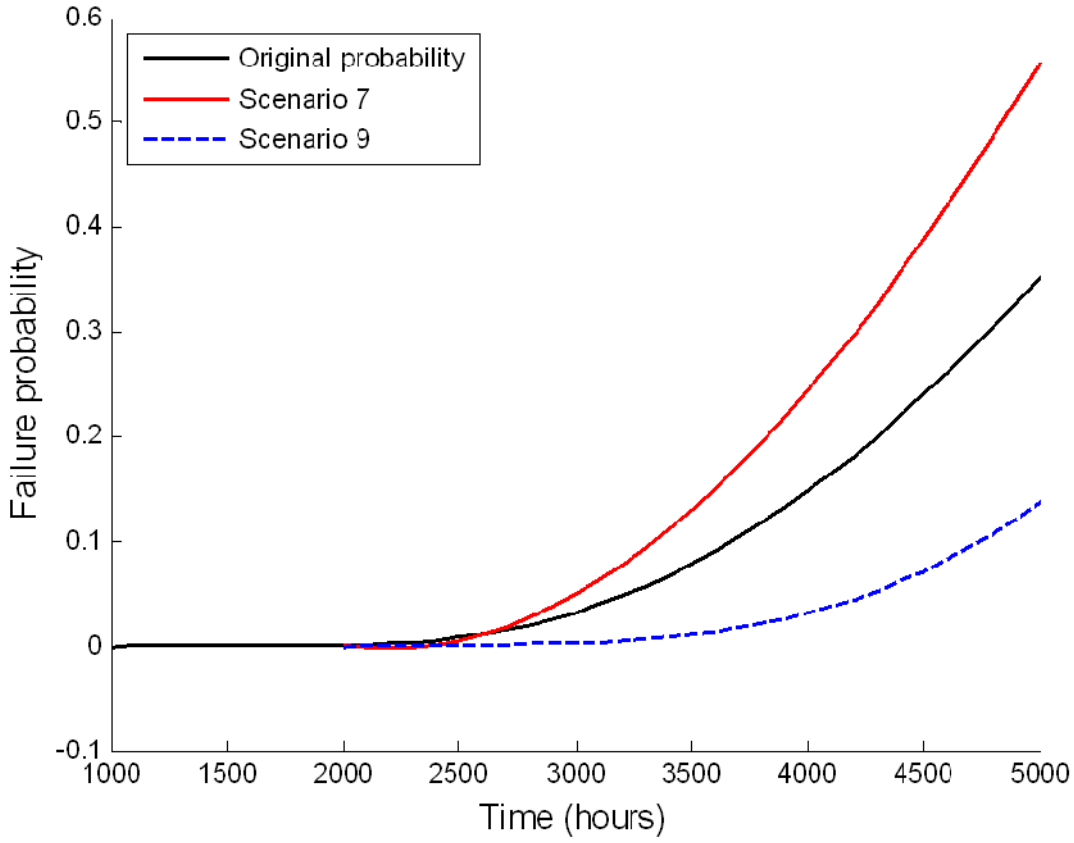

Figure 5.11 Comparison of updated probabilities for mixed case (Scenario 9 in Table 5.5)

Lastly, Figure 5.11 shows the updated probabilities for Scenarios 7 and 9. It turns out that the updated failure probability is much smaller compared for Scenario 9. The reason is, although a large crack is detected at member 1, no more cracks are detected at other locations (i.e. members 1-40 except for 5).

In these reliability update analyses, it is noteworthy that it took only a few minutes to perform the reliability updating in each scenario (using a general personal computer with 2.61 GHz CPU and 3.25 GB RAM), which is one of the powerful benefits from the proposed method

in efficiency. This is possible because, as previously stated, the reliability updating step is based on the results of the prior B^3 analysis and requires updating the probabilities of system failure and non-failure cases only without new FE simulations or B^3 analysis. This allows for significant saving in computational time because each FE analysis in this example takes several minutes.

5.6. Summary

This chapter introduces a new reliability updating method for fatigue-induced sequential failures, by integrating the B^3 method with existing formulations of reliability updating. For effective risk-based maintenance, it is essential to estimate the reliability of a structure against fatigue-induced sequential failures and update the original reliability based on the observations from inspections. The proposed reliability updating is a two-step procedure: 1) B^3 analysis is performed to identify system failure and non-failure cases as well as calculate upper and lower bounds on system failure probability; and 2) the probabilities of the identified system failure and non-failure cases are updated to obtain the updated upper and lower bounds. Since the B^3 analysis identifies most critical failure and non-failure cases, the updated probabilities conditioned on inspection events also provide accurately-updated upper and lower bounds on system failure probability with a reasonable gap. In addition, the new method allows us to update the original probability efficiently because it reuses the results of the B^3 analysis. The proposed method was demonstrated by two numerical examples, multi-layer Daniels system and aircraft longeron structure. In the first example, the results from the proposed method were compared with the ones from Monte Carlo simulation, which showed that the proposed method enabled us to obtain accurately-updated reliability estimates of truss and continuum subject to the risk of fatigue-induced sequential failures. In addition, the impact of various inspection conditions on

the reliability updating was investigated in both of the numerical examples, such as the number of inspections, crack detecting resolution, inspection interval, and measured crack length. The investigation confirmed that the method allows for reliability updating under various inspection scenarios. Lastly, especially in the aircraft longeron example, it is noteworthy that it took only a few minutes to obtain the updated reliability bounds in each scenario because the reliability updating method does not require new system reliability analysis or FE simulations.

6. CONCLUSIONS

6.1. Summary of Major Findings

This thesis developed novel methods for finite-element-based system reliability analysis and updating of structures subject to fatigue-induced sequential failures. As the first step, a framework for finite element system reliability analysis (FE-SRA) was proposed by integrating FE simulation with the matrix-based system reliability (MSR) method. In addition, a new Branch-and-Bound method employing system reliability Bounds (termed the B^3 method) was developed to perform system reliability analysis of fatigue-induced sequential failures of truss structures while accounting for load re-distribution. The method was further developed for applications to continuum structures. Lastly, a new inspection-based system reliability updating method was developed based on the use of the B^3 method. The proposed methods were applied to several numerical examples of discrete and continuum structures and successfully demonstrated. This study provided the following major findings:

- As a computational platform of the proposed FE-SRA framework, an interface code, FERUM-ABAQUS, was developed. In the framework, the reliability analysis package FERUM repeatedly calls ABAQUS® to obtain structural responses during a component reliability analysis, and a system reliability analysis using the matrix-based system reliability (MSR) method is performed by use of the results of the individual reliability analyses in the component level. The proposed framework allows us to compute the probabilities of general system events and their sensitivities with respect to design parameters based on the results of the component-level FE reliability analyses. Also, FERUM-ABAQUS is a more versatile computing platform than other existing FE-RA

software because it employs FERUM and ABAQUS®, both of which are respectively specialized in reliability and FE analyses. Finally, the proposed framework and FERUM-ABAQUS were successfully demonstrated through numerical examples of an aircraft wing torque box and a bridge pylon.

- The B^3 method can estimate the probability of system failure caused by fatigue-induced sequential failures by identifying critical system failure sequences efficiently and accurately. Due to the proposed disjoint cut-set formulation employing a recursive formulation of limit-states and systematic search procedure, the B^3 method can identify critical sequences of fatigue-induced failures causing a system failure in the decreasing order of their likelihood. Since the conventional branch-and-bound approaches employing non-disjoint cut-set provide only upper bound, there is a risk of underestimating the actual system failure probability. However, the proposed method provides both lower and upper bounds on the system failure probability while the size of the updates on each bound is diminishing monotonically. Every structural analysis or finite element simulation performed during the search contributes to narrowing the bounds. This significantly reduces the computational time required for accurate results especially when computational cost for structural analyses is dominant. The updated bounds provide reasonable criteria for terminating a branch-and-bound search without missing critical sequences. After a demonstration by a multi-layer Daniels system, the method was tested by a three-dimensional offshore structure with 66 members. The results by the B^3 method were verified by crude Monte Carlo simulations. The merits of the proposed approach were successfully demonstrated through comparison with the results by a conventional branch-and-bound approach.

- The B^3 method was further developed for FE-based system reliability analysis of fatigue-induced sequential failures of continuum structures. Despite merits over existing branch-and-bound approaches, the B^3 method which was originally developed for truss is not readily applicable to continuum structures because of its limitations in (1) describing general stress distributions in limit-state formulations; (2) evaluating stress intensity range based on the crack length; and (3) dealing with slow convergence of the bounds for continuum. In order to overcome these limitations, (1) the limit-state function was modified to incorporate general stress distribution instead of using far-field stress assumption; (2) an external computer program such as AFGROW® was incorporated into the B^3 computational framework to estimate the stress intensity range for the given stress distribution; and (3) the termination criteria of B^3 analysis was modified to avoid performing unnecessary simulations that would make insignificant updates on the lower bound. The B^3 method for continuum was demonstrated by a numerical example of multi-layer Daniels system, and the results were verified by the B^3 method for truss and Monte Carlo simulation. Furthermore, the proposed method was applied to a numerical example of aircraft longeron system. In the example, first of all, it was proved that the termination criteria newly introduced for the B^3 method for continuum enabled us to reduce computational and time costs significantly, by avoiding identifying many negligible failure sequences. In addition, it was shown that the proposed method enable us to calculate the system-level risk of fatigue-induced sequential failures using a large-scale FE models, efficiently and accurately. Lastly, the method can identify the most critical failure sequences in the decreasing order of their probabilities.

- The new method for system reliability updating enables us to update the original structural reliability based on inspection results in an accurate and efficient way. The reliability updating procedure is two folds: 1) B^3 analysis is performed to identify system failure and non-failure cases as well as calculate upper and lower bounds on system failure probability; and 2) the probabilities of the identified system failure and non-failure cases are updated to obtain the updated upper and lower bounds. Since the B^3 analysis identifies most critical failure and non-failure cases, their updated probabilities conditioned on inspection events also provide accurately-updated upper and lower bounds on system failure probability with a reasonable gap. In addition, the new method allows us to update the original probability efficiently because it reuses the results of the B^3 analysis. The proposed method was first applied to a numerical example of multi-layer Daniels system, and the results were verified by Monte Carlo simulation (MCS). The verification using MCS was not an easy task if any observations were of the equality type. In order to overcome this challenge, a new method (Straub 2011) using a likelihood function has been employed. In this example, first of all, it was successfully shown that the proposed method updated the original probabilities accurately for various inspection scenarios. In addition, it was observed that the probabilities of the failure sequences involved with the structural member where no crack or a small crack was detected decreased significantly. On the other hand, the probabilities of the failure sequences involved with the structural member having a large crack increased. However, it could not provide perfectly accurate results, with relative errors around 5-10%, when the inspection results included equality information. The proposed method was also applied to an example of aircraft longeron, and it was successfully shown that the method could

perform system reliability updating of fatigue-induced sequential failures for various inspection scenarios, efficiently and accurately.

6.2. Future Research Topics

The proposed methods can be further developed to further improve accuracy and efficiency of reliability analysis and updating as well as applicability to complex structural systems in practice. The following future research topics are suggested:

- Apply the proposed FE-SRA framework and computational platform FERUM-ABAQUS to structural reliability problems in consideration of the nonlinear behavior of structures. In reality, the reliability of structural systems should be estimated by considering their nonlinear properties in both material and geometry. However, the current framework and computational platform were tested by linear elastic problems only. The developed framework and platform have potentials of dealing with system-level risk assessment of nonlinear problems.
- Perform system reliability analysis of sequential failures induced by extreme loading. Yielding failure caused by extreme environmental loading is another important failure mode of structures, and sequential failures resulting in an entire system collapse may occur due to both fatigue and yielding. However, the current B^3 method is able to deal with fatigue-induced sequential failures only. Therefore, the method needs to be further developed such that it can perform system reliability analysis of sequential failures caused by yielding.
- Perform a parametric study about the approximation introduced to the B^3 method for continuum. Although it was shown in Section 4.3 that the approximation introduced in the B^3 method for continuum did not have a significant impact on the reliability analysis results in the numerical example, it is still necessary to investigate more cases in various

conditions: for example, different geometric functions from the one in Eq. (4.12) can be employed.

- Further develop the B^3 method so that it can re-define possible cracking locations/members. Currently, the B^3 method requires defining possible cracking locations before the analysis. In many nonlinear structural systems, however, it is hard to pre-define the cracking locations because the locations may vary with the prior local failures during a sequential failure. If the B^3 method can automatically re-define possible failure locations in each damage status (e.g., from the stress distribution), it will allow us to solve nonlinear structural systems more accurately.
- In reality, if inspection results indicate that the target structure is damaged to have insufficient level of safety, the damaged structural members may be repaired or replaced. For reliability-based inspection planning and structural maintenance, the reliability of the structure should be updated again after such maintenance efforts. However, the current B^3 method cannot update the structural reliability based on such changes. There have been some studies about such post-repairing reliability updating methods which are applicable to simple structures (Moan and Song 2000). Inspired by the existing research, the B^3 method can be expanded to estimate how the reliability of a damaged structure is updated by repairing. Based on the research, optimized inspection planning or risk based inspection (RBI) can also be suggested.

REFERENCES

Alford, R.E., Bell, R.P., Cochran, J.B., and Hammond, D.O. (1992). C-141 WS 405 Risk assessment. WL-TR-92-4045. *Proceedings of the 1991 USAF Structural Integrity Program Conference*, San Antonio, Texas.

Almar-Naess, A. (1985). *Fatigue Handbook: Offshore Steel Structures*, Tapir Forlag, Trondheim, Norway.

Ambartzumian, R., Der Kiureghian, A., Ohanian V., and Sukiasian, H. (1998). Multinormal probability by sequential conditioned importance sampling: theory and application. *Probabilistic Engineering Mechanics*, 13(4), 299-308.

Ayala-Uraga, E. and Moan, T. (2007). Fatigue-reliability-based assessment of welded joints applying consistent fracture mechanics formulations. *International Journal of Fatigue*, 29, 444-456.

Baker, M.J. and Descamps, B. (1999). Reliability-based methods in the inspection planning of fixed offshore steel structures. *Journal of Constructional Steel Research*, 52(1), 117-132.

Beck, J.L. and Au, S.-K. (2002). Bayesian updating of structural models and reliability using Markov chain Monte Carlo simulation. *Journal of Engineering Mechanics*, 128(4), 380-391.

Bjerager, P. and Krenk, S. (1989). Parametric sensitivity in first-order reliability theory. *Journal of Engineering Mechanics*, 115(7), 1577-1582.

Boole, G. (1854*). Laws of thought*, American Reprint of 1854 ed., Dover, New York.

Borrego, L.P., Ferreira, J.M., and Costa, J.M. (2001). Fatigue crack growth and crack closure in an AlMgSi alloy. *Fatigue and Fracture of Engineering Materials and Structures*, 24(4), 255-266.

Box, G.E.P. and Tiao, G.C. (1992). *Bayesian inference in statistical analysis*, Wiley, New York, NJ.

Byers, W.G., Marley, M.J., Mohammadi, J., Nielsen, R.J., and Sarkani, S. (1997). Fatigue reliability reassessment applications: state-of-the-art paper. *Journal of Structural Engineering*, 123(3), 277-285.

Daniels, H.E. (1945). The statistical theory of the strength of bundles of threads. *Proc. of the Royal Society of London. Series A, Mathematical and Physical Sciences*, 183(995), 405-435.

Deodatis, G., Fujimoto, G., Ito, S., Spencer, J., and Itagaki, H. (1992). Non-periodic inspection by Bayesian method I. *Probabilistic Engineering Mechanics*, 7(4), 191-204.

Der Kiureghian, A. (2005). First- and second-order reliability methods. *Engineering Design Reliability Handbook*, edited by E. Nikolaidis, D.M. Ghiocel, and S. Singhal, CRC Press, Boca Raton, FL, Chapter 14.

Der Kiureghian, A. and Song, J. (2008). Multi-scale reliability analysis and updating of complex systems by use of linear programming. *Reliability Engineering & System Safety*, 93(2), 288-297.

Ditlevsen, O. (1979). Narrow reliability bounds for structural systems. *Journal of Structural Mechanics*, 7(4), 453-472.

Ditlevsen, O. and Bjerager, P. (1989). Plastic reliability analysis by directional simulation. *Journal of Engineering Mechanics*, 115(6), 1347-1362.

Estes, A.C. and Frangopol, D.M. (1998). RELSYS: a computer program for structural system reliability. *Structural Engineering and Mechanics*, 6(8), 901-919.

Forman, R.G., Kearney, V.E., and Engle, R.M. (1967). Transactions of the American Society of Mechanical Engineers. Series D; *Journal of Basic Engineering*, 89(3), 459–465.

Frangopol, D.M. and Maute, K. (2003). Life-cycle reliability-based optimization of civil and aerospace structures. *Computers and Structures*, 81, 397-410.

Genz, A. (1992). Numerical computation of multivariate normal probabilities. *Journal of Computational and Graphical Statistics*, 141-149.

Gharaibeh, E.S., Frangopol, D.M., and Onoufriou, T. (2002). Reliability-based importance assessment of structural members with applications to complex structures. *Computers and Structures*, 80, 1113-1131.

Gollwitzer, S., Kirchgäßner, B., Fischer, R., and Rackwitz, R. (2006). PERMAS-RA/STRUREL system of programs for probabilistic reliability analysis. *Structural Safety*, 28 (1), 108-129.

Gooteman, F. (2008). A stochastic approach to determine lifetimes and inspection schemes for aircraft components. *International Journal of Fatigue*, 30, 138-149.

Guenard, Y.F. (1984). Application of system reliability analysis to offshore structures. *Report 1*, Reliability of Marine Structures Program, Stanford Univ., Stanford, CA.

Haldar, A. Ed. (2006). *Recent Developments in Reliability-based Civil Engineering*. World Scientific Publishing Company, Singapore.

Harter, J.A. (2006). AFGROW user guide and technical manual (Ver. 4.0011.14). *AFRL-VA-WP-TR-2006-XXXX*, Air Force Research Laboratory, WPAFB, OH.

Haldar, A. and Mahadevan, S. (2000). *Probability, Reliability, and Statistical Methods in Engineering Design*. John Wiley & Sons, New York.

Haukaas, T. (2003). *Finite Element Reliability and Sensitivity Methods for Performance-Based Engineering*. Ph.D. Thesis, Department of Civil and Environmental Engineering, University of California, Berkeley, CA.

Haukaas, T., Hahnel, A., Sudret, B., Song, J., and Franchin, P. (2003). *FERUM*. Department of Civil and Environmental Engineering, University of California, Berkeley, CA, URL: http://www.ce.berkeley.edu/FERUM/ [cited 6 Apr. 2012].

Heida, J.H. and Grooteman, F.P. (1998). Airframe inspection reliability using field inspection data. *Proceedings of Airframe Inspection Reliability under Field/Depot Conditions*, Brussels.

Hohenbichler, M and Rackwitz, R. (1983). First-order concepts in system reliability. *Structural Safety*, 1(3), 177-188.

Hu, Y., Chen, B., and Ye, N. (1998). Fatigue reliability analysis of redundant structural systems by using Monte Carlo simulation. *Proc. 17th International Conference on Offshore Mechanics and Arctic Engineering*, 5-9 July 1998. Lisbon, Portugal. OMAE.

Imai, K. and Frangopol, D.M. (2002). System reliability of suspension bridges. *Structural Safety*, 24, 219-259.

Itagaki, H. and Ito, S. (1998). A simplified quantitative analysis method for reliability of aging structures. *Structural Safety and Reliability*, N. Shiraishi, M. Shinozuka, and Y.K. Wen, (Eds), A.A. Balkema, 1 , 217-24.

Jiao, G. and Moan, T. (1990). Methods of reliability model updating through additional events. *Structural safety*, 9(2), 139-153.

Kang, W.-H. (2011). *Development and application of new system reliability analysis methods for complex infrastructure systems*. Ph.D. thesis, University of Illinois, Urbana-Champaign, IL.

Kang, W.-H. and Song, J. (2010). Evaluation of multivariate normal integrals for general systems by sequential compounding. *Structural Safety*, 32(1), 35-41.

Kang, W.-H., Lee, Y.-J., Song, J., and Gencturk, B. (2012). Further development of matrix-based system reliability method and applications to structural systems. *Structural and Infrastructure Engineering: Maintenance, Management, Life-cycle Design and Performance*, 8(5), 441-457.

Kang, W.-H., Song, J., and Gardoni, P. (2008). Matrix-based system reliability method and applications to bridge networks. *Reliability Engineering & System Safety*, 93, 1584-1593.

Karamchandani, A., Dalane, J.I., and Bjerager, P. (1991). Systems reliability or offshore structures including fatigue and extreme wave loading. *Marine Structures*, 4, 353-379.

Karamchandani, A., Dalane, J.I., and Bjerager, P. (1992). Systems reliability approach to fatigue of structures. *Journal of Structural Engineering*, 118(3), 684-700.

Karsan, D.I. and Kumar, A. (1988). Fatigue failure paths for offshore platform inspection. *Journal of Structural Engineering*, 116(6), 1679-1695.

Kirkemo, F. (1988). Applications of probabilistic fracture mechanics to offshore structures. *Applied Mechanics Reviews*, 41(2), 61-84.

Lee, Y.-J. and Song, J. (2011a). Risk analysis of fatigue-induced sequential failures by branch-and-bound method employing system reliability bounds. *Journal of Engineering Mechanics*, 137(12), 807-821.

Lee, Y.-J. and Song, J. (2011b). Risk quantification of fatigue-induced sequential failures by branch-and-bound method employing system reliability bounds. *11th International Conference on Applications of Statistics and Probability in Civil Engineering (ICASP11)*, August 1–4, Zurich, Switzerland.

Lee, Y.-J., Song, J., Gardoni, P., and Lim, H.-W. (2011). Post-hazard flow capacity of bridge transportation network considering structural deterioration of bridges. *Structure and Infrastructure Engineering: Maintenance, Management, Life-cycle Design and Performance*, 7(7), 509-521.

Lee, Y.-J., Song, J., and Tuegel, E.J. (2008). Finite element system reliability analysis of a wing torque box. *Proc. 10th AIAA Nondeterministic Approaches Conference*, April 7-10, Schaumburg, IL.

Madsen, H.O. (1985). Random fatigue crack growth and inspection. *Proc. 4th International Conference on Structural Safety and Reliability (ICOSSAR'85)*, May 27-29, Kobe, Japan.

Melchers, R.E. (1994). Structural system reliability assessment using directional simulation. *Structural Safety*, 16, 23-37.

Melchers, R.E. and Tang, L.K. (1984). Dominant failure modes in stochastic structural systems. *Structural Safety*, 2(2), 127-143.

Millwater, H.R. and Wieland, D.H. (2010). Probabilistic sensitivity-based ranking of damage tolerance analysis elements. *Journal of Aircraft*, 47(1), 161-171.

Millwater, H.R., Wu, Y.-T., and Cardinal J.W. (1994). Probabilistic structural analysis of fatigue and fracture. *Proc. 35th AIAA Structures, Structural Dynamics, and Materials Conference*, 18-20 April 1994. Hilton Head, SC.

Moan, T. (2005). Safety of offshore structures. *Center for Offshore Research and Engineering CORE*, Report 2005-04.

Moan, T. and Ayala-Uraga, E. (2008). Reliability-based assessment of deteriorating ship structures operating in multiple sea loading climates. *Reliability Engineering and System Safety*, 93, 433-446.

Moan, T. and Song, R. (2000). Implications of inspection updating on system fatigue reliability of offshore structures. *Journal of Offshore Mechanics and Arctic Engineering*, 122(3), 173-180.

Moan, T., Hovde, G.O., and Blanker, A.M. (1993). Reliability-based fatigue design criteria for offshore structures considering the effect of inspection and repair. *Proc. Offshore Technology Conference*, 3-6 May 1993. Houston, TX.

Moses, F. (1982). System reliability development in structural engineering. *Structural Safety*, 26(1), 3-13.

Murotsu, Y. (1984). Automatic generation of stochastically dominant modes of structural failure in frame. *Structural Safety*, 2(1), 17-25.

Newman, J.C., Raju, I.S. (1981). An empirical stress intensity factor equation for the surface crack. *Engineering of Fracture Mechanics*, 15, 185-192.

Nguyen, T.H., Paulino, G.H., Song, J., and Le, C.H. (2010a). A computational paradigm for multiresolution topology optimization (MTOP). *Structural and Multidisciplinary Optimization*, 41(4), 525-539.

Nguyen, T.H., Song, J., and Paulino, G.H. (2010b). Single-loop system reliability-based design optimization using matrix-based system reliability method: theory and applications. *Journal of Mechanical Design*, ASME., 132, 011005-1~11.

Nguyen, T.H., Song, J., and Paulino, G.H. (2011). Single-loop system reliability-based topology optimization considering statistical dependence between limit states. *Structural and Multidisciplinary Optimization*, 44(5), 593-611.

Pandey, M.D. (1998). An effective approximation to evaluate multinormal integrals. *Structural Safety*, 20, 51-67.

Paris, P.C. and Erdogan, F. (1963). A critical analysis of crack propagation laws. *J. Basic Eng., Trans*. ASME., 85: 528-534.

Shabakhty, N., Boonstra, H., and Van Gelder, P. (2003). System reliability of jack-up structures based on fatigue degradation. In T Bedford & van Gelder (Eds.), *Safety and Reliability*, 1437-1445.

Shi, P. and Mahadevan, S. (2001). Aircraft structures reliability under corrosion fatigue. *Proc. 42th AIAA Structures, Structural Dynamics, and Materials Conference*, April 16-19, Seattle, WA.

Sivia, D.S. (1996). *Data analysis: A Bayesian tutorial*, Clarendon, Oxford, UK.

Soares, C.G. (2000). Dealing with strength degradation in structural reliability. *Proc. workshop "Risk Based Design of Civil Structures"*, Delft University of Technology, Jan. 11, pp. 23-41.

Song, J. and Der Kiureghian, A. (2003). Bounds on system reliability by linear programming. *Journal of Engineering Mechanics*, ASCE., 129(6), 627-636.

Song, J. and Kang, W.-H. (2009). System reliability and sensitivity under statistical dependence by matrix-based system reliability method. *Structural Safety*, 31(2), 148-156.

Song, J. and Ok, S.-Y. (2010). Multi-scale system reliability analysis of lifeline networks under earthquake hazards. *Earthquake Engineering & Structural Dynamics*, 39(3), 259-279.

Song, J., Kang, W.-H., Lee, Y.-J., and Ok, S.-Y. (2008). Applications of matrix-based system reliability method to complex structural systems. *Proc. IFIP 08-WG7.5*, August 6-9, Toluca, Mexico.

Straub, D. (2004). *Generic approaches to risk based inspection planning for steel structures*. Ph.D. thesis, Swiss Federal Institute of Technology, Zurich, Switzerland.

Straub, D. (2011). Reliability updating with equality information. *Probabilistic Engineering Mechanics*, 26(2), 254-258.

Straub, D. and Der Kiureghian, A. (2007). Risk acceptance in deteriorating structural systems. *Proc. JCSS Workshop on Risk Acceptance and Risk Communication*, Stanford, CA.

Sudret, B. and Der Kiureghian, A. (2000). *Stochastic Finite Element Methods and Reliability: A State-of-the-Art Report*. Department of Civil and Environmental Engineering, University of California, Berkeley, CA.

SwRI. (2009). *NESSUS (ver 9.0)*, Southwest Research Institute, http://www.nessus.swri.org/ [cited 3 Jan. 2010].

Tada, H., Paris, P.C., and Irwin, G.R. (1985). The stress analysis of cracks handbook (2nd Ed.): 2.11. Paris Productions, Inc., St. Louis, MO.

Tang, W.H. (1973). Probabilistic updating of flaw information. *Journal of Testing and Evaluation*, 1(6), 459-467.

Taylor, J. (1998). Probability and statistics in engineering design. *Proceedings of the Institution of Mechanical Engineers, Part G: Journal of Aerospace Engineering*, 212(3), 177-181.

Thoft-Christensen, P. (1998). On industrial application of structural reliability theory. *Proc. IFIP 98-WG7.5*, May 11-13, Krakow, Poland.

Thoft-Christensen, P. and Murotsu, Y. (1986). *Application of Structural System Reliability Theory*, Springer-Verlag, Berlin, Germany.

Tiffany, C.F. (1978). Durability and damage tolerance assessments of United States air force aircraft. *Proc., the AIAA Structural Durability and Damage Tolerance Workshop*, April 6–7, Washington DC, pp. 25–47.

Toyoda-Makino, M. and Tanaka, H. (1998). Optimal inspection strategy based on cost-minimization using a diffusive crack growth model. *Structural Safety and Reliability*, N. Shiraishi, M. Shinozuka, and Y. K. Wen, (Eds), A.A. Balkema, 2, 1203-1210.

U.S. Department of Defense. (2005). *Military Handbook - MIL-HDBK-5H: Metallic Materials and Elements for Aerospace Vehicle Structures (Knovel Interactive Edition)*

Van Dijk, G.M. and De Jonge, J.B. (1975). Introduction to FALSTAFF. *Eighth ICAF Symposium*, ICAF-801, June 2-5, Lausanne, Swiss.

Walker, K. (1970). The effect of stress ratio during crack propagation and fatigue for 2024-T3 and 7075-T6 aluminum. *Effects of Environment and Complex Load History on Fatigue Life*, ASTM STP 462, American Society for Testing and Materials, West Conshohocken, PA, 1-14.

Wang, Y., Shi, Y., Wang, C., and Li, S. (2006). A new method for system fatigue reliability analysis of offshore steel jacket. *Advances in Structural Engineering*, 9(2), 185-193.

Wirsching, P.H., Torng, T.Y., Geyer, J.F., and Stahl, B. (1990). Fatigue reliability and maintainability of marine structures, *Marine Structures*, 3(4), 265-284.

Yang, J.N. and Trapp, W.J. (1974). Reliability analysis of aircraft structures under random loading and periodic inspection. *AIAA Journal*, 12(12), 1623-1630.

Yang, J.N. and Trapp, W.J. (1975). Inspection frequency optimization for aircraft structures based on reliability analysis. *Journal of Aircraft*, 12(5), 494-496.

Yarema, S.Y. (1980). Correlation of the parameters of the Paris equation and the cyclic crack resistance characteristics of materials. *Strength of Materials*, 13(9), 1090-1098.

Zhao, Z., Haldar, A., and Breen, F.L. (1994). Fatigue-reliability updating through inspections of steel bridges. *Journal of Structural Engineering*, 120(5), 1624-1642.

Zhu, J. and Wu, J. (2011). Study on system reliability updating through inspection information for existing cable-stayed bridges. *Advanced Materials Research*. Vols. 250-253, 2011-2015.